To the Graduate Council:

I am submitting here with a thesis written by Y. C. Lin entitled "Effect of Aging on the Structure of a Ni-10 at.%Ta and in a Ni-10 at.%Ta-16 at.%Cr Alloy." I have examined the final copy of this thesis for form and content and recommend that it be accepted in partial fulfillment of the requirements for the degree of Master of Science, with a major in Metallurgical Engineering.

C. R. Brooks, Major Professor

We have read this thesis
and recommend its acceptance

Accepted for Council:

Vice Provost and
Dean of the Graduate School

EFFECT OF AGING ON THE STRUCTURE OF A NI-10 at.% Ta AND IN A NI-10 at.% Ta-16 at.% CR ALLOY

A Thesis

Presented for the

Master of Science

Degree

THE University of Tennessee, Knoxville

Yee C. Lin

December 1986

DEDICATION

This thesis is dedicated to my parents, two sisters and my wife. Without their love, support, and encouragement, this graduate education would have been impossible.

ACKNOWLEDGEMENTS

The author would like to express deep gratitude to his major professor, Dr. C. R. Brooks, for his unceasing guidance, patience, and support through the entire duration of this research.

The financial support provided through teaching assistantships by the Department of Materials Science and Engineering, University of Tennessee, Knoxville is gratefully acknowledged.

The author would like to deeply thank Dr. B. F. Oliver for supplying the high-purity Ni, Ta, and Cr materials and for the help in operating the Balzers induction furnace.

The help received from Mr. Ted A. Long, head of the departmental electronic shop, and his efficient group: Mr. Stephen A. Stiner, Mr. Michael R. Neal and Mr. Ronald L. Johnson, in maintaining the electronic and furnace equipment is deeply appreciated.

Thanks are extended to Mr. H. B. Thompson, head of the departmental machine shop and his amiable group: Mr. Raymond Bellamy, Mr. Jack French, and Mr. Doug Fielden for their help in solving the Arc Melting Furnace problems.

Special gratitude is expressed to Mr. Bob L. McGill for his help with the scanning and transmission electron microscope, and to Mr. Albert W. J. Carter and Ms. Aileen Cagle for supplying laboratory materials.

Special appreciation is expressed to Dr. C. T. Liu at the Oak Ridge National Laboratory for his assistance with solution treatment and chemical analysis.

The author would like to express his appreciation to the ladies of the departmental office: Ms. Sancy Hail, Ms. Betty Frazier, Ms. Phyllis Davis, Ms. Inez McDonald, Ms. Phyllis Klindt, and Ms. Sue Turner for their goodwill, support, and help with official matters.

The author would like to thank his fellow graduate students for their friendship and support, and for providing a congenial work atmosphere.

ABSTRACT

In the compilations in the literature of the Ni-Ta phase diagram, extensive solubility of Ta in Ni is shown, with the intermetallic compound Ni_3Ta forming upon exceeding the solubility. Also the compounds Ni_2Ta, $NiTa_2$, NiTa and Ni_3Ta are reported to be stable in this system. However, examination of the literature reveals contradictions in the phase relations in the region from 0 to 15 at.% Ta. For example, a Ni_8Ta compound has been reported to be stable in this range. For the binary Ni-rich Ni-Ta alloys, aging studies in this composition range have not revealed any significant hardening. However, the addition of Cr, Al, and Fe to these alloys produces considerable precipitation and hardening upon aging. In order to examine in more detail the phase relations and precipitation in the Ni-rich region, aging studies were conducted on a Ni-10 at.% Ta alloy and on a Ni-9.6 at.% Ta-16.6 at.% Cr alloy.

The ingots of both alloys were made in an arc melting furnace. For each alloy, after several ingots were made, they were then remelted together into a larger ingot in a Balzers induction furnace. These Ni-Ta and Ni-Ta-Cr ingots were heat treated at 1250°C for one week, then water quenched. The Ni-Ta ingot was reduced in diameter by several swaging and annealing steps; the Ni-Ta-Cr alloy was too brittle to be cold worked. The Ni-Ta-Cr alloy was reheated

to 1280°C for 4 hrs in order to dissolve one of the two second phases present in the matrix after the first solution heat treatment. Both solution treated alloys were aged from 600°C to 1000°C for times up to 1000 hrs. The microstructures were characterized using X-ray diffractometry, optical microscopy, scanning and transmission electron microscopy, and microhardness measurements were made.

The microstructure of the Ni-Ta alloy was single phase in the solution treated condition, and remained so during aging. The initial hardness for the cold worked material was about 355 DPH; it remained at about this value during aging at 600°C, but decreased to about 200 DPH upon recrystallization during aging at the higher temperatures. The X-ray diffractometer traces did not show any Ni_8Ta structure present after aging from 600°C to 1000°C for times up to 1000 hrs. Only an FCC structure was detected, which indicates that this Ni-Ta alloy is a Ni-rich solid solution (γ phase). However, the electron diffraction patterns showed that this alloy sometimes contained small amounts of Ni_2Ta and DO_{22} structure which were not detected by the X-ray diffractometry. The Ni_8Ta structure was not observed in the present work, which is contradictory to the work of Nash and West published in 1983, but is consistent with the phase diagram revised by Moffatt, where the Ni_8Ta compound was reported to be present only below 570°C at around 10 at.%

Ta. It is very difficult to modify the partial phase diagram for the Ni-Ta system at 0 to 15 at.% Ta to give agreement simultaneously with the results of several previous articles and the present work. Ni-Ta alloys in this compositions range need to be examined in more detail by TEM.

The Ni-Ta-Cr alloy in the first solution treated condition (1250^{o}C for 7 days, then water quenched) contained about 15% of two phases, but contained 10% of only one phase (plate-like particles) after the second solution treatment (1280^{o}C for 4 hrs, then water quenched). The hardness was 335 DPH after the first solution treatment, and increased to 530 DPH upon reheating to 1280^{o}C for 4 hrs. It remained approximately the same during aging at 600^{o}C, but decreased to about 330 DPH when aging from 700^{o}C to 1000^{o}C for times up to 1000 hrs. The matrix decomposed by a complex process, which included high angle boundary migration and formation of transformation products from the second phase and the matrix. The matrix of the ternary alloy was taken to be FCC structure by X-ray diffractometry. The structure of the second phase (plate-like particles) was taken to be BCT Ni_3Ta by comparing the experimentally observed X-ray diffractometer traces with those listed in the ASTM X-ray data file. Although the microstructure of the first solution treated condition showed what looked like two phases present in the matrix, its diffractometer trace was similar to that

of the second solution treated condition which contained apparently only one second phase. Thus, these two second phases may have the same structure.

The X-ray diffractometer traces of the transformation product which formed on aging were compared with the reference data listed in the ASTM file. Examination of the ASTM data revealed that some of the listed d-spacings and relative intensity are questionable. The X-ray diffractometer traces of alloys containing the transformation product did not agree exactly with any of those of the ASTM files for the binary Ni-Ta compounds. The transformation products could consist of orthorhombic and/or monoclinic Ni_3Ta. However, based on the similarity of the microstructures to that of one in the literature which contained orthorhombic Ni_3Ta, only this compound may be present. Thus, the transformation after aging from 700°C to 1000°C can be written as γ (90% of structure) + BCT Ni_3Ta (10% of structure) $\longrightarrow$ γ (5%) + BCT Ni_3Ta (10%) + orthorhombic Ni_3Ta (85%).

For the Ni-Ta-Cr alloy, EDS analysis was done to examine the chemical content of different areas. It is concluded that the structure of the second phase (plate-like particles) present in the solution treated condition and after aging is $Ni_3(Ta_{0.79}\ Cr_{0.21})$.

The effect of Cr on the lattice parameter of Ni_3Ta is to decrease the mismatch in parameter if substituting for

Ta. The reduction in the lattice mismatch due to the presence of Cr in the Ni-Ta-Cr alloy is an important factor in aiding precipitation. The addition of Cr to the binary alloy increases the microhardness considerably which is an important consideration in developing high strength Ni-Ta alloys.

TABLE OF CONTENTS

CHAPTER PAGE

LIST OF TABLES

Table PAGE

TABLE PAGE

FIGURE PAGE

FIGURE PAGE

FIGURE PAGE

FIGURE PAGE

FIGURE PAGE

FIGURE PAGE

FIGURE PAGE

FIGURE PAGE

CHAPTER 1

INTRODUCTION

There are three important methods by which the resistance to plastic deformation of a metal may be increased, namely by cold working, by solid solution strengthening and by precipitation hardening. Many modern high strength alloys depend on the use of one or more of these effects.

The principle of precipitation hardening is reviewed as follows. At high temperature, an alloy will exist as a homogeneous solid solution. If, after solution heat treatment, the alloy is then rapidly cooled to room temperature by quenching into water or other fluid, the separation of a second phase is suppressed, and an unstable supersaturated solid solution is produced. Merica et al. (1) suggested that hardening resulted from precipitation of the second phase taking place when the quenched alloy was aged for a sufficient time, and that the precipitate was in the form of a fine submicroscopic dispersion. The strengthening reaches a maximum value at an average particle size denoted by the term critical dispersion. Within a given amount of precipitate, larger particles would have less strengthening effect.

In the Ni-Ta system, there is a marked change in solubility of Ta with temperature, the precipitating phase

being Ni_3Ta. This phase is body-centered tetragonal Al_3Ti type (2) at temperatures above 1593 K and at lower temperatures has been reported to be orthorhombic structure of the βCu_3Ti type (3) or monoclinic $\beta NbPt_3$ type (4) In addition to Ni_3Ta, the compounds NiTa, $NiTa_2$, Ni_2Ta, and Ni_8Ta are present in the Ni-Ta system, and will be described in more detail later. It is expected that aging of supersaturated, nickel-rich solid solution compositions would lead to the precipitation of substantial amounts of Ni_3Ta, but it has been found that the rate of precipitation is quite low. However, this rate can be accelerated considerably by the addition of some other elements, e.g., Cr (5).

In the Ni-rich Ni-Ta alloys, hardening occurs by the precipitation of metastable phases, denoted r' and r" (to be described later), by employing small addition of iron and aluminum. Some nickel-base alloys can be strengthened by the precipitation of Ni_3X, where X is Al in the prototype structure. A few commercial nickel-base alloys, an example of which is Inconel 718 (but which does not contain Ta), are strengthened by the DO_{22}, r' phase. The r" phase is an ordered, fully coherent, phase with an ideal stoichiometry of Ni_3X, where X may be Ta or Nb. This phase has never been observed to form in the binary Ni-Ta alloy, but it does form as a metastable phase in some other nickel-base alloys, e.g., Ni-Ta-Fe (6).

In the Ni-Ta equilibrium phase diagram, some contradiction exists in the region around 10 at.% Ta according to several published articles. The structure and phases are still not well defined in the Ni-rich region from 0 to 15 at% Ta.

The purpose of the research reported in this thesis was to determine the phase relations and structural development upon aging (up to 1000 hours) from 600°C to 1000°C a Ni-10 at.% Ta alloy and a Ni-9.6 at.% Ta-16.6 at.% Cr alloy.

CHAPTER 2

LITERATURE REVIEW

PHASE DIAGRAM

Kornilov and Pylaeva (7) have determined the partial diagram (25~100 at. % Ta) from metallographic, X-ray and thermal analysis of alloys prepared from 99.8% pure Ta and high-purity Ni. These data are incorporated with the 0~25 at. % Ta equilibria that was recommended by Hansen (8) and are shown in Figure 1 (9). The diagram is characterized by three peritectically formed, intermetallic phases -Ni_2Ta, NiTa, $NiTa_2$-and the congruently melting compound Ni_3Ta.

According to the Metals Handbook (10), the crystal structure data of Ni-Ta systems are shown in Table 1.

The maximum solubility of Ta in Ni is 15.4 at. % at 1360°C, at which temperature there is an eutectic reaction producing γ and Ni_3Ta (7).

β-Ni_3Ta melts congruently at 1813 K (1540°C) (11), stable above 1593 K (1320°C), and is body-centered tetragonal of the Al_3Ti type (space group I 4/mmm) with a = 3.527 Å and c = 7.455 Å (2). The structure β', stable below 1593 K (1320°C), has been found to be orthorhombic of the Cu_3Ti type (3,4) (space group p /mmm), the lattice parameters of which have been reported as a = 5.114 Å, b = 4.25 Å, c = 4.542 Å (4), or a = 5.10 Å, b = 4.24 Å, c = 4.52 Å (3).

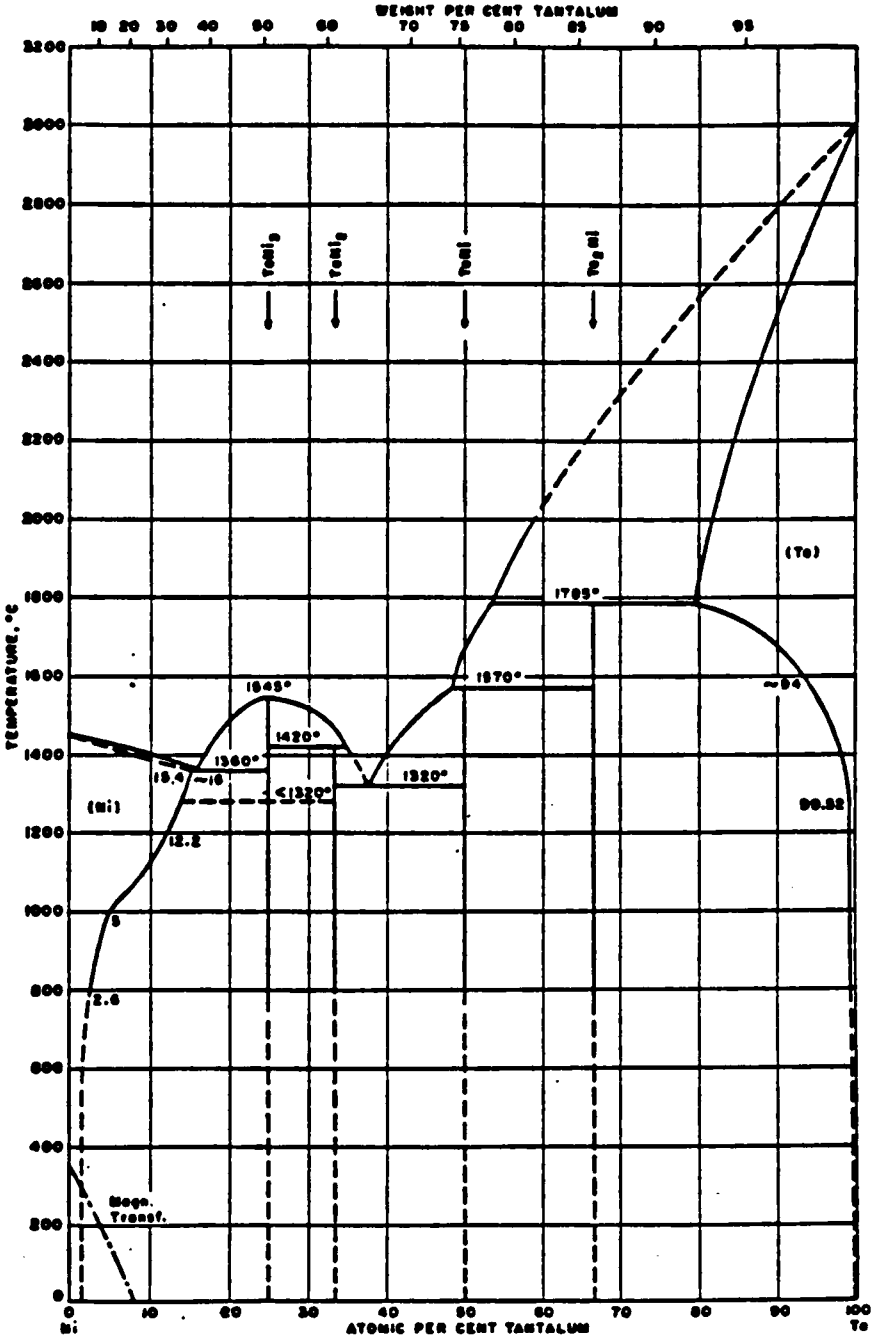

Figure 1. The Ni-Ta phase diagram containing the intermetallic phases NiTa, Ni_2Ta, $NiTa_2$, and Ni_3Ta (9).

Table 1. The crystal structure of Ni-Ta compounds (10).

Phase	Formula	Symmetry	Prototype
β	Ni_3Ta	body-centered tetragonal	Al_3Ti
β'	Ni_3Ta	orthorhombic	Cu_3Ti
β'	Ni_3Ta	monoclinic	$CuPt_3$ (β $NbPt_3$)
γ	Ni_2Ta	body-centered tetragonal	$MoSi_2$
-	Ni_8Ta	face-centered tetragonal	Ni_8Nb

Giessen and Grant (12) found another structural form which was determined as being of the monoclinic $\beta NbPt_3$ type (space group $p\ 2_1/m$) with a = 5.126 Å, b = 4.523 Å, c = 25.37 Å, α=90°50'. It was concluded that this is the stable form of Ni_3Ta, at least for temperatures higher than 1158 K (885°C).

Shunk (9) shows Ni_2Ta melting congruently at 1693 K (1420°C) (Figure 1). The structure of Ni_2Ta is body-centered tetragonal, $MoSi_2$ type (13) (space group $I\ 4/mmm$) with a = 3.154 Å, c = 7.905 Å (13) or a = 3.157 Å, c = 7.919 Å (14).

In the Metals Handbook (15), the Ni-Ta phase diagram clearly indicates the compositions of β, β', γ, δ, and ϵ phases (Figure 2).

Another compound Ni_8Ta has been reported to be stable up to 1573 K (1300°C) and to accommodate a range of stoichiometry of between 2~4 at. % Ta (16). Larson et al. (17) did not find this Ni_8Ta phase after quenching from 1473 K. However, they determined an order-disorder temperature for the formation of Ni_8Ta as 843 K (570°C), and found the crystal structure of Ni_8Ta to be face-centered tetragonal.

Nash and West (16) found that an alloy with 80 at. % Ni-15 at. % Ta-5 at. % Al was three-phase $Ni_8Ta + \delta + \eta$ at 1523 K and at 1273 K, thus confirming the existence of the binary compound. Ni_8Ta phase is not an equilibrium phase reported in the Ni-Ta equilibrium phase diagram of Fig. 1. No previous aging studies have been reported in the

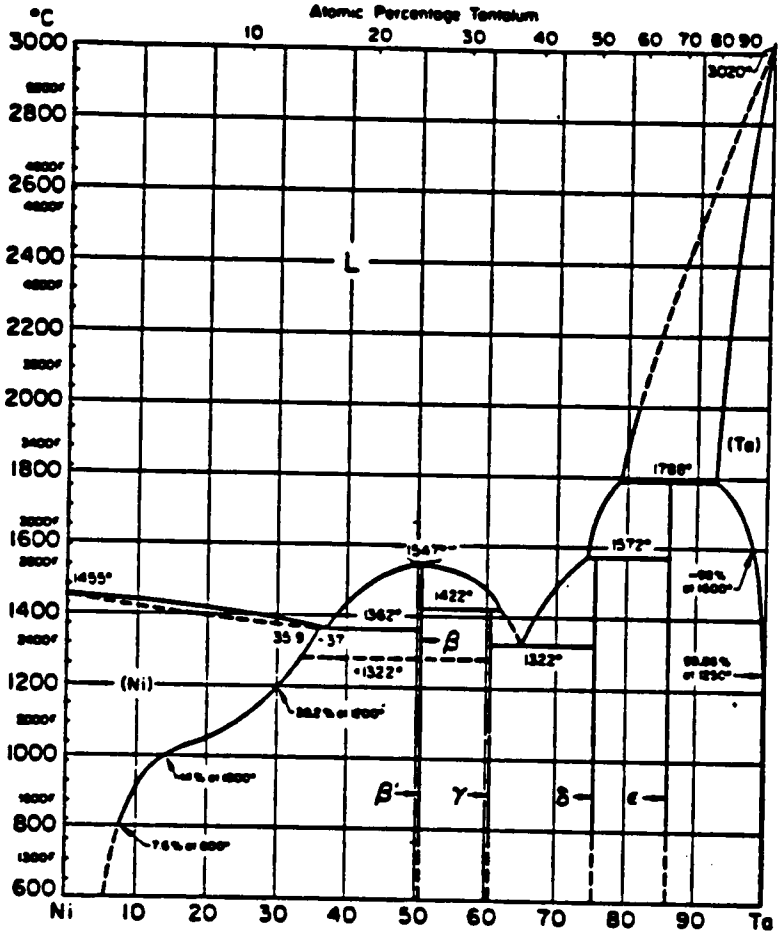

Figure 2. The Ni-Ta phase diagram. It shows the NiTa (δ), Ni_2Ta (γ), $NiTa_2$ (ϵ), and Ni_3Ta (β-β') compounds (15).

temperature range over which the ordered phase has been observed to form (17).

The data of Pimenov et al. (18) indicate that Ni_8Ta is an incongruently melting compound and from these data it seems probable that it forms by a peritectoid reaction $\delta + \gamma \rightarrow Ni_8Ta$ between 1537 K (1264°C) and 1613 K (1340°C) (16).

Larson, Taggart and Polonis (17) concluded the following:

(a) The phase Ni_8Ta is isomorphic with the fct Ni_8Nb structure and forms by a nucleation and growth reaction from supersaturated primary solid solutions of nickel and tantalum. Ni_8Ta first appears as spheres which eventually grow into cuboids elongated in the z direction. The cube faces of the precipitates are parallel to the {001} planes of the Ni-Ta matrix.

(b) The transformation of the fcc Ni-Ta matrix to fct Ni_8Ta is a type of order-disorder reaction with the critical temperature at 843 K. The fct Ni_8Ta unit cell is contracted slightly relative to the fcc Ni-Ta unit cell. The fct Ni_8Ta lattice parameters are $a = b = 10.754$ Å, and the $3c/a$ ratio is greater than 1.0.

(c) The Ni_8Ta phase can be nucleated only after quenching very rapidly from the solution temperature range and then aging in the temperature range from 623 K to 823 K. The quench rate sensitivity is a strong indication that

nucleation of the Ni_8Ta requires a supersaturation of lattice vacancies.

The lattice parameter value determined for the fcc structure of the disordered Ni-11.1 at. % Ta matrix was a = 3.589 Å. The corresponding parameter of the fct unit cell was a'= 10.754 Å for Ni_8Ta. The lattice parameter of the fct cell was determined from a Debye-Scherrer pattern for a Ni-11.1 at.% Ta alloy which had a domain size of approximately 1000 Å (17).

The Bravais lattice for the Ni_8Ta is body-centered tetragonal; however, since the Ni_8Ta phase precipitates coherently on the Ni-Ta matrix, it is much more convenient to describe the Ni_8Ta phase as a face-centered tetragonal structure (17).

For the Ni_8Ta superlattice, the Miller indices of the fct structure are designated h', k', l'. Then, h' = 3 h, k' = 3k, l' = l (17).

Figure 3 is a partial Ni-Ta equilibrium phase diagram at high temperature showing the existence of Ni_8Ta (18).

Thermal effects observed by Therkelsen (19) in the solid state, especially at 1623 K (1350°C), could be due to a transformation in the Ni_3Ta phase or to the peritectoid formation of an additional compound with a composition between NiTa and Ni_2Ta_3. A transformation in the Ni_3Ta phase below the eutectic temperature involving Ni_3Ta and Ni_2Ta_3 is mentioned by Therkelsen (19), and a transformation of the

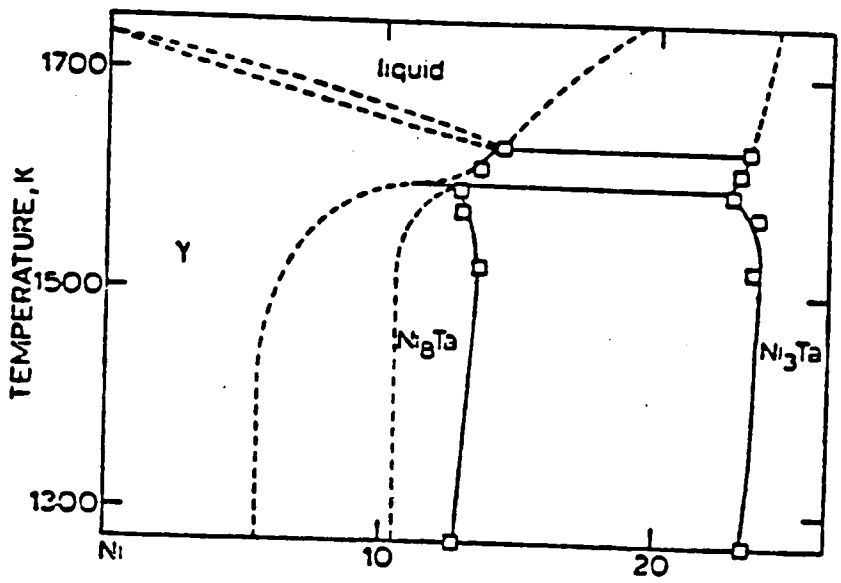

Figure 3. Part of Ni-Ta equilibrium phase diagram incorporating electron microprobe analysis data obtained from a Ni-20 at.%Ta alloy (18).

Ni_3Ta phase at 1350°C was reported by Wallbaum (20), but denied by Kubaschewski and Speidel (11).

The lattice parameter of Ni-rich Ni-Ta binary alloy vs. 0 to 25 at.% Ta is shown in Figure 4a (21). In Figure 4b, the lattice parameters of Ni-rich phase in Ni-Ta-Cr alloys are plotted against atomic percentage of Ni; an expansion of the FCC nickel lattice up to 30 at.-% (Ta+Cr) is shown, but the respective at. % of Ta and Cr are not given in Kubaschewski and Speidel's paper (11).

CRYSTAL STRUCTURE

The crystal structure of Ni_3Ta is shown in Figure 5. Its structural type is reported in the Metals Handbook as DO_{22} (8).

As mentioned above, Ni_2Ta has the structure of $MoSi_2$ type. The crystal structures of $MoSi_2$ is shown in Figure 6 (22).

The FCT unit cell of Ni_8Ta and its corresponding reciprocal lattice are illustrated in Figure 7 (17).

Figure 8a (23) shows the reciprocal space for Ni_8Nb alloy (which is similar to Ni_8Ta alloy) containing the precipitated compound, extended over the volume occupied by one reciprocal lattice unit cell of the parent matrix (as determined by electron diffraction). Figure 8b is the proposed unit cell for the Ni_8Nb compound which is identical to that of Ni_8Ta (Figure 7). The dark spheres represent niobium atoms, the light ones nickel atoms (23).

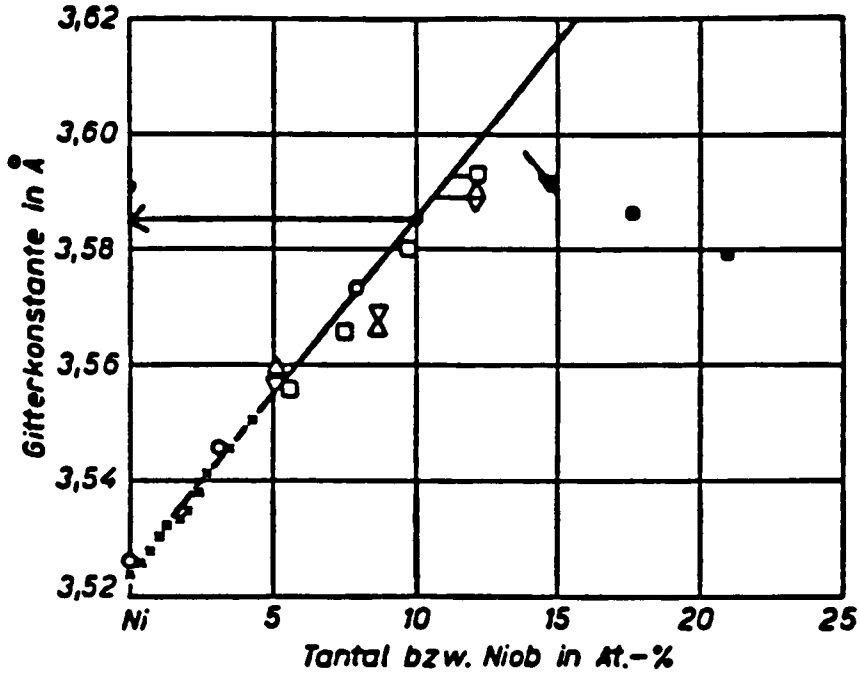

4a. Lattice parameter of the FCC structures Ni-rich Ni-Ta alloys vs. at.% Ta (21).

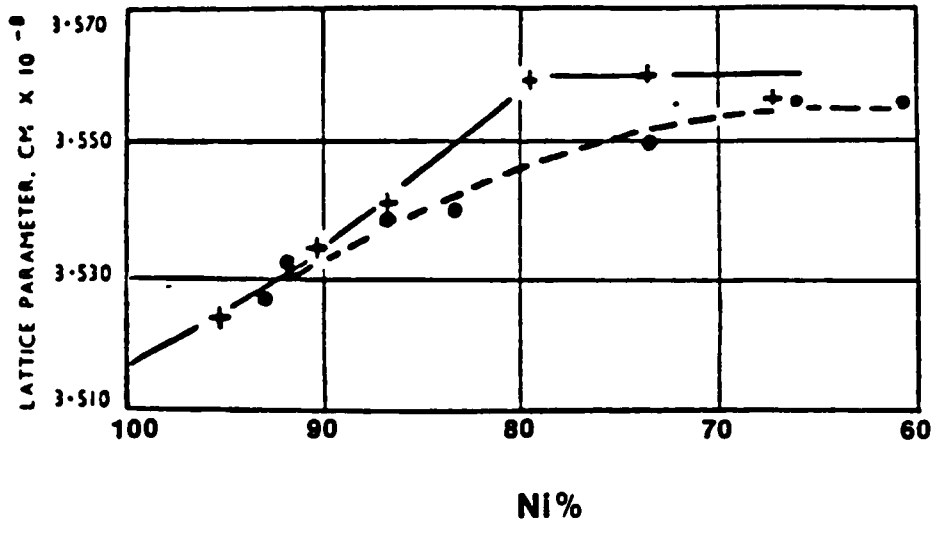

4b. Lattice parameter of the FCC structures of alloys in the Ni-rich corner of the Ni-Ta-Cr system (11).

Figure 4. Lattice parameter of the Ni-Ta and the Ni-Ta-Cr alloy.

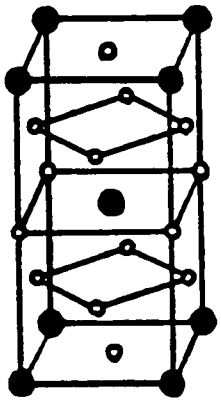

● — Ta

o — Ni

Figure 5. The crystal structure of Ni_3Ta (DO_{22} phase) (10).

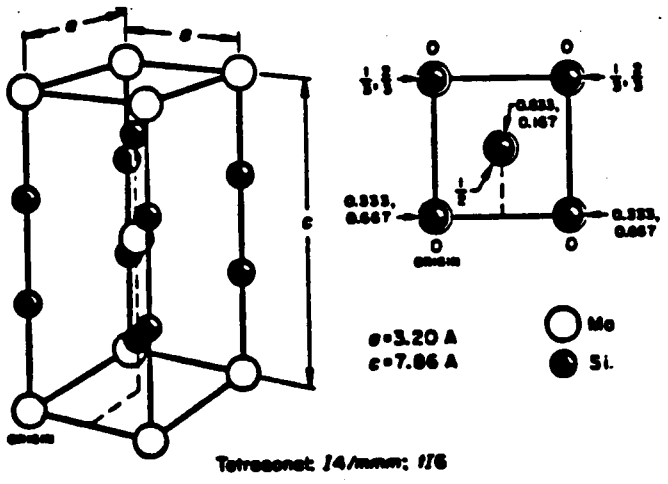

Figure 6. The crystal structure of $MoSi_2$ (Ni_2Ta) (22).

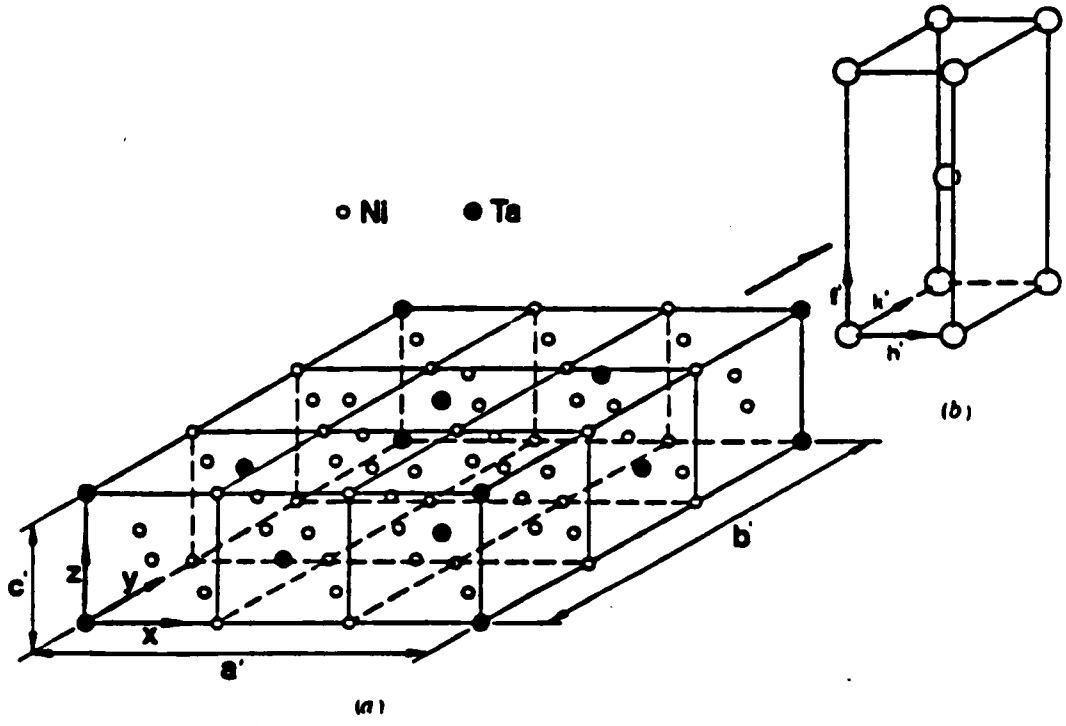

(a) The FCT Ni_8Ta unit cell.
(b) The reciprocal lattice of the FCT Ni_8Ta structure (17).

Figure 7. The reciprocal lattice and the unit cell of the FCC Ni_8Ta.

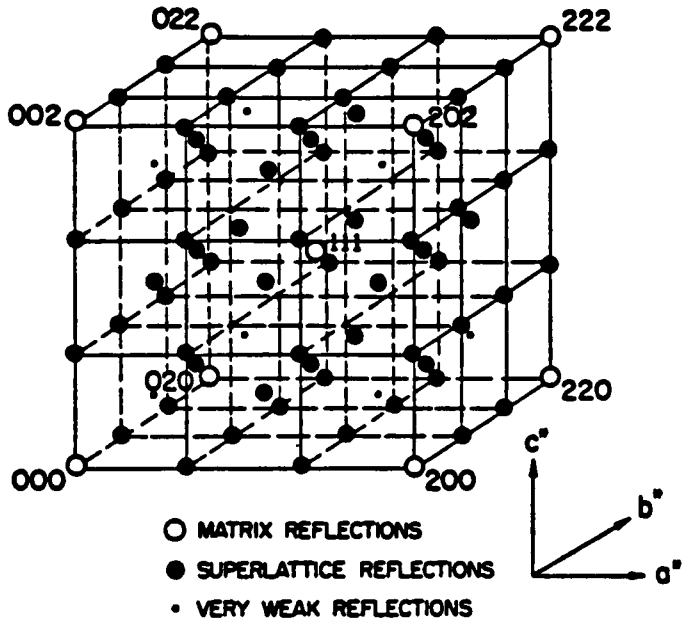

8a. The reciprocal space of Ni_8Nb and FCC matrix (23).

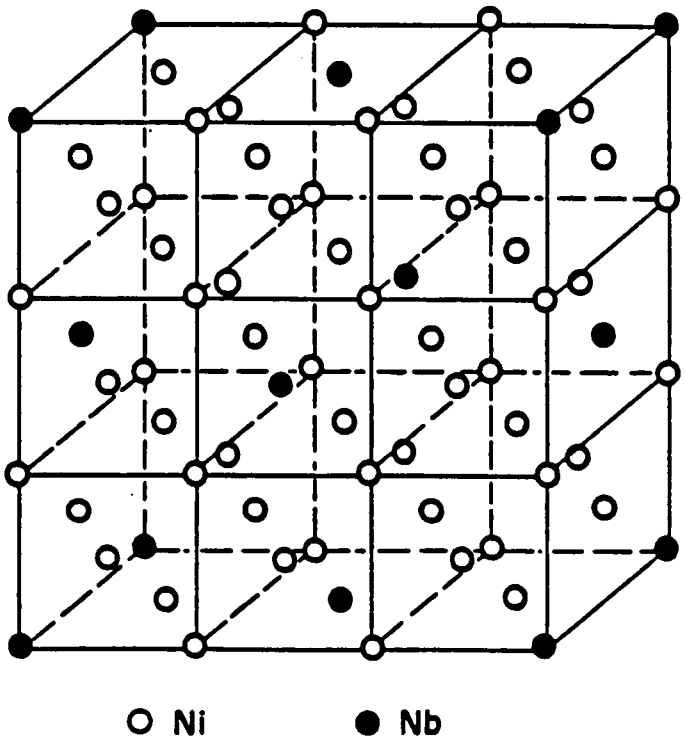

8b. The unit cell for the Ni_8Nb (Ni_8Ta) compounds (23).

Figure 8. The reciprocal space and unit cell for the Ni_8Nb compounds.

Ni_3Ta has been reported to exist as three different kinds of crystal structures : (a) β-Ni_3Ta, tetragonal with Al_3Ti type of which the space group is I4/mmm and the structure type is listed as DO_{22} in the Metals Handbook (10), (b) β'-Ni_3Ta, orthorhombic, Cu_7Ti_2 type listed in the Metals Handbook (24). This formula is questionable; Hansen (8,10) called it Cu_3Ti type, (c) monoclinic with $\beta NbPt_3$ type (12, 24), the space group of which is p 2_1 /m.

ORDER-DISORDER STRUCTURE OF NI_8TA

In Ni-base alloys at the composition Ni_8X, where "X" may be combinations of V, Nb, and Ta, the ordering reactions have been investigated by employing electrical resistivity and electron diffraction techniques. Recent investigations of phase transformations in alloys of nickel with two of the elements in group V of the periodic table have led to the discovery of the ordered phase Ni_8Ta (17). The Ni-rich portion of the binary phase diagrams for Ni with Ta, Nb, and V, as presented by Pearson (25), exhibits several similarities.

Rudman (26) has considered the effects of the atomic size factor upon the existence of ordered phases. His arguments show that in alloys containing atomic species of different size it is not possible to account for the existence of ordered phases on the basis of size effects alone; furthermore, a negative enthalpy of mixing is required if the ordered phases are to exist. The atomic size will determine the "visibility" of the phase, so that

systems with large atomic size differences are expected to exhibit ordered phases that are stable up to high temperatures and extend over a wide range of composition. The atomic diameters of V, Ta, and Nb are markedly different from that of Ni, and these elements exhibit similar alloying behavior when combined with nickel (25). Under these conditions an order-disorder reaction might occur in ternary nickel-base alloys of the type Ni_8X where X is a combination of V with either Ta or Nb.

The electron diffraction patterns in Figure 9 are identical to those reported for ordered phases of the type Ni_8X in the Ni-Ta system (27) The unit cell of the Ni_8X structure can be described as fct comprising three multiples of the fcc lattice in the a and b dimension and one unit cell in the c direction (see Fig. 7).-Three variations of orientation of the ordered phase form in the fcc matrix, with the following crystallographic relationship :

$(001)Ni_8X // \{001\}fcc : [100]Ni_8X // \langle 100\rangle fcc$

It has been shown (17) that the formation of Ni_8Nb and Ni_8Ta upon aging is sensitive to the quench-rate from the solution anneal temperature and that a rapid quench is essential for measurable rates of ordering in these alloys.

Figure 10 (27) shows composition dependence of the order-disorder critical temperature for the Ni_8X phase. The ordering energy for the Ni_8V composition is expected to be lower than that of the Ni_8Ta composition because of the smaller size difference between the Ni and V atoms, only

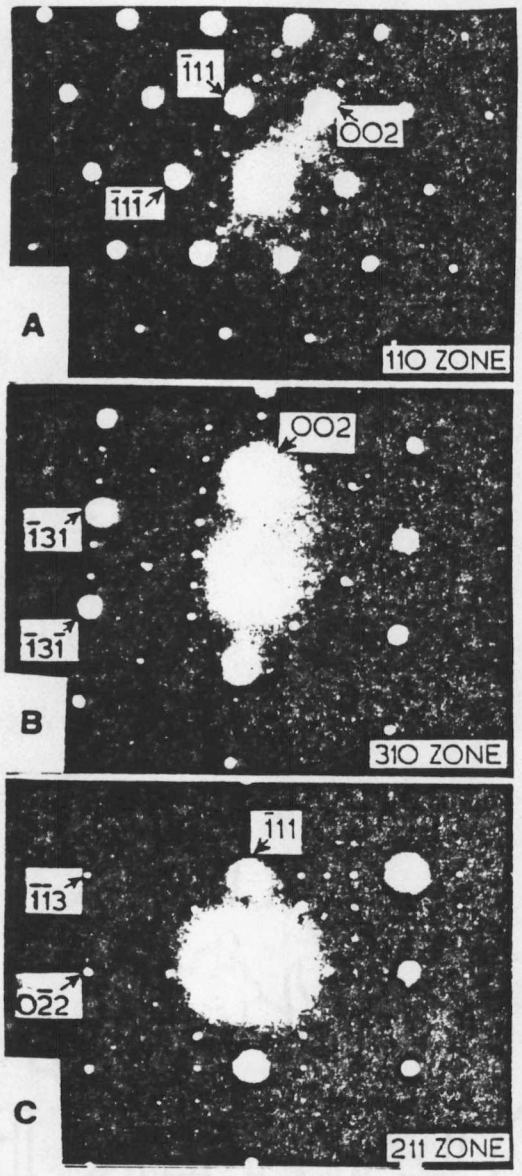

Figure 9. Electron diffraction patterns of aged Ni_8V alloys. These patterns are identical to those reported for ordered phases of the Ni_8X type in the Ni-Ta systems (27).

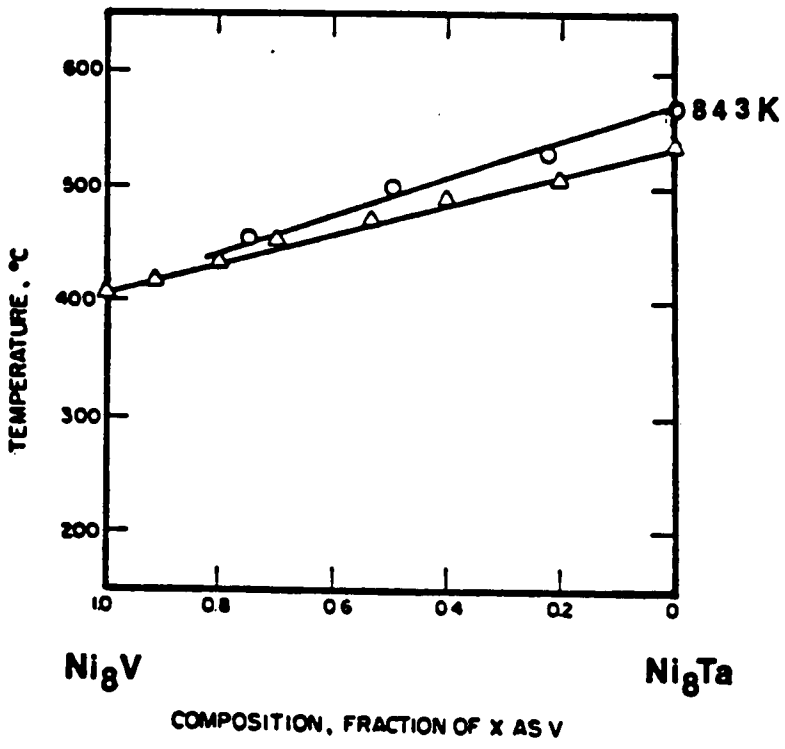

Figure 10. Composition dependence of the order-disorder critical temperature for Ni_8X phases (27).

0.09 Å, compared to a difference of 0.18 Å between Ni and Ta. The atomic radii of the atoms as given by Pearson are Ni = 1.24 Å and Ta = 1.42 Å. These values lead to a misfit of Ta in Ni of 0.18 Å. We get a critical temperature for Ni_8Ta of 843 K (570°C) from Figure 10.

We can also get some information about Ni_8Ta from a similar structure Ni_8Mo. Mayer and Urban (28) reported a new ordered Ni_8Mo phase in a Ni-11.1 % at Mo alloy of which the chemical composition was close to that of my Ni-Ta alloy. They (28) explained these results on the basis of radiation-enhanced ordering and argued that ordered Ni_8Mo was an equilibrium phase. The atomic arrangement on the (001) fcc plane is shown in Figure 11, where the large circles represent Mo atoms, the small ones nickel and the shaded circles atoms at the c/2 level. The structure can be further described, in a manner similar to DO_{22} and Ni_2Mo, by the successive stacking of nickel and Mo atoms on {420} fcc planes.

The electron diffraction pattern is characterized by superlattice spots at the 1/3{420} and 1/3{200} positions, shown in Figure 12. It should be noted that in Figure 12 the 1/3{420} is also the position for Ni_2Mo reflections.

Larson et al. (17) showed electron diffraction patterns of the Ni_8Ta structure in their paper published in 1970. Their specimens were heat treated at 1270°C for 15 min in a purified helium atmosphere and quenched in a 10 pct NaOH aqueous solution at room temperature. The specimens were

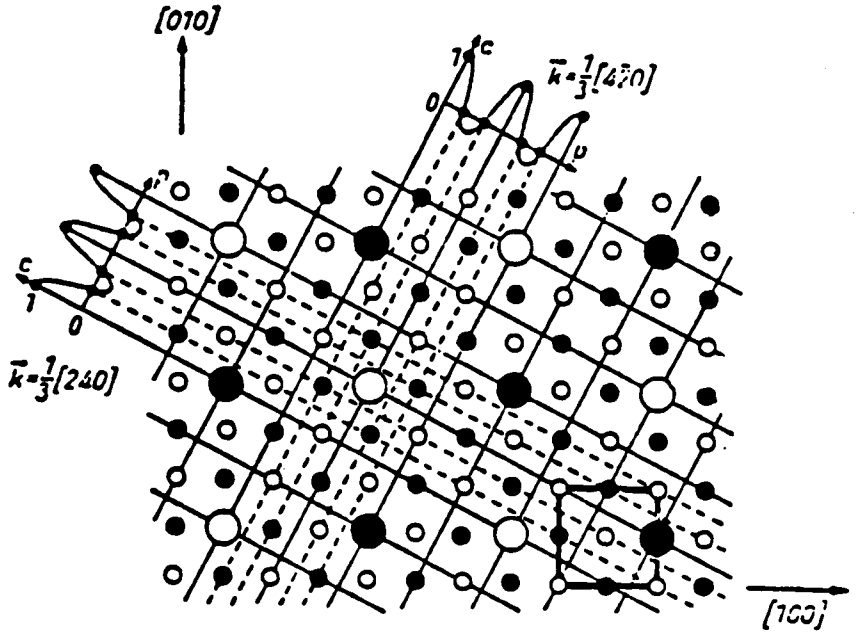

Figure 11. Atomic arrangement in the (001) plane of Ni_8Mo (Ni_8Ta); small circles denote Ni atoms, large circles Mo and dark circles atoms at c/2; the FCC unit cell is shown at right corner (28).

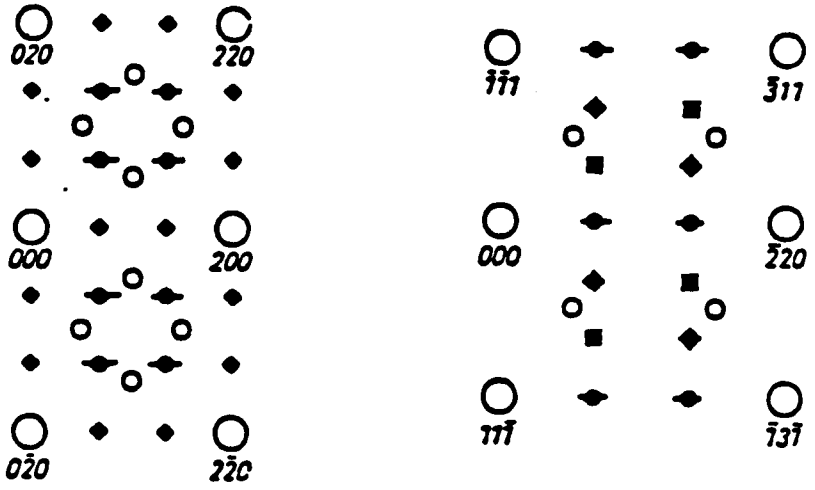

(001) (112)

Figure 12. (001) and (112) reciprocal lattice sections. Large and small open circles respectively denote fundamental and SRO spots; filled circles and squares denote respectively 1/3{420} and 1/3{200} Ni_8Mo spots. Three variants of 1/3{420} spots are shown : [100] by dash, [010] by vertical dash, and [001] by inclined cross (28).

then aged at temperatures in the range of 400°C and 600°C (which were lower than the present work) for times up to 3500 hours (longer than mine). Figure 13 is electron diffraction patterns of the Ni_8Ta structure showing <011>fcc zone, <013>fcc zone, and <001>fcc zone (17). They also gave the X-ray 2θ values for Ni_8Ta, but the relative intensity was not available in their paper. The lattice parameter measurements obtained from their X-ray diffraction data indicated that the ordered Ni_8Ta precipitate contracts relative to the disordered stoichiometric Ni_8Ta matrix (FCC). A stoichiometric Ni_8Ta alloy was quenched from 1325°C and aged for 3500 hr at 550°C, resulting in the formation of domains of Ni_8Ta that were 10,000 Å in size. At this point the Ni-Ta matrix was completely transformed. Also none of the reported equilibrium Ni_3Ta phase was detected by Larson et al. (17). Neither Ni_8Ta nor Ni_3Ta was detected in the same alloy which has been quenched and aged at 650°C for 2 hr and then lowered to 500°C for 600 hr. The above observations presented a good case for the existence of Ni_8Ta as a thermodynamically stable phase below the 570°C critical temperature. However, their study did not rule out the formation of Ni_3Ta after several thousand hours at an appropriate aging temperature.

The results of the microprobe analyses on the Ni-Ta alloy done by Nash and West in 1983 (16) are shown in Fig. 3. Their work confirmed the existence of the Ni_8Ta up to 1593 K (1320°C) at around 10~13 at.% Ta. The peritectoid

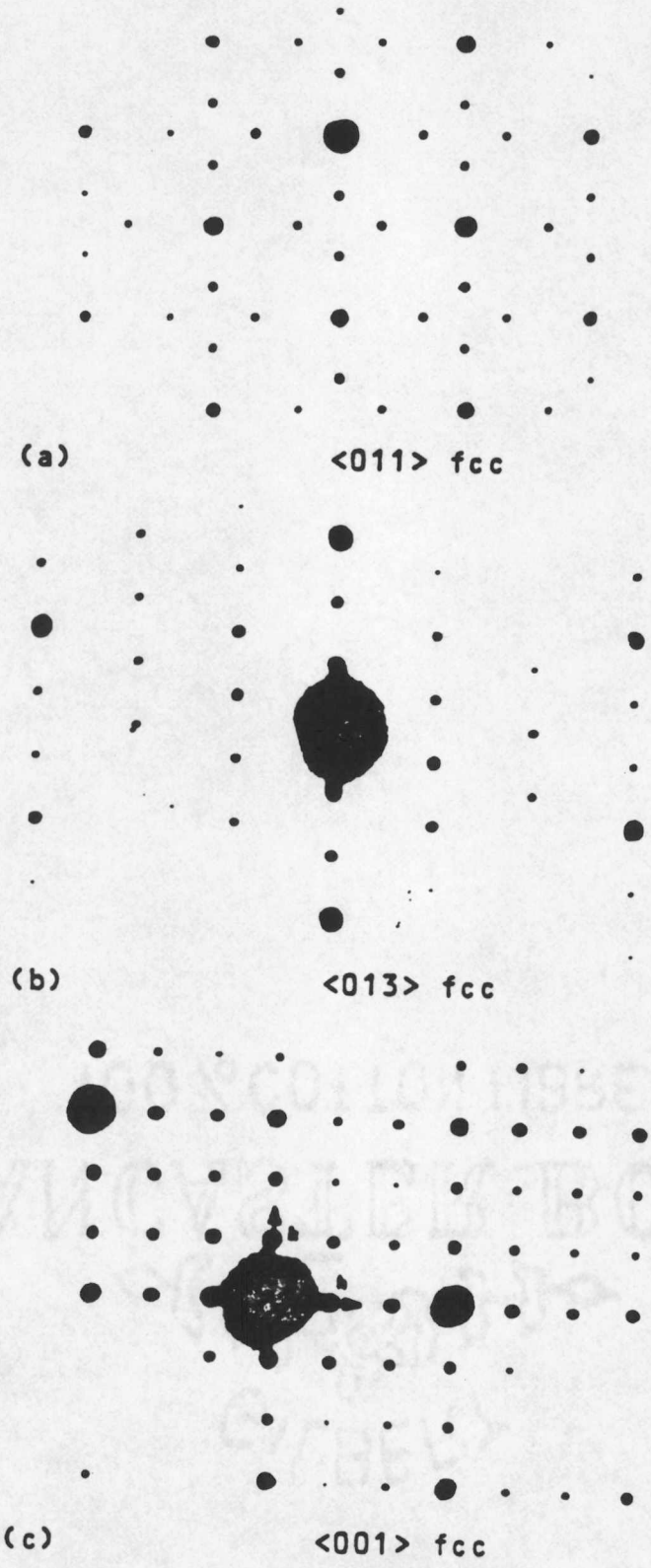

Figure 13. Electron diffraction patterns of the Ni_8Ta structure showing <011>fcc, <013>fcc, and <001>fcc zone axes (17).

temperature was found to lie between 1593 and 1613 K by them which indicates that Ni_8Ta is an ordered, stable, equilibrium phase at 10 at.% Ta for temperature above 843 K to 1593 K. There is an evident contradiction by comparing the result of Nash and West to that of Larson et al. (17). The partial equilibrium phase diagram of Ni-Ta alloy at Ta < 15 at.% is not well established. The structure reported in several articles at this region is not consistent with each other.

PRECIPITATION PROCESS

The precipitation of intermetallic phases from a supersaturated solid solution occurs by a nucleation and growth process. First, it is necessary to form the beginning of the second phase crystals, a process called nucleation. Following nucleation, the precipitate particles grow in size by diffusion; this is called growth. No precipitation can occur until nucleation begins. Nucleation may occur simultaneously with the growth of particles previously formed.

The rate at which precipitation occurs varies with temperature (Figure 14) (29). At very low temperatures, long times are required to complete the precipitation because the diffusion rate is very low. The rate of the reaction is controlled by the rate at which atoms can migrate. The rate of precipitation is also very low at temperatures just below the solvus line. In this case, the solution is only slightly oversaturated and the free energy decrease resulting from

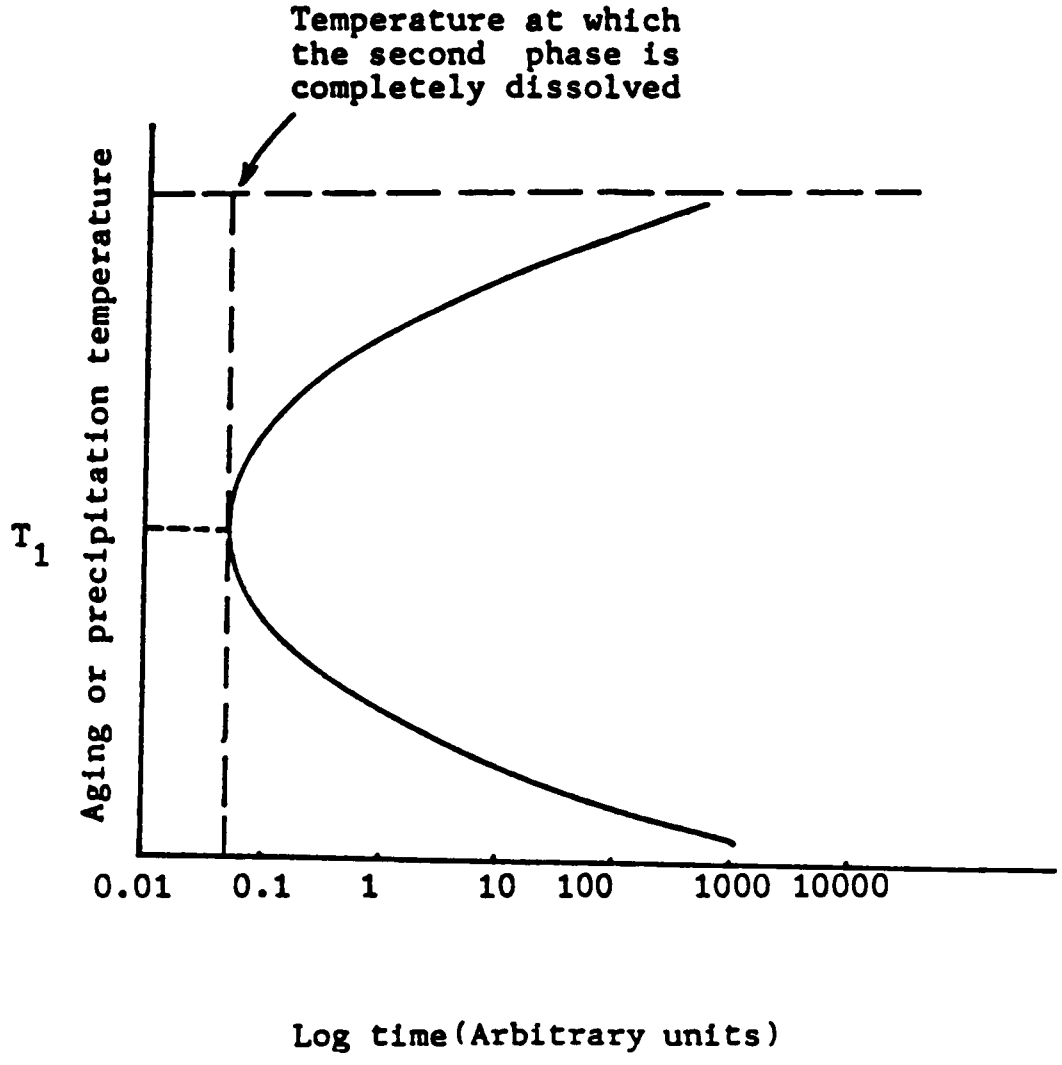

Figure 14. Schematic representation of the time for the beginning of the precipitation in a supersaturated alloy (29).

precipitation is very small. Nucleation is, accordingly, slow.

At intermediate temperatures T_1, the precipitation rate is a maximum, so that the time to complete the precipitation is a minimum. In this range, the combination of moderate diffusion and high nucleation rate make precipitation most rapid.

In the binary Ni-Ta alloy, the aging of supersaturated solid solutions of appropriate compositions leads to the precipitation of Ni_3Ta. Quist, Taggart and Polonis (30) found great difficulty in achieving nucleation of Ni_3Ta in the Ni-Ta system. It appeared, therefore, that the nucleation energy for Ni_3Ta precipitation was very high, probably due to poor lattice matching and because the diffusion rate of Ta is low. The low diffusivity was illustrated by the fact that even when grain boundary nucleation had occurred discontinuous precipitation proceeded very slowly.

The aging of a supersaturated solid solution in a Ni-25% Ta-10% Cr alloy causes copious matrix precipitation of a body-centered tetragonal Ni_3Ta phase and a considerable strengthening effect (31). It is proposed (31) that the effect of Cr may be attributable to a reduction in the matrix/precipitate lattice mismatch

MECHANICAL PROPERTIES

As we know, an important effect of the precipitation of the second phase is that the alloy is hardened. Figure 15

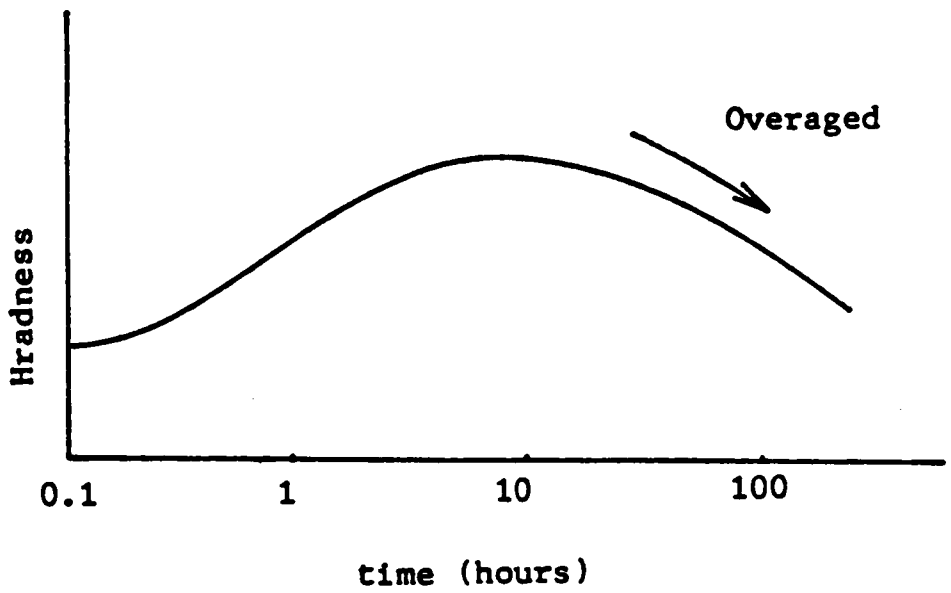

Figure 15. Schematic illustration of the change in hardness during aging (29).

shows a typical hardening curve. The most important feature of this curve is the maximum it possesses. Holding, or aging, the specimens for too long at a given temperature causes them to lose their hardness. This effect is known as overaging.

We know that the shape of the aging curve is primarily a function of two variables : (a) the temperature at which aging occurs, and (b) the composition of the alloy. Figure 16 shows the effect of temperature on the aging curve during precipitation hardening. We have three different temperatures in this figure where $T_3 > T_2 > T_1$.

The curve marked T_1 in Figure 16 represents aging at too low a temperature. In this case, atomic motion is so slow that no appreciable precipitation occurs and hardening occurs slowly. Temperature T_2 corresponds to an optimum temperature, a temperature at which maximum hardening occurs within a reasonable length of time. At T_3, hardening occurs quickly due to rapid diffusion, but softening effects are accelerated also, causing a lower hardness.

The changes in properties, such as hardness and electrical resistivity, are induced by the various phenomena of precipitation. With regard to electrical resistivity, the orderly motion of electrons through a crystal, which constitutes an electric current, is badly disturbed when an extremely small and uniformly distributed precipitate, such as G. P. zones, is present. Thus, when precipitation starts there is an initial rise in resistivity, which then

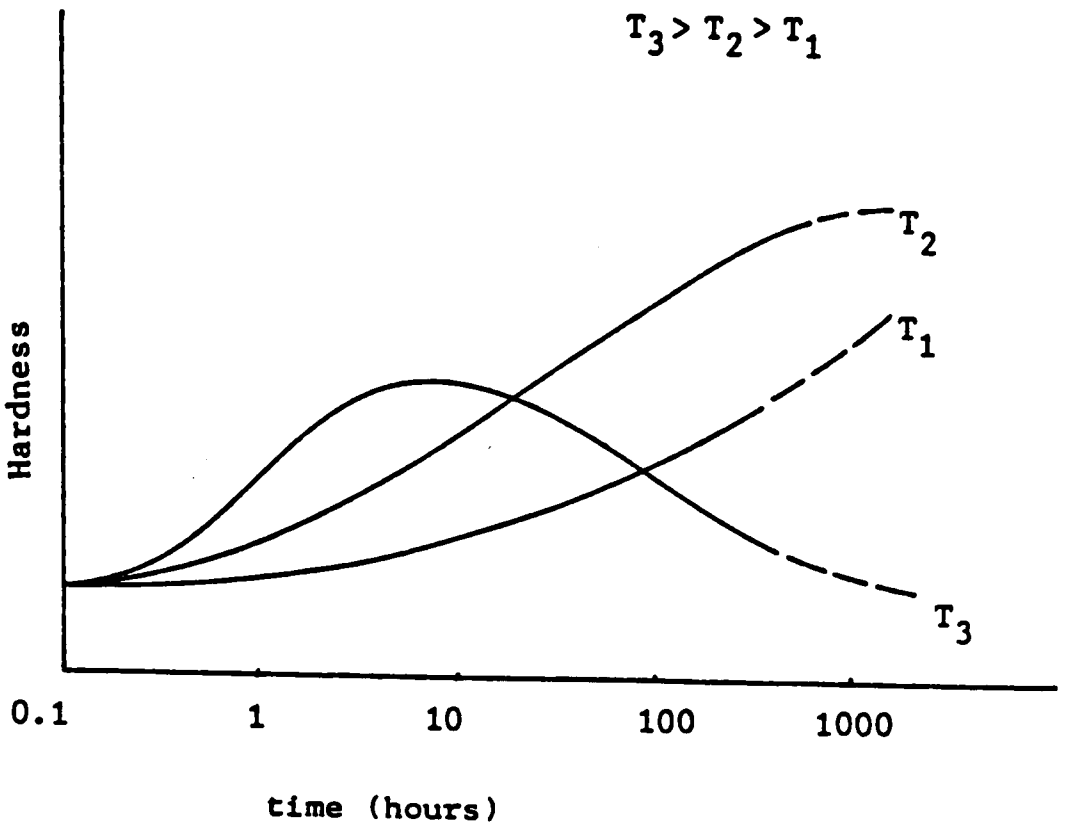

Figure 16. Schematic illustration of the effect of temperature on the aging curve during precipitation hardening (29).

decreases as the average particle separation distance increases during the progress of the precipitation.

EFFECT OF 3RD ELEMENT

(a) The influence of Cr on the Ni-Ta system

The binary Ni-Ta system shows a marked change in solid solubility with change in temperature (9), and it is therefore expected that aging of supersaturated solid solutions of appropriate compositions should lead to the precipitation of substantial amounts of Ni_3Ta. It has been found that this precipitation can be accelerated by the addition of Cr to the alloy (5).

According to the work by Aballe et al. (31), the Ni-25 wt.% Ta-2 wt.% Cr alloy did not harden on aging but the Ni-25 wt.% Ta-10 wt.% Cr alloy produced a marked hardening effect on aging (see Figure 17), associated with intermetallic compound precipitation.

The aging of supersaturated solid solution in Ni-Ta alloys (10~30 wt.% Ta) at various temperatures in the range 550-1080°C produced only slight precipitation of Ni_3Ta; the precipitation that was observed was mainly discontinuous and occurred at high supersaturations (i.e., in alloy with 25 and 30 wt. % Ta) (31).

The addition of 10 wt.% Cr to a Ni-Ta alloy (25 wt.% Ta) gave rise to a rapid, marked age-hardening response in the range 650°C to 800°C, associated with copious matrix

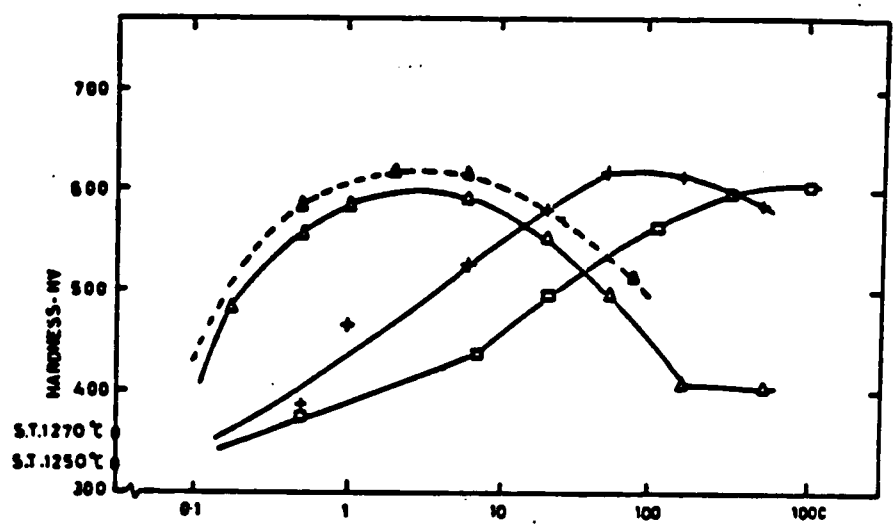

TIME - HOURS

▲ — Solution treated 1270°C, aged 800°C;

△ — Solution treated 1250°C, aged 800°C;

\+ — Solution treated 1250°C, aged 700°C;

□ — Solution treated 1250°C, aged 650°C.

Figure 17. Hardness vs. aging time for Ni-25 wt.% Ta-10 wt.% Cr alloy (31).

precipitation of a body-centered tetragonal Ni_3Ta phase. On prolonged aging at 800°C or above, this phase was replaced by the stable, orthorhombic Ni_3Ta phase.

The mechanism by which chromium enhanced the precipitate nucleation is of particular interest, and it appears that a reduction in lattice mismatch due to the presence of chromium is an important factor in aiding precipitation.

Figure 17 (31) is a plot of hardness versus aging time for Ni-25 wt. % Ta-11 wt.% Cr alloy. We can compare these results with the curves of Figure 16.

(b) The influence of Fe and Al on Ni-Ta system

Ni-Ta alloys with small additions of iron and aluminum exhibit precipitation of both the r' and r" phases during isothermal aging. These two metastable phases precipitated independently of each other in the ternary and quaternary alloys investigated by Axter and Polonis (6). The coherency strains and the corresponding surface energies associated with both types of precipitate particles are small, thereby resulting in a high resistance to coarsening.

The kinetics of r" formation is determined by diffusion-controlled precipitate growth. The r' phase begins to coarsen at earlier times, but the rate of coarsening is extremely low and is controlled by the diffusion of aluminum.

The difference in the observed growth rates for the γ" phase between the ternary and quaternary alloys has been identified with the influence of aluminum and iron additions on the solubility of tantalum in the matrix phase.

CHAPTER 3

EXPERIMENTAL METHODS

ALLOY PREPARATION

Table 2 shows the compositions and solution treatment temperatures of the two research alloys.

Alloy 1 was prepared by arc melting Ni and Ta in an atmosphere of argon. Pure Ni and Ta were weighed to give an approximate 150 gram charge which was arc melted. Due to the limitation of the pocket of the arc furnace, the total amount of each ingot was about 150 grams. Seven ingots were made for Ni-Ta alloy and the final total amount was 553 grams. For the Ni-Ta-Cr alloy, the smaller pocket was used and the weight was less than 100 grams (around 80 grams is best to get perfect melting) for each ingot. Seven ingots were melted with the final total as 536 grams. The charges were placed in a small pocket in the water cooled, copper base of a tungsten electrode arc melting furnace, and completely melted at least five times for each side of the ingots to increase the homogeneity of the melt. After these cylindrical ingots (diameter was about 2 cm, 8 cm in length for the larger ones; 1 cm in diameter and 7 cm in length for the smaller ones) were made with the same composition, they were then put into a Zirconia crucible and remelted together into a larger specimen in a Balzers induction furnace (VSG 02 type) in an atmosphere of 40 cm argon. The molten alloys were then cast into a water cooled, Cu mold.

Table 2. Alloy composition and solution treatment temperature for Ni-Ta and Ni-Ta-Cr alloy.

Alloy		Nominal composition		Chemical analysis		Solution treatment temperature (°C)
		wt%	at%	wt%	at%	
1	Ni	74.50	90.00	74.64	90.07	1250°C
	Ta	25.50	10.00	25.36	9.93	
2	Ni	62.50	73.80	61.79	73.38	1250°C
	Ta	25.00	9.60	25.57	9.92	
	Cr	12.50	16.60	12.46	16.70	

The Ni-Ta ingots were sealed in a quartz tube under vacuum and heat treated at 1250°C for 7 days, then water quenched. The next step was swaging. The specimens were heated up to 1250°C under vacuum for 30 minutes, then water quenched, before each cold swaging. Several swagings were done as follows. (a) 0.493 inch to 0.427 inch in diameter (25% reduction), (b) 0.427 inch to 0.357 inch (30% reduction), (c) 0.357 inch to 0.299 inch (30% reduction), (d) from 0.299 inch to 0.259 inch (25% reduction). The Ni-Ta-Cr alloy, was too hard for swaging, so only a solution treatment at 1250°C for 7 days was done. After the solution treatment, the sample was water quenched.

The cold-swaged Ni-Ta specimen was cut into 0.1 inch and 0.012 inch thick samples to do the aging. The 0.1 inch specimens were characterized using optical microscopy, scanning electron microscopy and microhardness measurements, while on the 0.012-inch ones X-ray diffraction analysis and transmission electron microscopy were carried out. To get the inside pressure of the quartz tube to be 1 atm at the aging temperatures, some argon was put in the tube instead of having it fully evacuated (26 cm Hg for 600°C, 23.28 cm Hg for 700°C, 21.1 cm Hg for 800°C, 19.3 cm Hg for 900°C, and 17.79 cm Hg for 1000°C). The aging temperatures were 600°, 700°, 800°, 900°, and 1000°C (all $\pm$ 10°C) and the aging times were set as 100 hr, 500 hr and 1000 hr for each temperature. The temperature was checked periodically by

inserting a platinum vs platinum-13% Rhodium (R-type) thermocouple. After the aging, the tubes were broken in water to quench the samples. The 0.1-inch thick specimens were cut into two pieces and mounted in Bakelite. The specimens were mounted so that the cross section and the inner portion of the samples could be viewed. The usual polishing procedures were used on the metallographic specimens. The samples were etched by immersion for 5 to 10 seconds in an etchant of 30 ml HF, 30 ml HCl and 15 ml HNO_3. The grain boundaries were observable optically after etching. The mounted samples were examined by optical microscopy, scanning electron microscopy, and the microhardness was measured. This alloy was also examined by transmission electron microscopy to study its structure.

The Ni-Ta-Cr alloy was solution heat treated at 1250^{o}C for seven days in vacuum, then water quenched. After this treatment, two second phases were present. The sample was reheated to 1280^{o}C in order to dissolve one of the second phases. The specimen was sealed in a quartz tube in vacuum and heated up to 1280^{o}C for about four hours, then water quenched. After this treatment, the sample was cut into 0.1 inch and 0.012 inch thick samples, the same as what was done to the Ni-Ta alloy. For aging, the samples were sealed in quartz tubes with some argon. The aging temperatures and times were the same as those of Ni-Ta alloy.

EXAMINATION METHODS

(1) Optical Microscopic Examination

The aged specimens were mounted in Bakelite at 290° F under pressure. After the Bakelite cooled down to room temperature, about 2 mm was ground from the specimen surface to remove any possible oxide layer. Then the samples were mechanically rough and fine ground, and finally rough and fine polished using conventional procedures for preparation for metallographic examination. Manual and vibrating polishing machines were employed at various polishing stages.

All of the etched specimens were examined initially by optical microscopy at a series of magnifications.

(2) Scanning Electron Microscopic Examination

The etched metallographic specimens were examined in the SEM. A conductive carbon paint was put around the specimen and the top of the Bakelite in order to prevent charging.

(3) Microhardness Measurements

Hardness measurements on polished metallographic specimens were made with a 136° apex angle diamond pyramid indenter, loaded with ten kilograms. Usually, the hardness was measured just after the last state of fine polishing. The diagonals of three to five impressions were measured, averaged and then converted to give a Diamond Pyramid

Hardness Number, DPH. A standard hardness block, 10 kg./DPH 801, was used to check calibration of the tester.

(4) Transmission Electron Microscopic Examination

Disks, 0.012 inches thick, were sliced from the heat treated and aged specimens, using a Gillings-Hamco's Thin Sectioning Machine with running water as the cooling system.

The slices were electrolytically polished and thinned in an electropolishing cell which was equipped with a light sensing system to detect the light upon the initial penetration of the specimens and turn off the power. The solution used for polishing contained 640 ml H_3PO_4, 150 ml H_2SO_4, 210 ml distilled water and 35 ml HCl. The polishing was conducted at 10°C with the cell potential at 10 volts and a current of 4 amperes.

The polished and penetrated specimens were rinsed in distilled water and methanol. Observation of the thin foils was conducted in a Phillips EM 300 transmission electron microscope operated at 100 kilovolts.

(5) X-Ray Diffraction Pattern Analysis

The etched metallographic specimens were examined using a Rigaku X-ray diffractometer operated at 35 KV and 20 mA. The mode was set at continuous scanning, 2θ/θ as drive axis, 10° to 120° as the range of scanning angle, 2 to 16 deg/min as scan speed, and 800 to 2000 cps as the counting rate.

CHAPTER4

RESULTS AND DISCUSSION

OPTICAL MICROSTRUCTURE

(a) Ni-Ta alloy

The Ni-Ta alloy was single phase in the solution treated condition, and as far as could be detected by optical microscopy, remained so during aging. Figure 18a shows the microstructure of the Ni-Ta alloy in the condition used for the aging treatments. The treatment to develop this condition consisted of annealing for 30 min. at 1250°C, water quenching, then cold working 50% by swaging. Thus, in Figure 18a the microstructure is that of the cold worked alloy, and the aging treatments were carried out on samples with this initial condition. The cold worked material was aged at 600°C to 1000°C for 100 hours up to 1000 hours. The material was swaged prior to aging, so the heat treatments involved aging the alloy in the cold worked condition. The optical microstructures are shown in Figures 18b through 21d. The aging conditions and magnification of each alloy are included in the captions.

The grain size of as-quenched material is almost the same as that after aging at 600°C for 100 hours to 1000 hours, and is larger than that after aging at higher temperatures (700°C to 900°C). There is almost no change in grain size after aging at 700°C to 900°C, but it increases a little at 1000°C. From the view of optical microstructures,

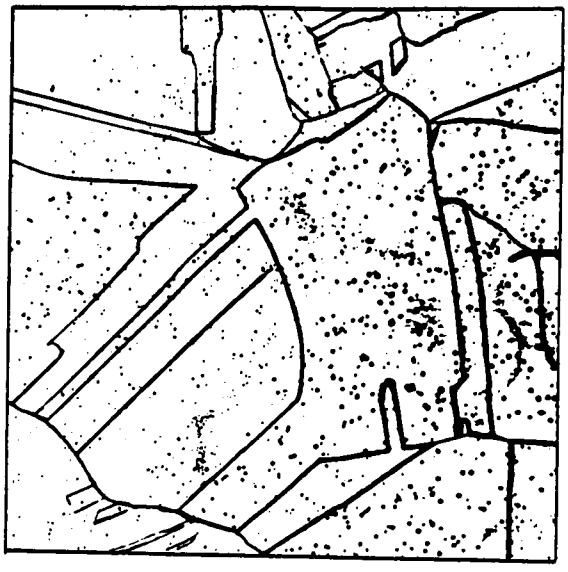

18a. Ni-Ta alloy, 1250°C, 7 days, water quenched, cold worked 50%, OM, 100 X.

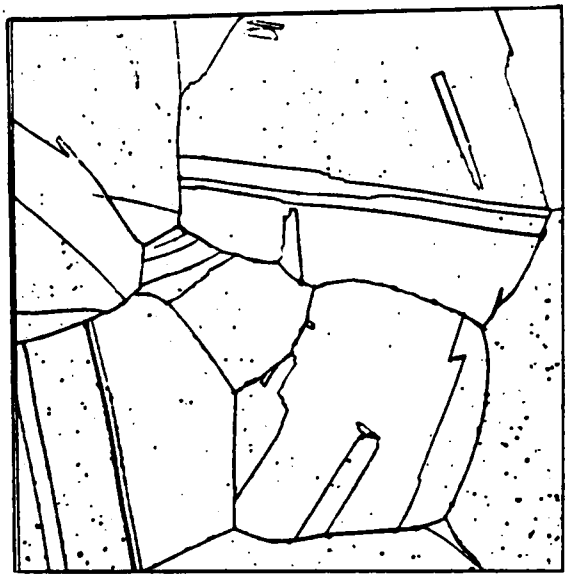

18b. Ni-Ta alloy, aged at 600°C for 100 hrs, water quenched, OM, 100 X.

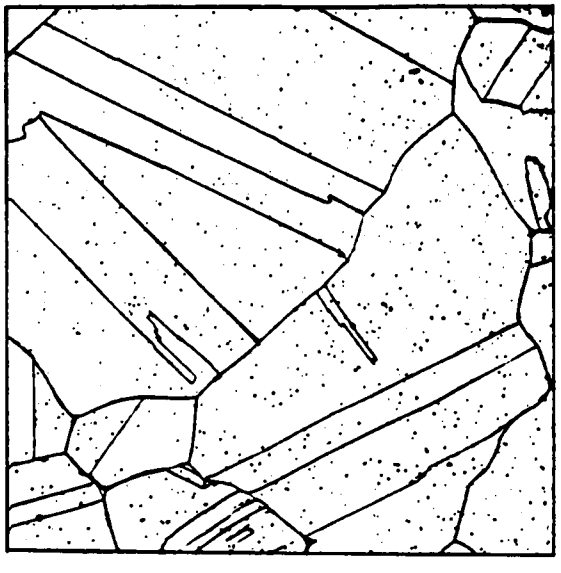

18c. Ni-Ta alloy, aged at 600°C for 500 hrs, water quenched, OM, 100 X.

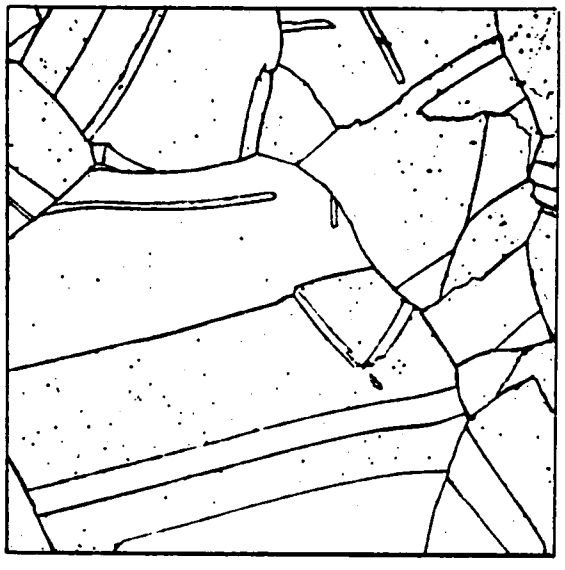

18d. Ni-Ta alloy, aged at 600°C for 1000 hrs, water quenched, OM, 100 X.

Figure 18. Optical microstructures of the Ni-Ta alloy after solution treatment and aging at 600°C.

19a. Ni-Ta alloy, aged at 700°C for 100 hrs, water quenched, OM, 100 X.

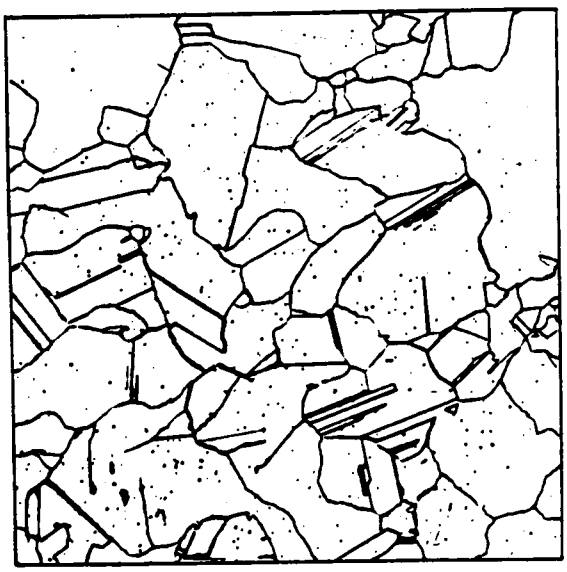

19b. Ni-Ta alloy, aged at 800°C for 100 hrs, water quenched, OM, 100X.

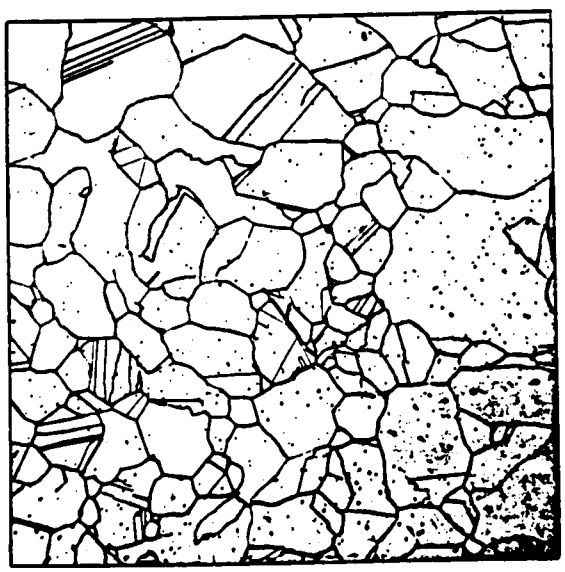

19c. Ni-Ta alloy, aged at 900°C for 100 hrs, water quenched, OM, 100 X.

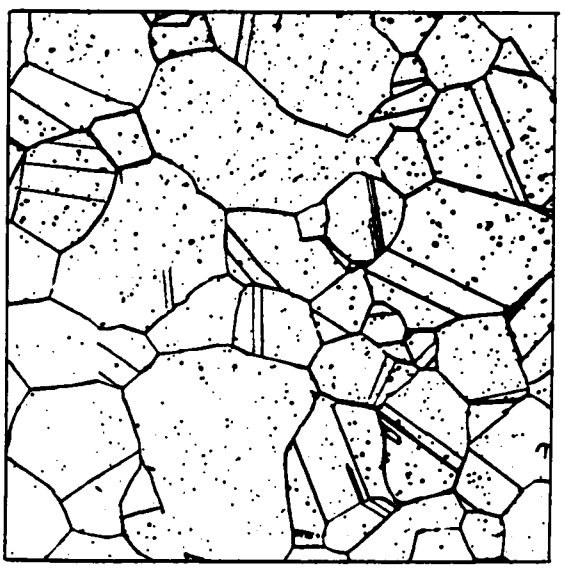

19d. Ni-Ta alloy, aged at 1000°C for 100 hrs, water quenched, OM, 100X.

Figure 19. Optical microstructures of the Ni-Ta alloy after aging at 700°C to 1000°C for 100 hrs.

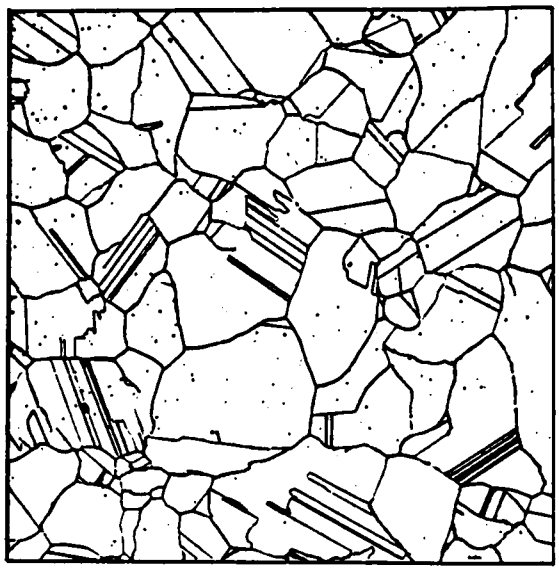

20a. Ni-Ta alloy, aged at 700°C for 500 hrs, water quenched, OM, 100 X.

20b. Ni-Ta alloy, aged at 800°C for 500 hrs, water quenched, OM, 100X.

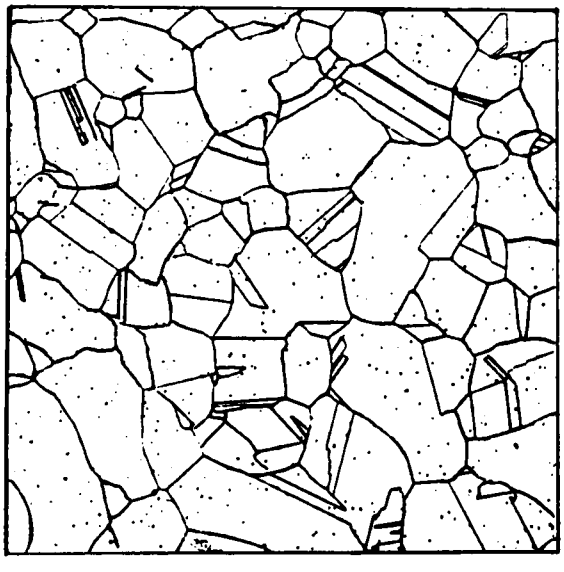

20c. Ni-Ta alloy, aged at 900°C for 500 hrs, water quenched, OM, 100 X.

20d. Ni-Ta alloy, aged at 1000°C for 500 hrs, water quenched, OM, 100X.

Figure 20. Optical microstructures of the Ni-Ta alloy after aging at 700°C to 1000°C for 500 hrs.

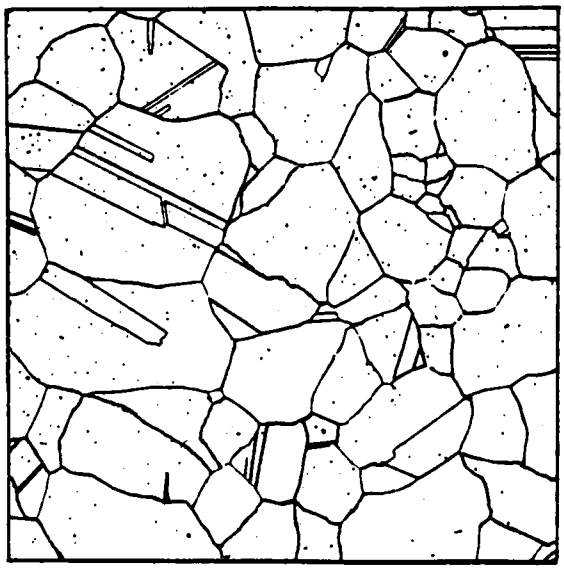

21a. Ni-Ta alloy, aged at 700°C for 1000 hrs, water quenched, OM, 100 X.

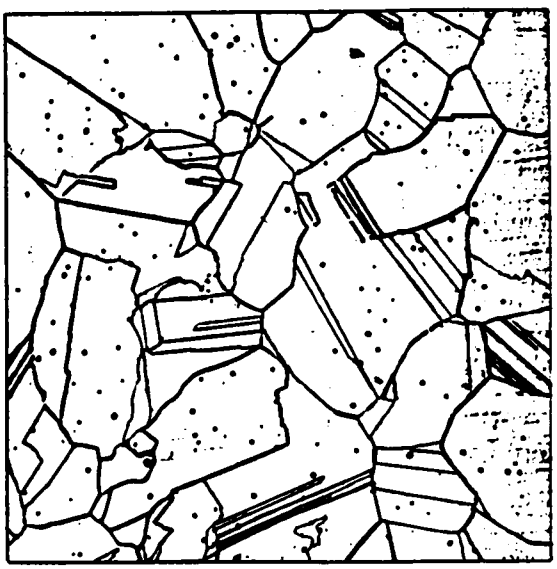

21b. Ni-Ta alloy, aged at 800°C for 1000 hrs, water quenched, OM, 100X.

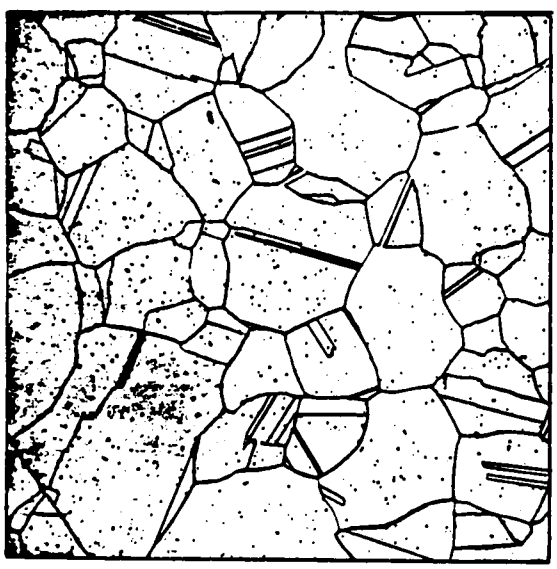

21c. Ni-Ta alloy, aged at 900°C for 1000 hrs, water quenched, OM, 100 X.

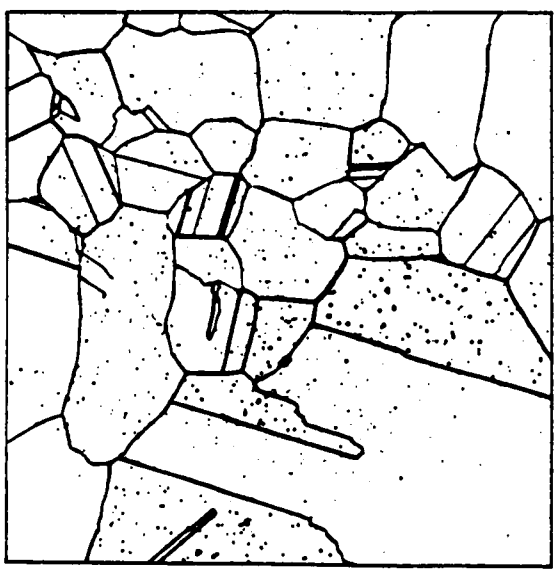

21d. Ni-Ta alloy, aged at 1000°C for 1000 hrs, water quenched, OM, 100X.

Figure 21. Optical microstructures of the Ni-Ta alloy after aging at 700°C to 1000°C for 1000 hrs.

there is no evidence of any Ni_3Ta structure having formed at the grain boundaries or inside the grains. The material is very brittle; some intergranular cracks occurred after aging at 600°C to 1000°C, then water quenching. No obvious change in structure by optical microscopy or scanning electron microscopy was seen. X-ray diffraction analysis and TEM examination were also conducted to study this material and the results will be discussed later.

(b) Ni-Ta-Cr alloy

The Ni-Ta-Cr alloy at the first step of the solution treated condition (1250°C for seven days, water quenched) contained about 20% of two second phases (noted 1 and 2 in Figure 22a). This as-quenched material was reheated to 1280°C for about four hours, after which the resulting material contained about 10% of only a single second phase. Figures 22a and 22b show the optical microstructures for these two solution treated conditions. The reheated material was used to do the aging.

After aging at 600°C for times up to 1000 hours, there was no change optically, as shown in Figures 23b through 23d compared with reheated material shown in Figure 23a. The structure changed after aging at higher temperatures. From Figures 24a through 27d we can observe that the matrix decomposed by a complex process, which included high-angle boundary migration and formation of transformation products.

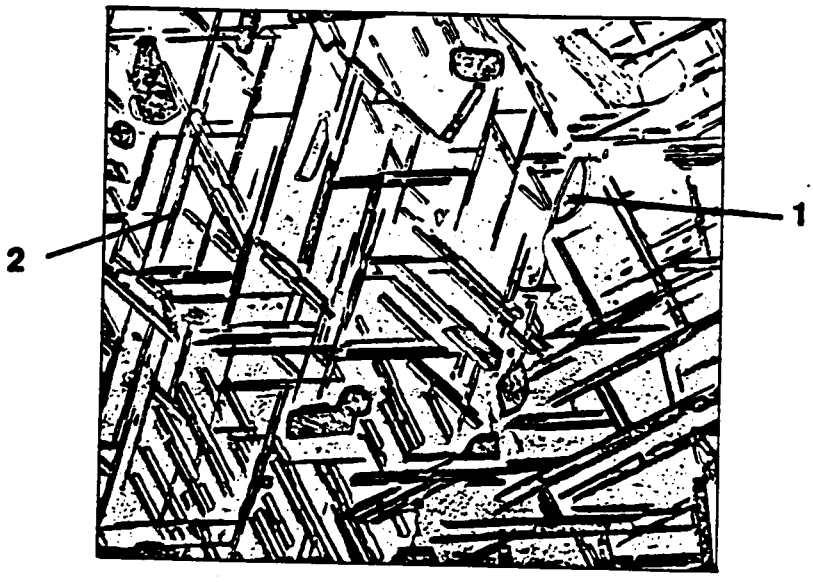

22a. Ni-Ta-Cr alloy, 1250°C for 7 days, water quenched; two second phases present in the matrix, OM, 500 X.

22b. Ni-Ta-Cr alloy, 1250°C for 7 days, water quenched, then reheated to 1280°C for 4 hrs, water quenched; one second phase present, OM, 200 X.

Figure 22. Optical microstructures of the Ni-Ta-Cr alloy after the first and the second solution treatment.

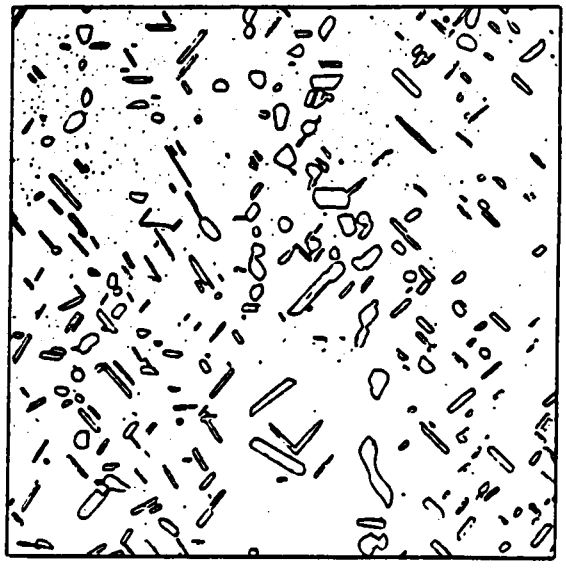

23a. Ni-Ta-Cr alloy, 1250°C, 7 days, water quenched, then reheated to 1280°C for 4 hrs, water quenched, OM, 200 X.

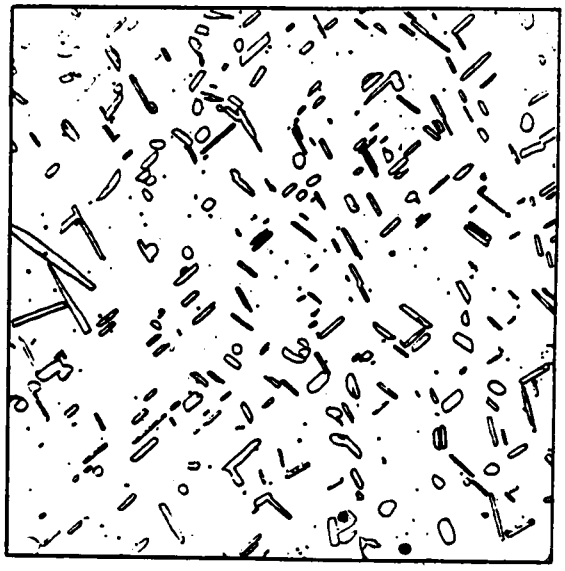

23b. Ni-Ta-Cr alloy, aged at 600°C for 100 hrs, water quenched, OM, 200 X.

23c. Ni-Ta-Cr alloy, aged at 600°C for 500 hrs, water quenched, OM, 200 X.

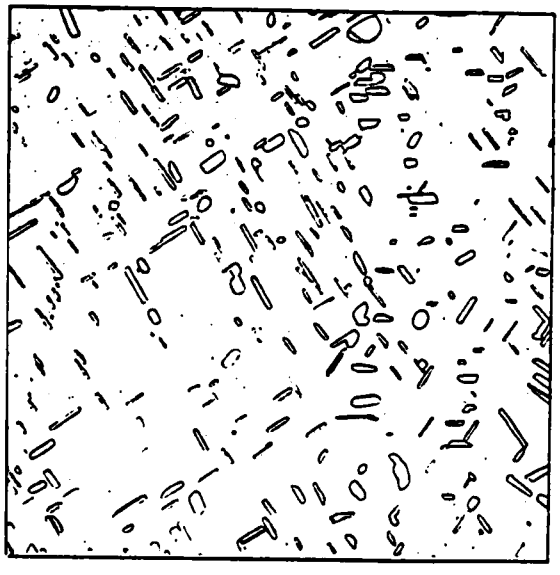

23d. Ni-Ta-Cr alloy, aged at 600°C for 1000 hrs, water quenched, OM, 200 X.

Figure 23. Optical microstructures of the Ni-Ta-Cr alloy after solution treatment and aging at 600°C.

24a. Ni-Ta-Cr alloy, aged at 700°C for 100 hrs, water quenched, OM, 200 X.

24b. Ni-Ta-Cr alloy, aged at 800°C for 100 hrs, water quenched, OM, 200 X.

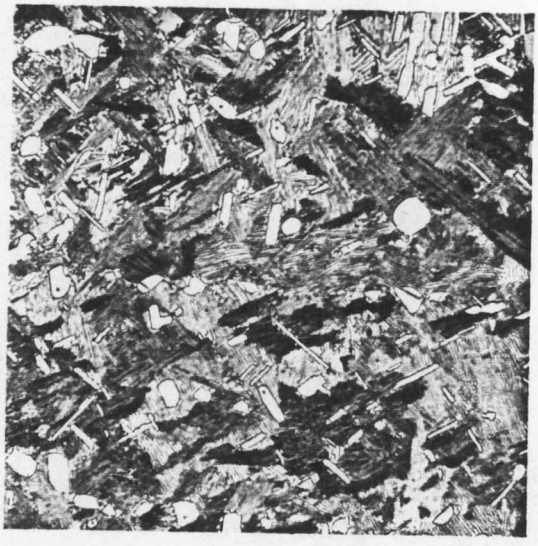

24c. Ni-Ta-Cr alloy, aged at 900°C for 100 hrs, water quenched, OM, 200 X.

24d. Ni-Ta-Cr alloy, aged at 1000°C for 100 hrs, water quenched, OM, 200 X.

Figure 24. Optical microstructures of the Ni-Ta-Cr alloy after aging at 700°to 1000°C for 100 hrs.

25a. Ni-Ta-Cr alloy, aged at 700°C for 500 hrs, water quenched, OM, 200 X.

25b. Ni-Ta-Cr alloy, aged at 800°C for 500 hrs, water quenched, OM, 200 X.

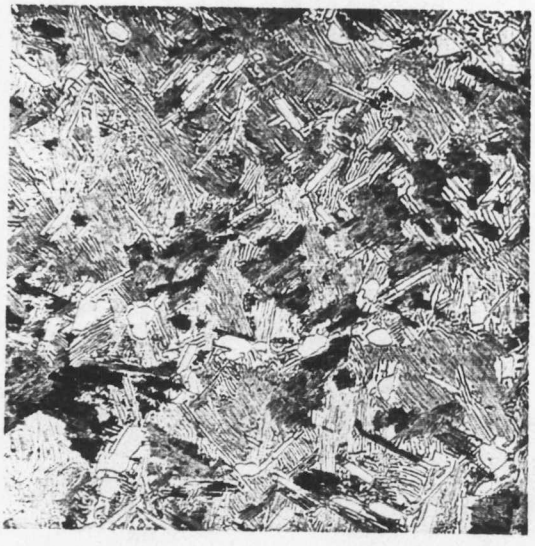

25c. Ni-Ta-Cr alloy, aged at 900°C for 500 hrs, water quenched, OM, 200 X.

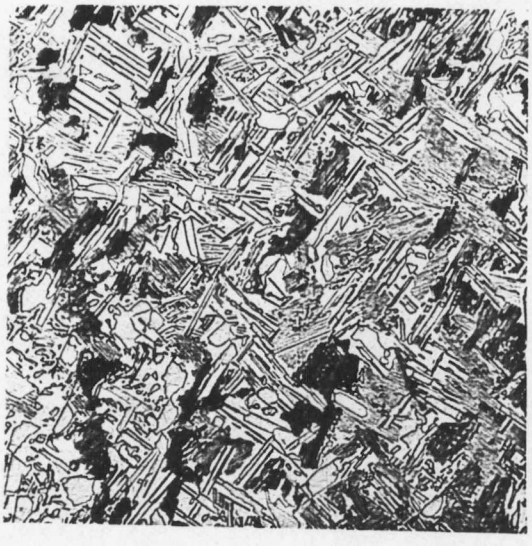

25d. Ni-Ta-Cr alloy, aged at 1000°C for 500 hrs, water quenched, OM, 200 X.

Figure 25. Optical microstructures of the Ni-Ta-Cr alloy after aging at 700° to 1000°C for 500 hrs.

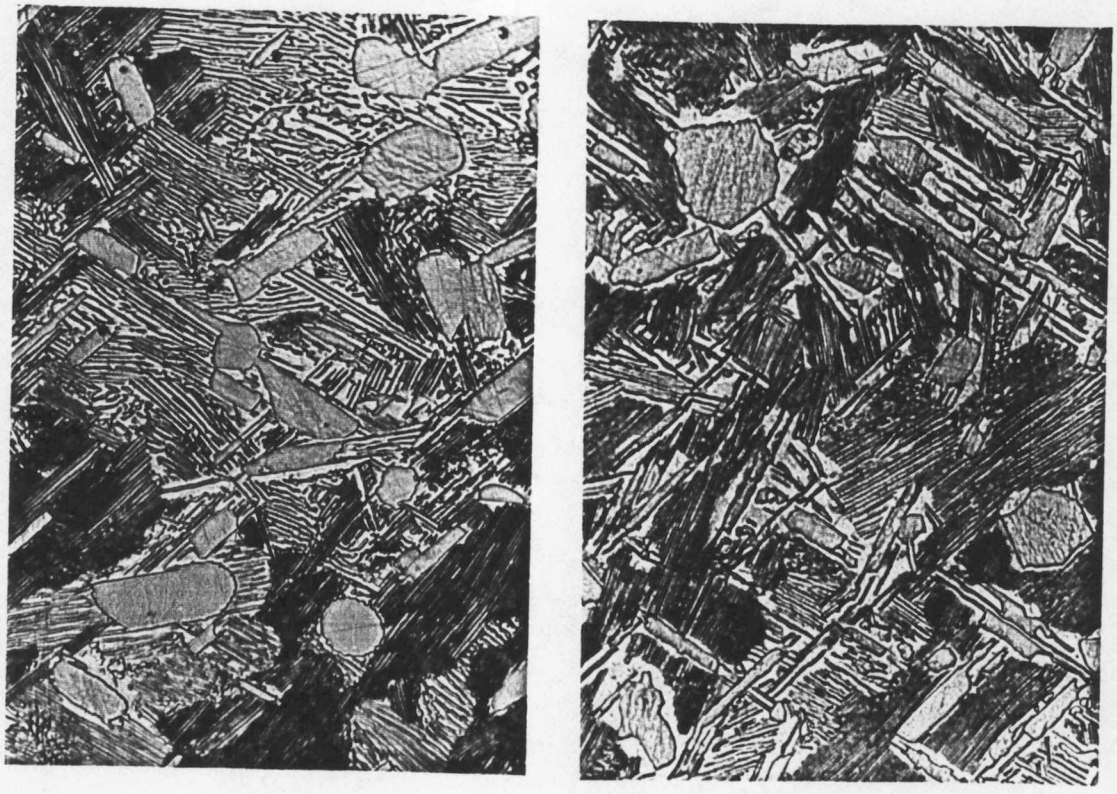

26a. Ni-Ta-Cr alloy, aged at 900°C for 500 hrs, water quenched, OM, 500 X.

26b. Ni-Ta-Cr alloy, aged at 1000°C for 500 hrs, water quenched, OM, 500 X.

Figure 26. Optical microstructures of the Ni-Ta-Cr alloy after aging at 900°and 1000°C for 500 hrs.

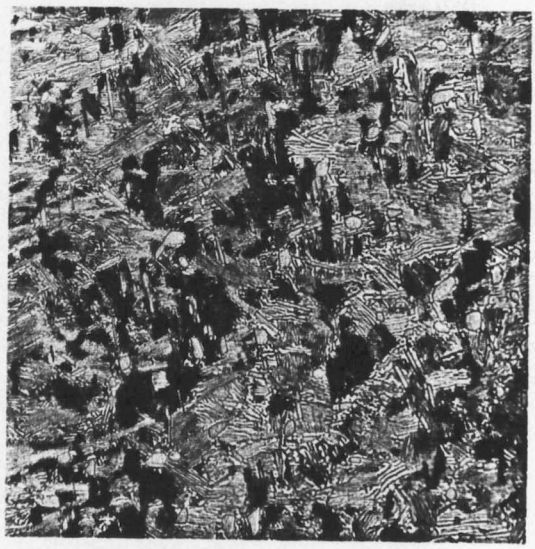

Fig.27a. Ni-Ta-Cr alloy, aged at 700°C for 1000 hrs, water quenched, OM, 200 X.

Fig.27b. Ni-Ta-Cr alloy, aged at 800°C for 1000 hrs, water quenched, OM, 200 X.

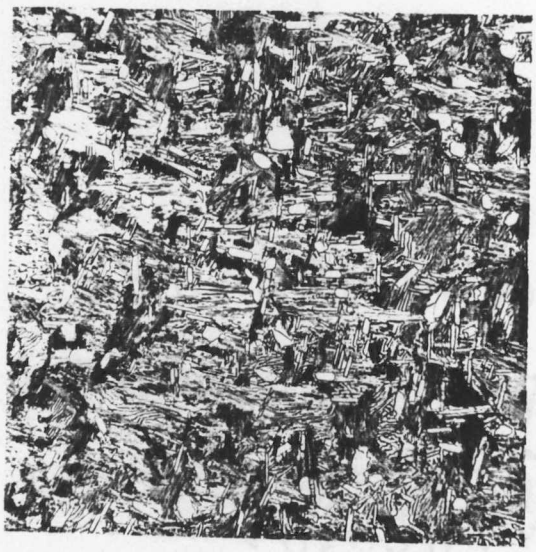

Fig.27c. Ni-Ta-Cr alloy, aged at 900°C for 1000 hrs, water quenched, OM, 200 X.

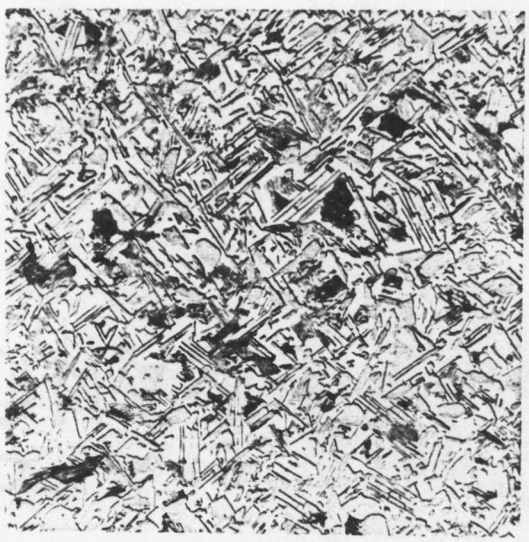

Fig.27d. Ni-Ta-Cr alloy, aged at 1000°C for 1000 hrs, water quenched, OM, 200 X.

Figure 27. Optical microstructures of the Ni-Ta-Cr alloy after aging at 700° to 1000°C for 1000 hrs.

The new structure formed either from the matrix or the second phase particles, and will be shown in more detail later by high magnification scanning electron microscope pictures. The structures shown in Figures 25a through 27d indicate that the new structure became coarser at higher aging temperatures for longer times. The microhardness (described later) decreases with the occurrence of these new products.

Table 3 shows the times when the changes in structure first began at different temperatures. Figure 28 is the plot of aging temperature versus this time.

MICROHARDNESS DATA

(A) Ni-Ta alloy

The initial hardness after the solution treatment was about 355 DPH; it remained at about 300 DPH during aging at 600°C, but decreased to around 200 DPH upon aging at higher temperatures. Table 4 shows the hardness values and the heat treatment conditions. Figures 29 through 31 show the microhardness in DPH versus the aging temperatures. Although the grain size of the solution treated and aged at 600°C materials is much larger than those aged at 700°C to 1000°C (Figures 18a through 21d), the hardness values decrease with an increase in temperature. According to the results of X-ray diffraction patterns, the material is all FCC structure (discussed later). The decrease in hardness is due to the

Table 3. The time when the change in structure first began corresponding to the aging temperature from 700°C to 1100°C (Ni-Ta-Cr alloy).

time / temp	10 min	15 min	25 min	40 min	50 min	1 hr	2 hr	25hr
700° C								X
800° C						X		
900° C				X				
1000° C		X						
1100° C	X							

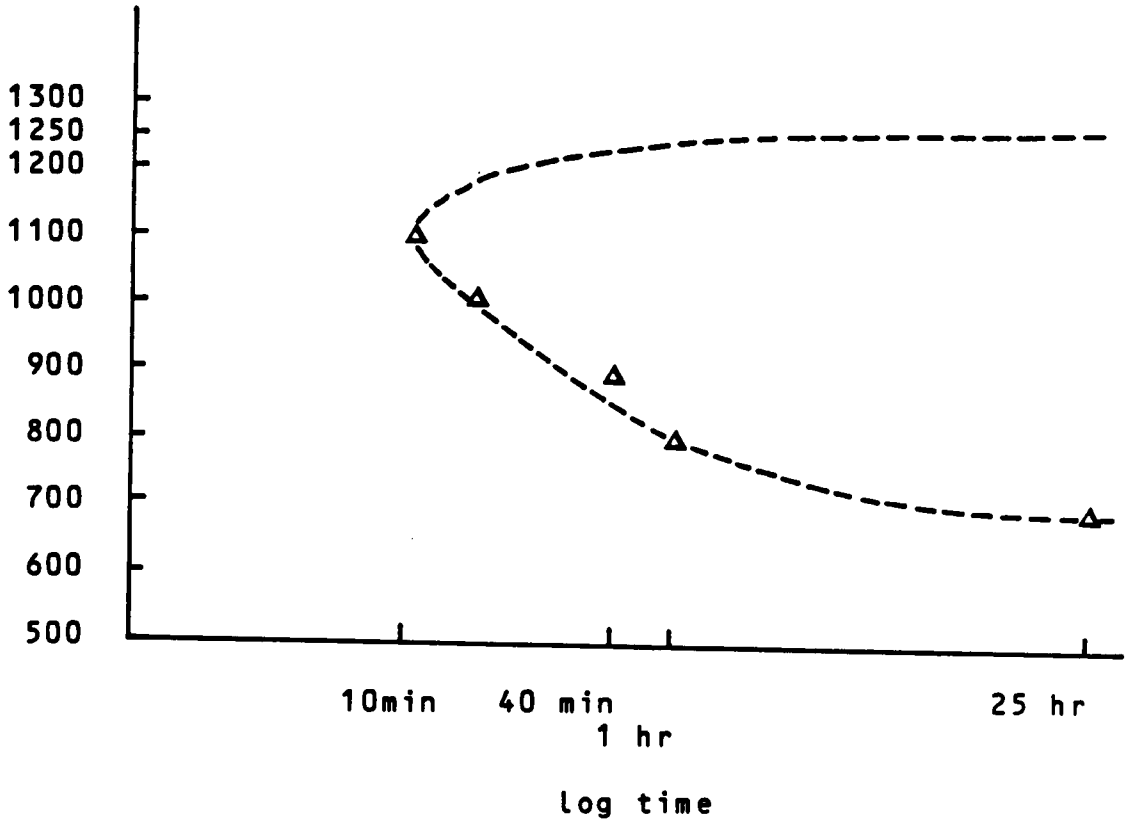

Figure 28. The aging temperature vs. the time when the new structure began to form in the Ni-Ta-Cr alloy.

Table 4 The microhardness values (in DPH) of Ni-Ta alloy corresponding to the heat treated conditions.

Heat treated condition	DPH		
1250°C, 7 days, water quenched.	348	366	355
600°C, 100 hrs	306	291	315
700°C, 100 hrs	199	204	205
800°C, 100 hrs	197	197	198
900°C, 100 hrs	194	198	204
1000°C, 100 hrs	199	185	200
600°C, 500 hrs	299	298	282
700°C, 500 hrs	199	206	200
800°C, 500 hrs	202	206	203
900°C, 500 hrs	186	188	190
1000°C, 500 hrs	197	192	199
600°C, 1000 hrs	304	292	300
700°C, 1000 hrs	199	198	198
800°C, 1000 hrs	195	198	203
900°C, 1000 hrs	198	201	203
1000°C, 1000 hrs	190	193	198

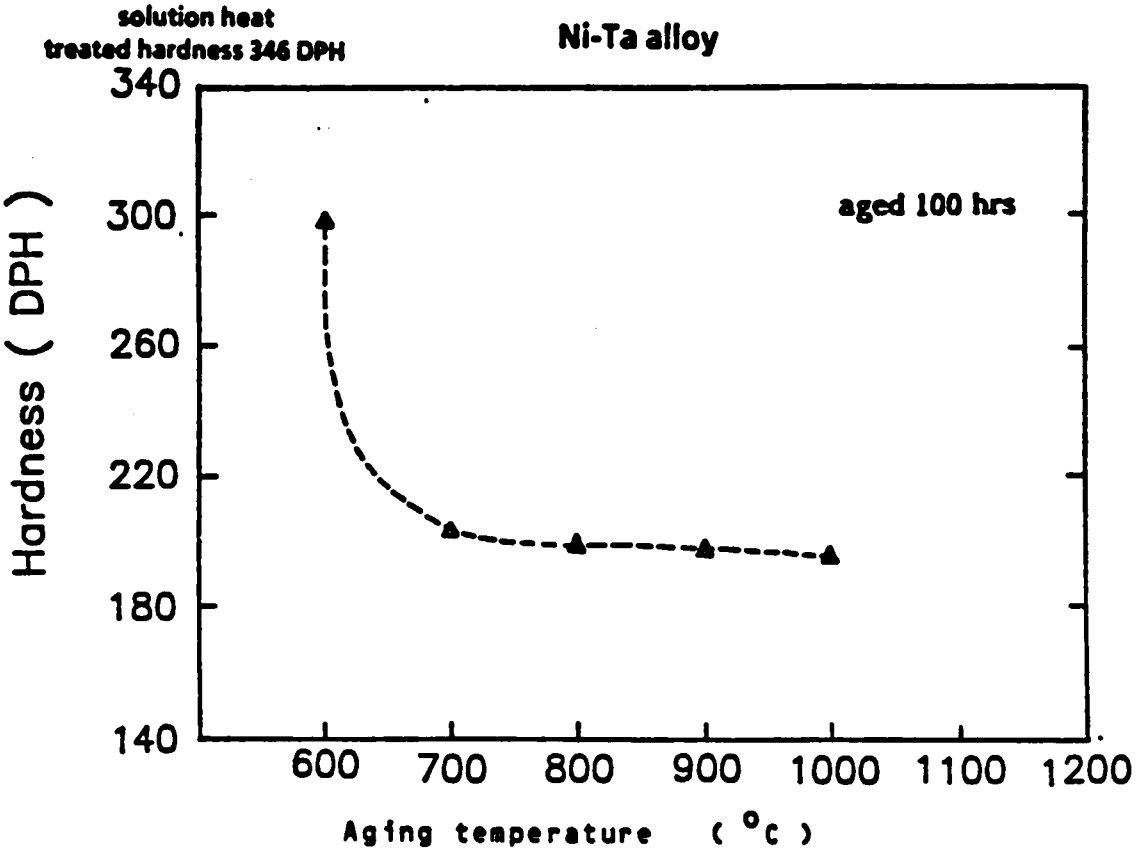

Figure 29. Hardness (in DPH) vs. aging temperature for Ni-Ta alloy, aged for 100 hrs.

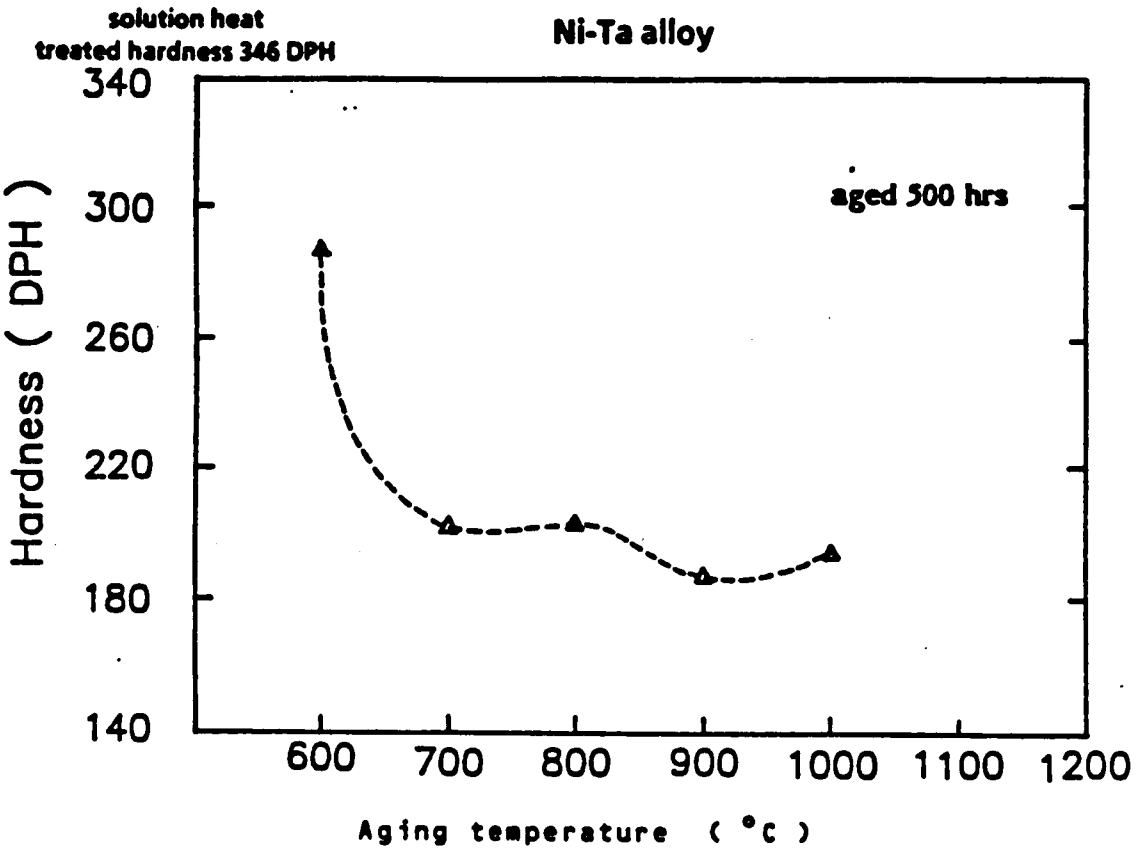

Figure 30. Hardness (in DPH) vs. aging temperature for Ni-Ta alloy, aged for 500 hrs.

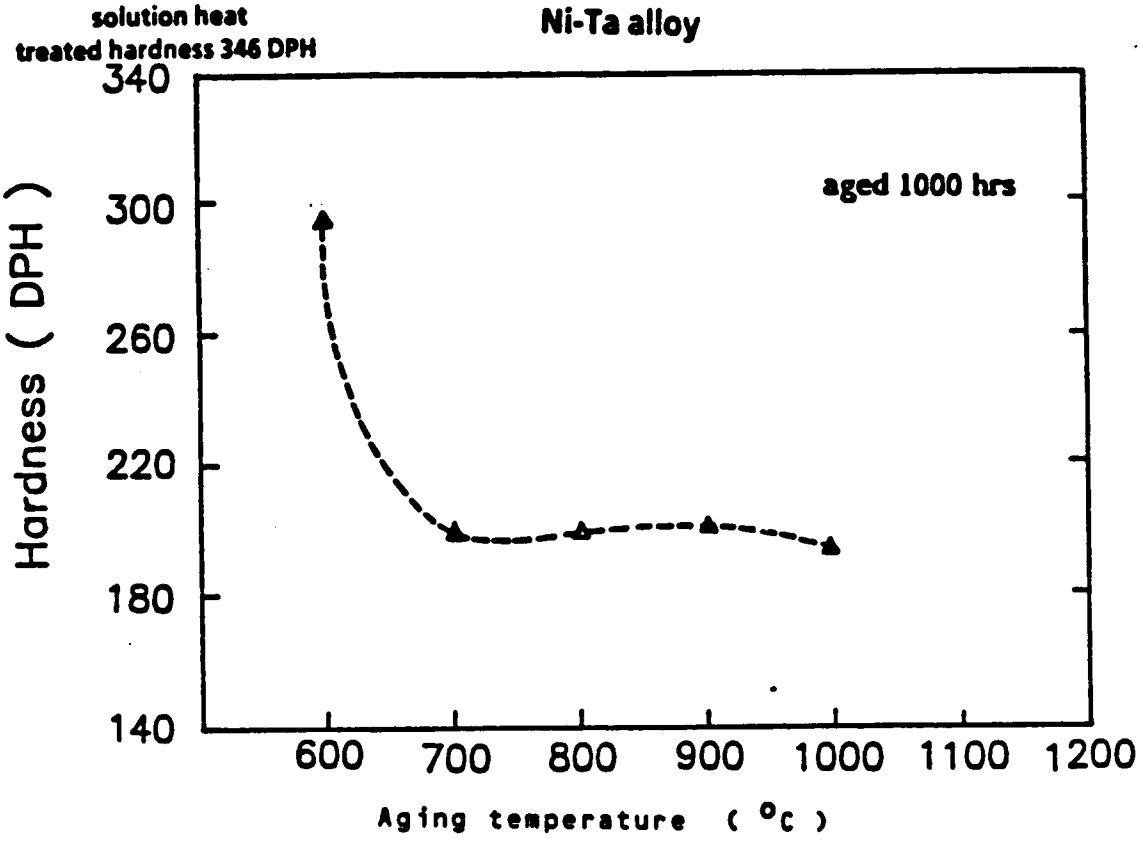

Figure 31. Hardness (in DPH) vs. aging temperature for Ni-Ta alloy, aged for 1000 hrs.

effect of recrystallization. This phenomenon is shown in the plots of microhardness versus aging time (Figure 32).

(B) Ni-Ta-Cr alloy

The hardness of the Ni-Ta-Cr alloy was high, from 335 DPH (1250°C, 7 days, water quenched) to 530 DPH (1280°C, 4 hours, water quenched; after the previous treatment), depending on the solution treating temperature. The alloy in the final solution heat treated condition contained about 10% of a second phase.

The hardness remained approximately around 580 to 620 DPH during aging at 600°C, but decreased to about 330 to 380 DPH (700°C to 1000°C, 500 hours) and 320 to 350 DPH (700°C to 1000°C, 1000 hours). Table 5 lists the microhardness results. Figure 33 is a plot of microhardness vs. the aging time, and Figures 34 through 37 are the plots of microhardness (DPH) versus the aging temperature.

No changes in the microstructure of the matrix were observed by optical microscope after aging at 600°C; also the hardness remained approximately constant.

At higher temperatures from SEM high magnification pictures (shown later) we can see that transformation occurred in the matrix. The hardness decreased a little bit after aging at 700°C for 50 to 100 hours and at 800°C for 50 hours (see Figures 34 and 35).

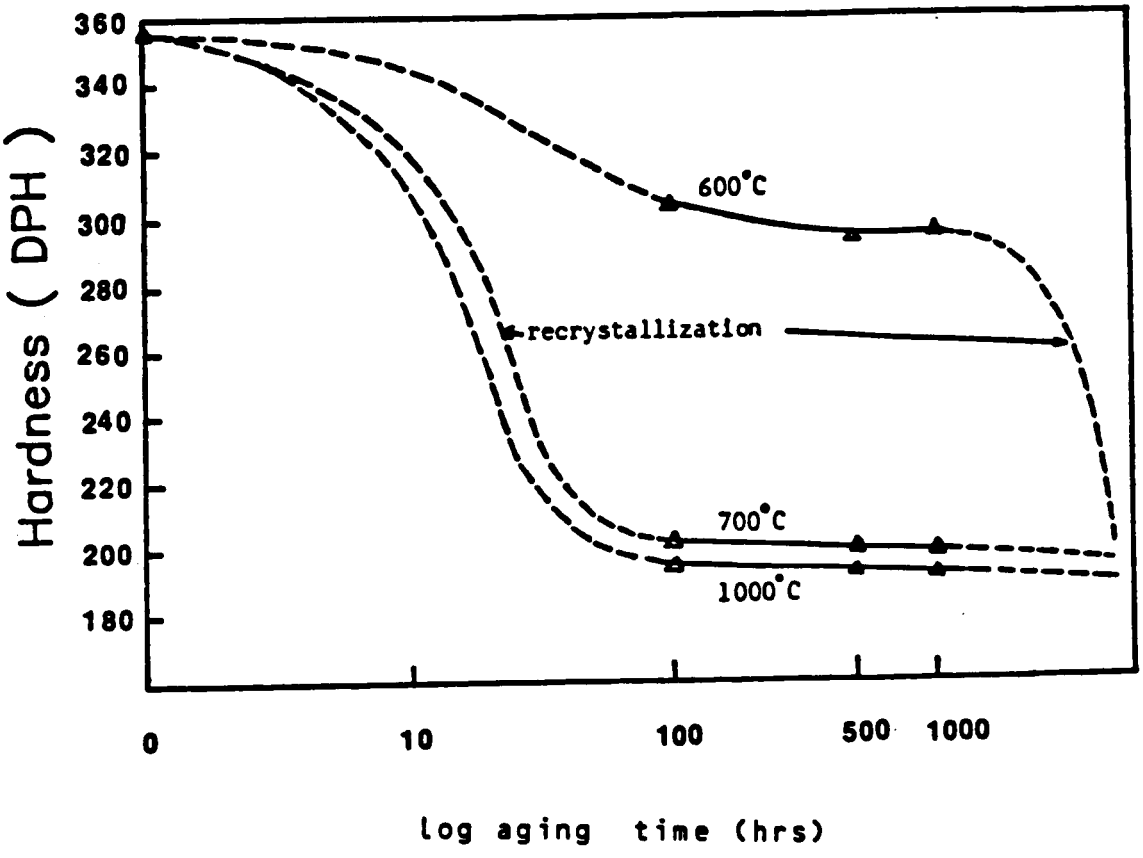

Figure 32. Hardness (in DPH) vs. aging time of Ni-Ta alloy; dashed lines denote the predicted curves.

Table 5. The microhardness values (in DPH) of the Ni-Ta-Cr alloy after solution heat treated and aging at 600°C to 1000°C up to 1000 hrs.

Heat treated condition				Hardness			
1250°C, 7 days, water quenched.				335 (DPH)			
1280°C, 4 hrs, water quenched, after 1250°C for 7 days.				532 (DPH)			
50 hrs, water quenched.				100 hrs, water quenched.			
temp.	DPH			temp.	DPH		
600°C	603	619	621	600°C	572	542	557
700°C	-	-	-	700°C	493	488	530
800°C	609	611	618	800°C	486	475	515
900°C	380	383	394	900°C	377	370	355
1000°C	380	380	380	1000°C	346	348	354
500 hrs, water quenched.				1000 hrs, water quenched.			
temp.	DPH			temp.	DPH		
600°C	588	589	612	600°C	602	621	634
700°C	402	386	411	700°C	366	361	363
800°C	361	362	372	800°C	314	314	314
900°C	351	353	358	900°C	285	343	308
1000°C	318	320	334	1000°C	324	325	334

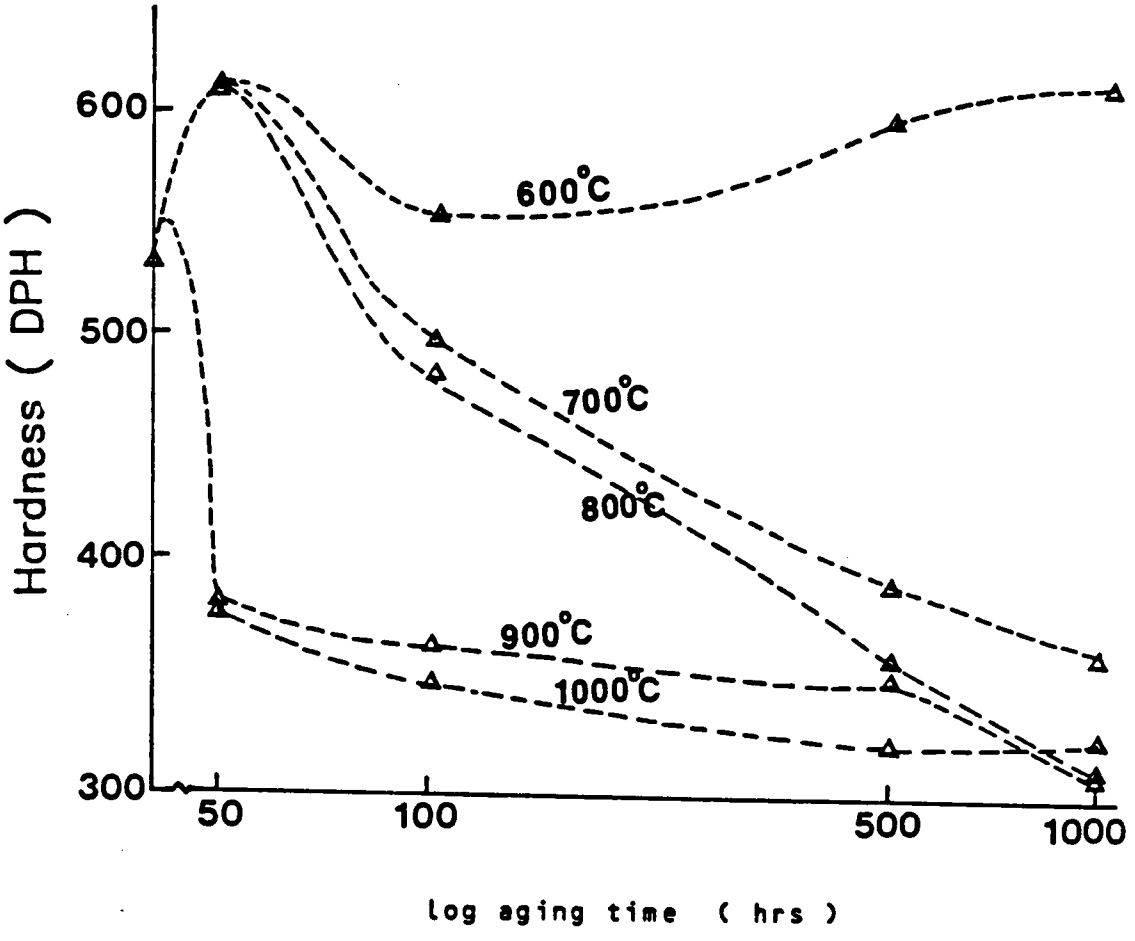

Figure 33. The microhardness (in DPH) vs. aging time for Ni-Ta-Cr alloy.

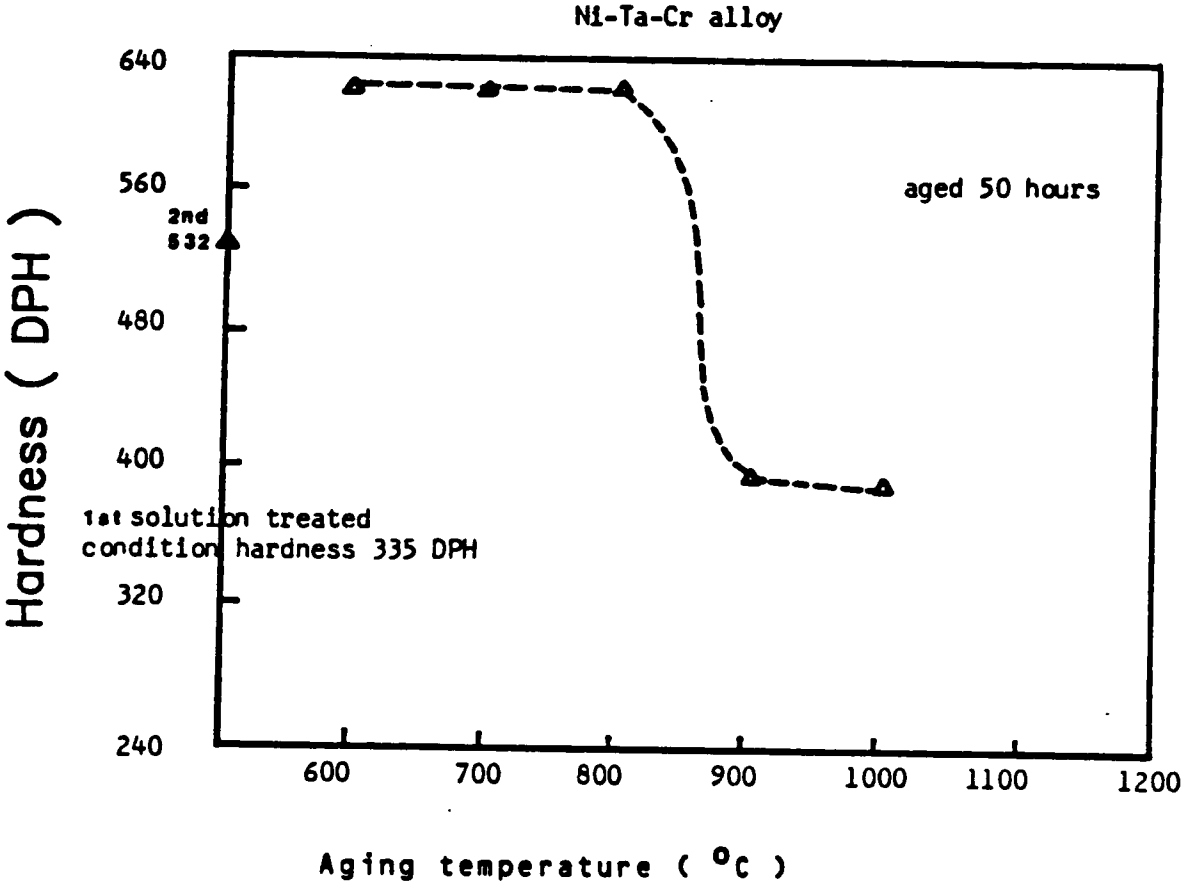

Figure 34. Hardness (in DPH) vs. aging temperature for Ni-Ta-Cr alloy, aged for 50 hrs.

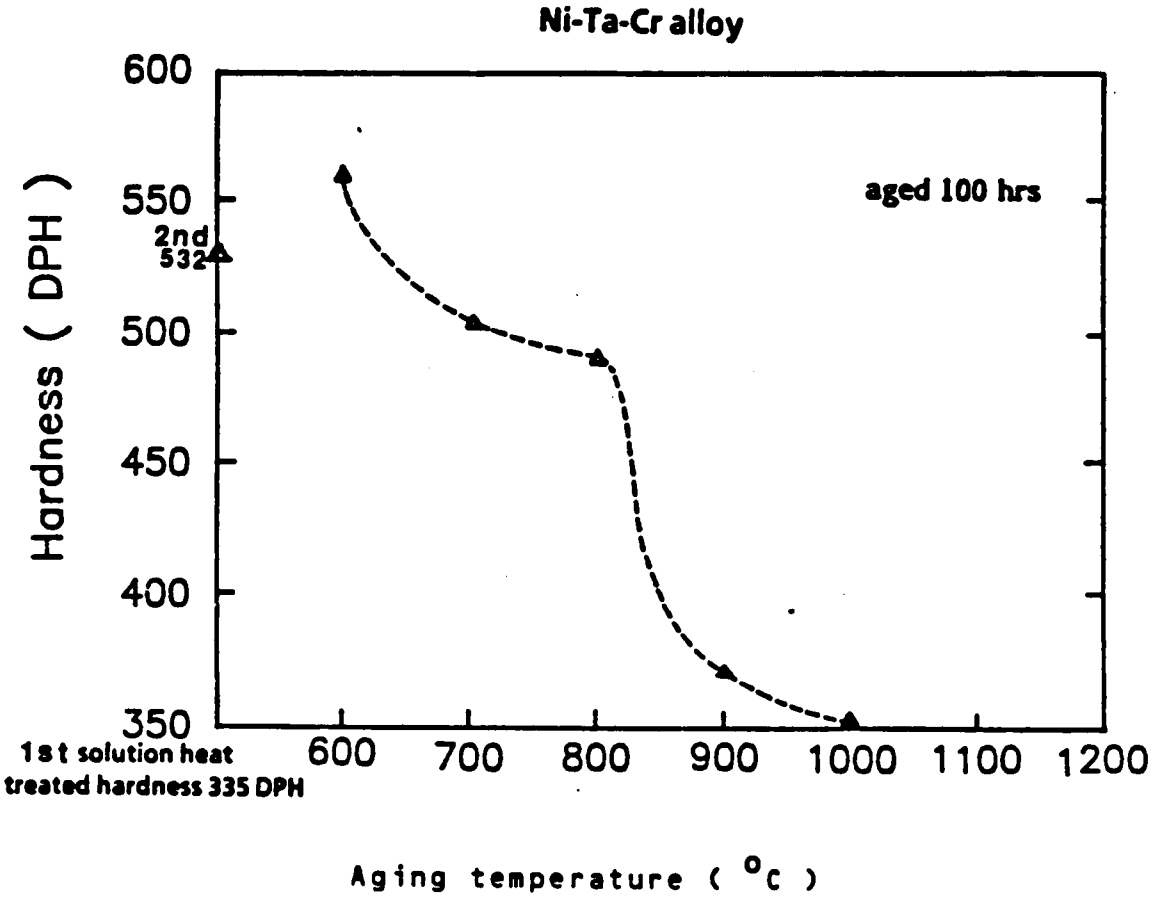

Figure 35. Hardness (in DPH) vs. aging temperature for Ni-Ta-Cr alloy, aged for 100 hrs.

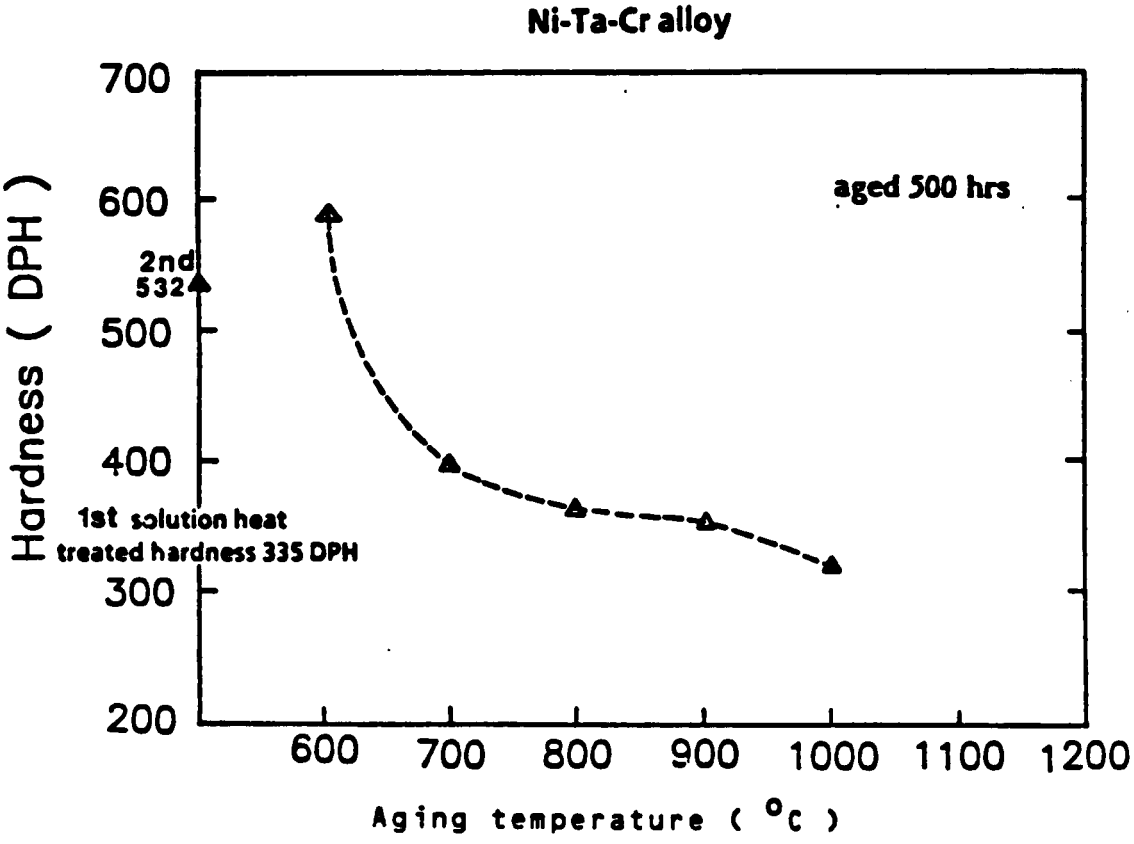

Figure 36. Hardness (in DPH) vs. aging temperature for Ni-Ta-Cr alloy, aged for 500 hrs.

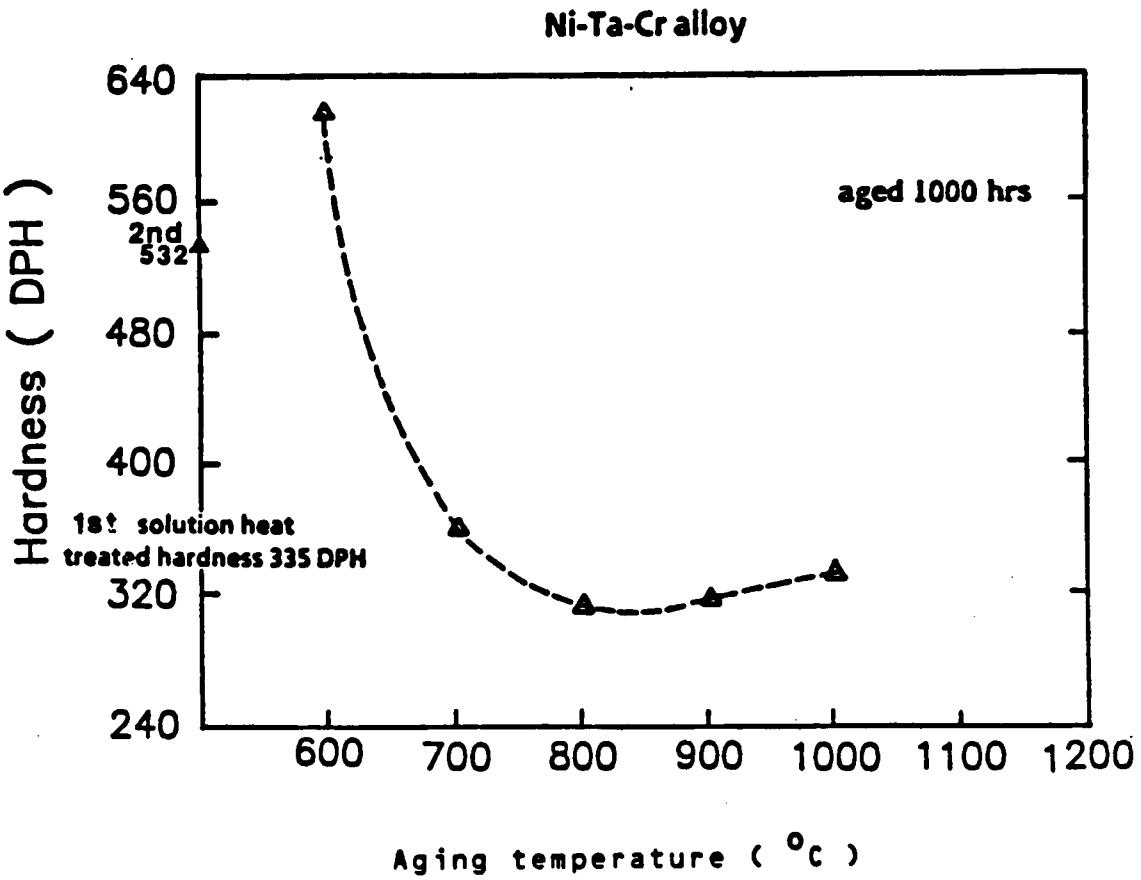

Figure 37. Hardness (in DPH) vs. aging temperature for Ni-Ta-Cr alloy, aged for 1000 hrs.

The hardness stayed at around 610 DPH after aging at 600°C to 800°C for 50 hours (Figure 34). There was no change in the microstructure of the matrix, as shown in the previous pictures (Figures 23b-d). The hardness dropped to about 385 DPH after aging at 900°C and 1000°C for 50 hours due to the structural change in matrix. The more the material transformed, the lower the hardness. The change in structure of the matrix, which occurred between 50 and 100 hours upon aging at 700°C and 800°C, caused the decrease in hardness. The structure formed from the matrix became coarser after aging at 1000°C for long time.

SCANNING ELECTRON MICROSCOPY

(a) Ni-Ta alloy

Using SEM, only a single phase structure was shown in the Ni-Ta alloy.

(b) Ni-Ta-Cr alloy

As shown in the optical microstructures, a second phase was present after solution treatment at 1280°C. This second phase always appeared all over the material no matter what aging temperature and time were used. Figure 38a shows that about 10% of this second phase is present in the solution treated condition. After aging at 600°C for times up to 1000 hours, neither the microstructure nor the hardness changed. Figure 38b is high magnification view of a second phase particle.

The matrix started to decompose both at around the second phase particles and inside the matrix regions, as shown in Figures 38c and d. It shows that the shape of the forming structure is something like a bundle of parallel hairs or pearlite-like structure. To look at this type of transformation product in more detail, high magnification (5000X) microstructures are shown in Figures 39a through 39d for which the alloy was aged for a short time (one hour). The formation of the structure seems to be started along the boundaries of the second phase and parallel to its two edges (if it is close to rectangular in shape). Figure 40 shows more clearly how the formation occurred along the particle. The newly formed structure grew and continued, sometimes passing around a neighboring second phase (Figures 41a and 41c). The higher the aging temperature, the higher the rate of growth. The transformed structures became coarser after aging at higher temperatures (Figures 41a-d, shown by arrows). Sometimes the transformation would occur inside the matrix without apparently associating with any second phase, as shown in Figure 42. The new structure formed at 1000°C is coarser than that formed upon aging at 900°C with the same aging time (Figures 43a-b).

X-RAY DIFFRACTION PATTERN ANALYSIS

The interpretation of the X-ray diffraction data have been complicated by two factors. One is due to the

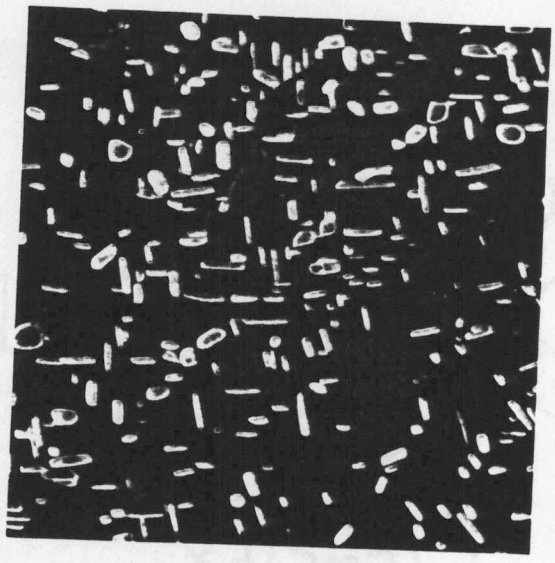

38a. Ni-Ta-Cr alloy, heated to 1280°C, 4 hrs after 1250°C, 7 days; only one second phase present, SEM, 200 X.

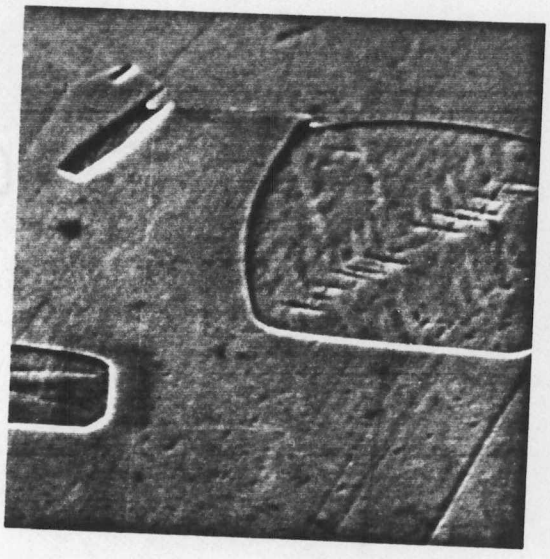

38b. Ni-Ta-Cr alloy, aged at 600°C for 100 hrs, water quenched, SEM, 5000X.

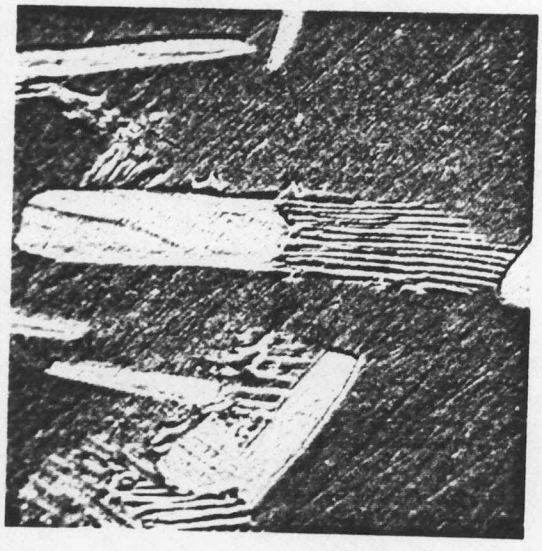

38c. Ni-Ta-Cr alloy, aged at 700°C, 100 hrs, then water quenched, SEM, 2000 X.

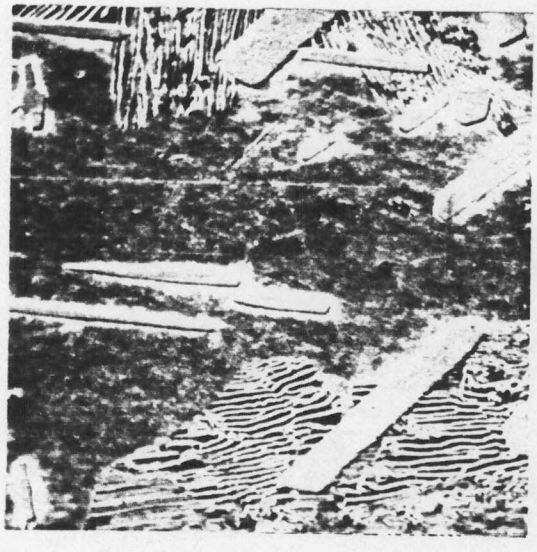

38d. Ni-Ta-Cr alloy, aged at 700°C, 100 hrs, then water quenched, SEM, 2000 X.

Figure 38. Scanning electron microstructures of the Ni-Ta-Cr alloy after solution treatment and aging at 600°C, 700°C for 100 hrs.

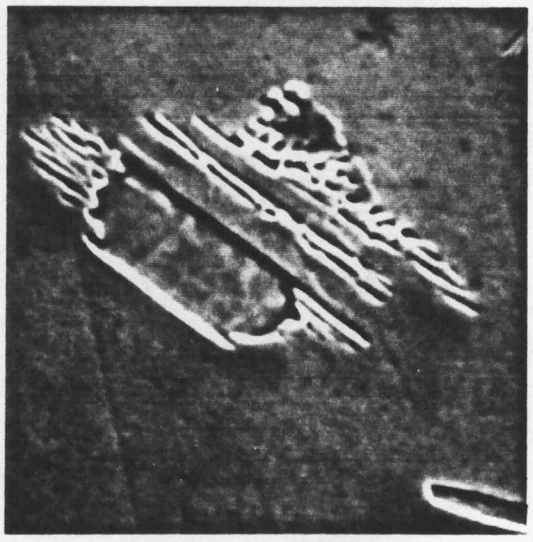

39a. Ni-Ta-Cr alloy, aged at 800°C, 1 hr, then water quenched, SEM, 5000 X.

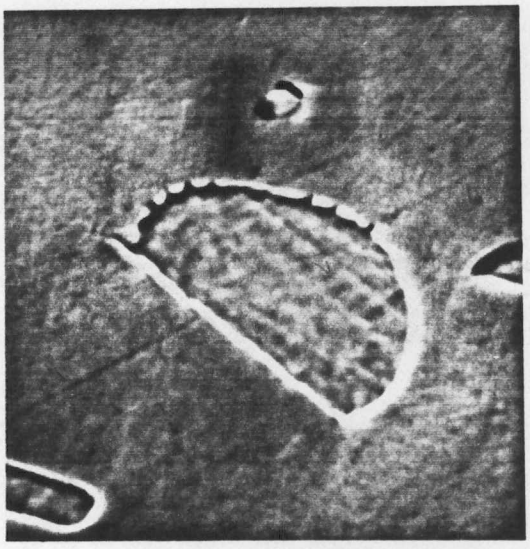

39b. Ni-Ta-Cr alloy, aged at 800°C, 1 hr, then water quenched, SEM, 5000 X.

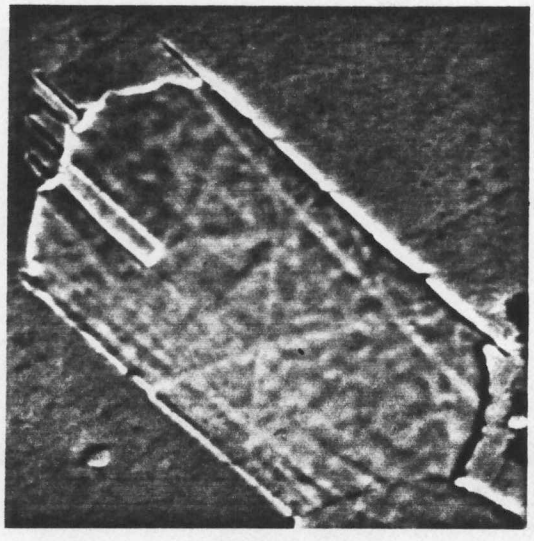

39c. Ni-Ta-Cr alloy, aged at 800°C, 1 hr, then water quenched, SEM, 5000 X.

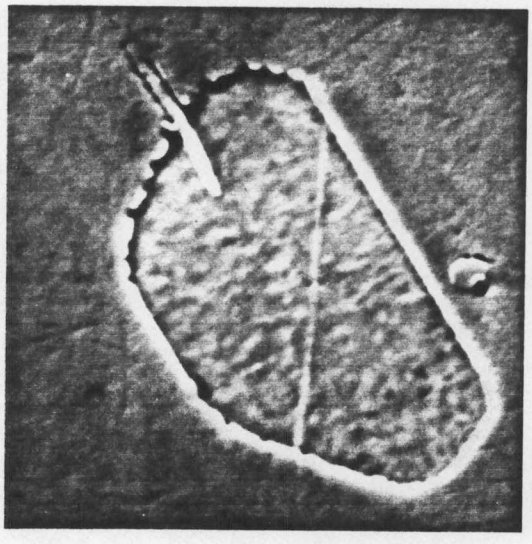

39d. Ni-Ta-Cr alloy, aged at 800°C, 1 hr, then water quenched, SEM, 5000 X.

Figure 39. Scanning electron microstructures of the Ni-Ta-Cr alloy after aging at 800°C for 1 hr.

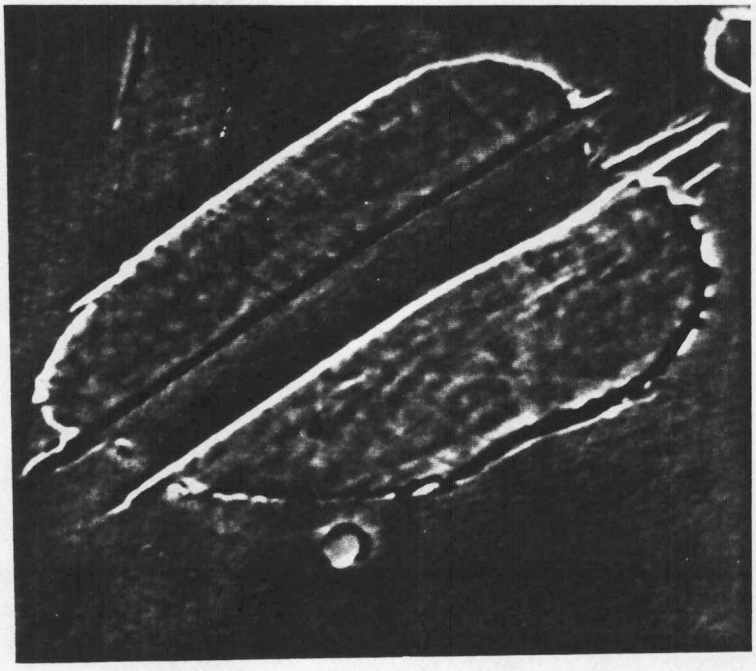

Figure 40. Ni-Ta-Cr alloy, aged at 800°C, 1 hr, water quenched, SEM, 5000X.

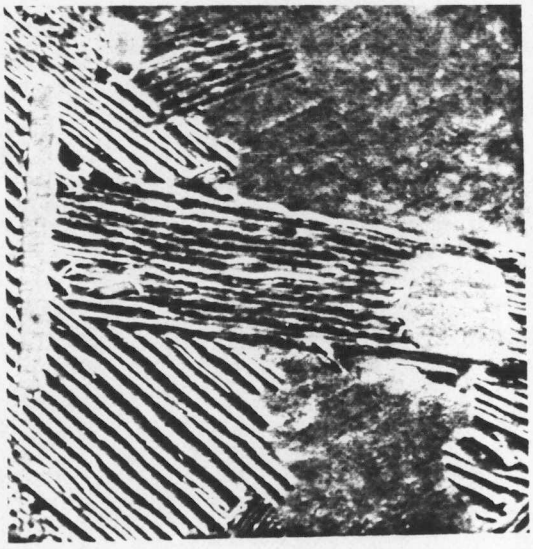

41a. Ni-Ta-Cr alloy, aged at 700°C, 500 hrs, then water quenched, SEM, 2000 X.

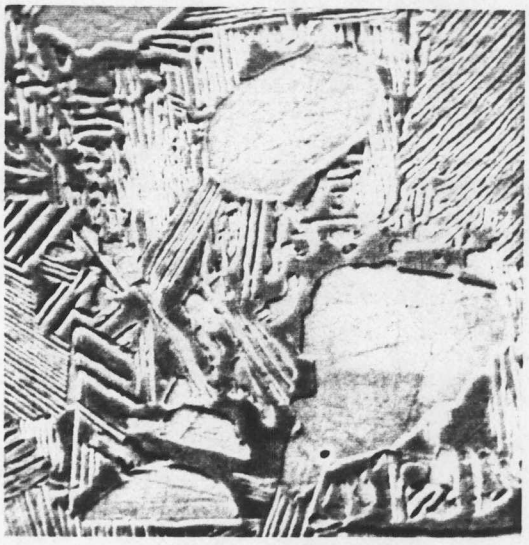

41b. Ni-Ta-Cr alloy, aged at 800°C, 500 hrs, then water quenched, SEM, 2000 X.

41c. Ni-Ta-Cr alloy, aged at 900°C, 500 hrs, then water quenched, SEM, 2000 X.

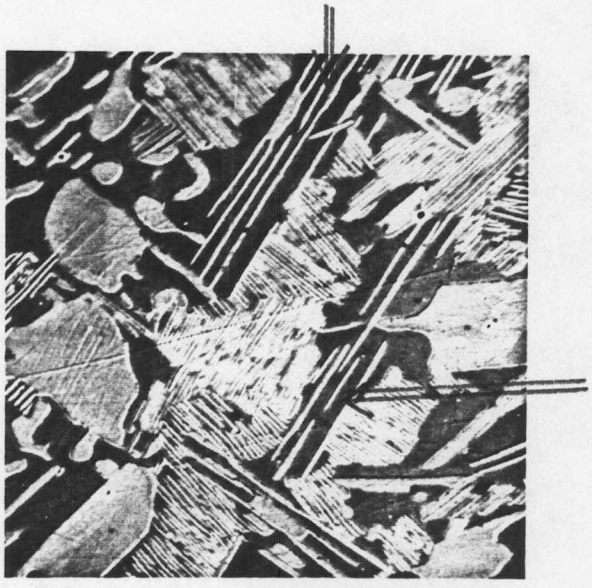

41d. Ni-Ta-Cr alloy, aged at 1000°C, 500 hrs, water quenched, SEM, 1000 X.

Figure 41. Scanning electron microstructures of the Ni-Ta-Cr alloy after aging at 700°C to 1000°C for 500 hrs.

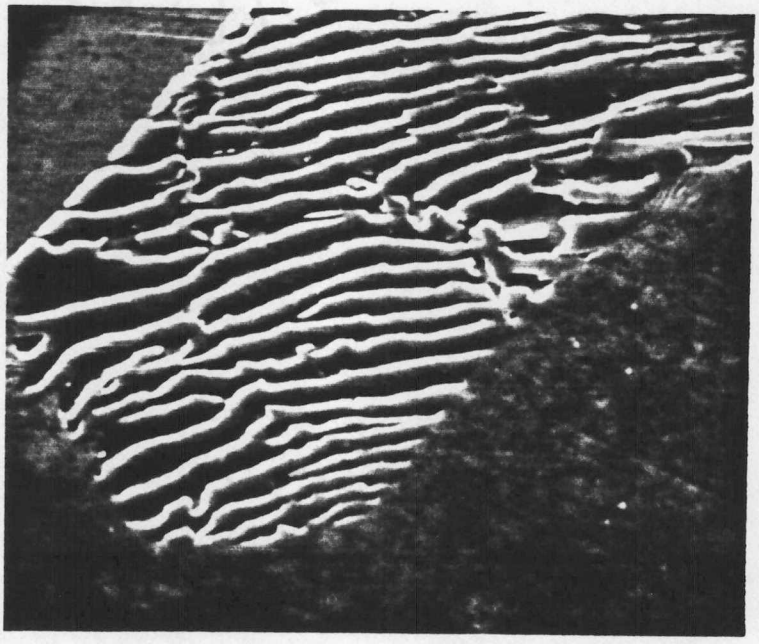

Figure 42. Ni-Ta-Cr alloy, aged at 700° C, 500 hrs, water quenched, SEM, 5000 X.

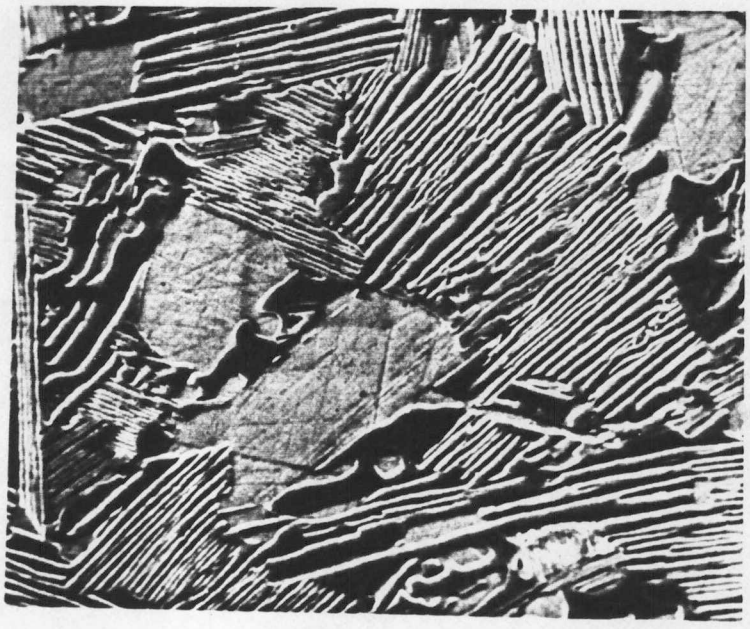

43a. Ni-Ta-Cr alloy, aged at 900°C, 1000 hrs, water quenched, SEM, 2000 X.

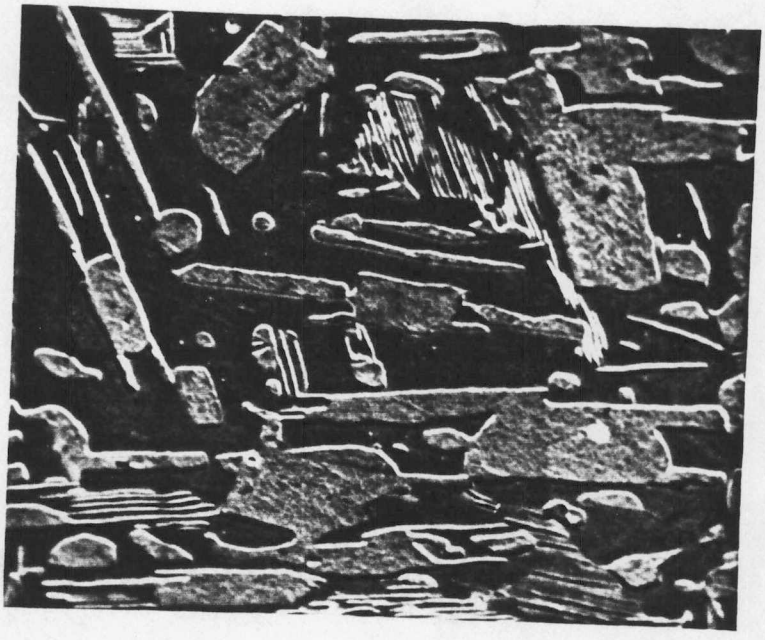

43b. Ni-Ta-Cr alloy, aged at 1000°C, 1000 hrs, water quenched, SEM, 2000 X.

Figure 43. Scanning electron microstructures of the Ni-Ta-Cr alloy after aging at 900°C and 1000°C for 1000 hrs.

experimental procedure of employing the metallographic samples for obtaining the diffractometer traces. Preferred orientation may have been present in the samples, and the grains of the samples (of the matrix and of any second phases present) may not have been sufficiently numerous nor sufficiently randomally oriented to allow obtaining a representative diffractometer trace of the actual structures present in the sample. The effect of this is that the intensity of the peaks may not have the proper relative value, and indeed some peaks may be missing.

The other factor relates to the literature data which were used to deduce the structures present. Initially, data were taken from the ASTM X-ray diffraction data files. However, these were found often to be quite contradictory, so the original sources were examined. It was then found that in some cases the original paper did not agree well with the data given in the ASTM file from the source given. Also, in many papers lack of detail about sample preparation techniques and heat treatments made comparison of these results to those obtained in the present research difficult and sometimes questionable.

For the reasons listed above, in the following section is presented again a brief review of the X-ray diffraction literature pertinent to the Ni-Ta and the Ni-Ta-Cr alloys, before discussing the experimental results.

(A) Brief review of x-ray results from literature for Ni_8Ta

An ordering reaction was observed by Larson et al. (17) in 1970 in a Ni-11.1 at.% Ta alloy that was aged below 570°C following quenching from elevated temperatures (1275°C). This reaction was investigated by employing electron diffraction microscopy, X-ray diffraction, and electrical resistivity techniques. The critical temperature for the order-disorder reaction was estimated to be 843 K (570°C) for Ni_8Ta by Moreen et al. (27) in 1971 (see Figure 10). In 1983, Nash and West worked on a Ni-20 at.% Ta alloy in order to clarify the phase equilibria in the Ni-rich region of Ni-Ta system. Their results confirmed the existence of the compound Ni_8Ta up to 1593 K. The peritectoid temperature was found to lie between 1593 and 1613 K. The phase diagram revised by Moffatt (32) includes the existence of Ni_8Ta only below 843 K. This phase was not found by Larson et al. (17) after quenching from 1473 K; it was found by Chakravorty and West (33) to be present after annealing in the range 1423-1573 K, but not for annealing at 1613 K. The work of Chakravorty and West published in 1983 (33) shows that $Ni_8(Ta,Mo)$ has a body-centered tetragonal structure after annealing at 1523 K (1250°C), determined by X-ray diffraction data. This indicates that Ni_8Ta exists as an ordered structure at temperatures higher than the order-disorder formation temperature 570°C given by Larson et al. (17) and Moreen et al.(27) as mentioned above. It's obvious

that there exists some contradiction in these results. For the Ni-rich binary Ni-Ta alloy, the region around 10 at.% Ta is still not well defined in the equilibrium phase diagram.

(B) The experimental results of the present work and the methods of identifying the structure

The X-ray diffraction data obtained consist of diffractometer traces from the metallographic samples. For such traces, the 2θ locations of the peaks depend upon the crystal structure of the phase, but the phase must be present in amounts exceeding approximately 5% to be detectable. Also, as mentioned at the beginning of this section, the intensity is quite sensitive to a number of experimental factors. Prominent among these is preferred orientation, which can be sufficiently developed to make peaks even be missing.

In the experimental method used in this research to obtain the diffractometer traces, no attempt was made to avoid or minimize the experimental problems which might affect intensity. Also, no attempt was made to analyze the X-ray diffraction data to deduce the crystal structure. Instead, the approach taken to use the X-ray diffraction data for phase identification has been to compare visually the X-ray diffractometer traces to the location of peaks reported for phases which are known to form, or suspected to form, in Ni-Ta or Ni-Ta-Cr alloys.

The phases for which comparison was made were identified from the literature and from the ASTM X-ray diffraction files. Thus, in addition to the expected face-centered cubic disordered phase, there are several ordered compounds which might be present. The ASTM X-ray diffraction files listed the d-spacings, and these were combined with the wavelength (used to obtain the experimental diffractometer traces in the present research) to calculate the 2θ locations for the peaks. For the compounds, the literature listed many peaks, many of which were listed as weak intensities (e.g., 5% out of 100%). It was expected that many of these weak peaks would not be present in an experimental diffractometer trace, but the stronger peaks would if the phase was present in sufficient amount (e.g., greater than 5 volume per cent), and if preferred orientation is not too severe. Thus, for the compounds, only the locations of the stronger peaks were used for comparison to the experimental diffractometer traces.

For ease of comparison, a trace of the peak for each compound was sketched, with each strong peak located at the proper 2θ value and the listed relative intensity correct. These traces will be referred to as reference traces. In the figures to follow which present the experimental diffractometer traces of the alloys, above these traces is presented the sketched reference traces for various compounds.

A search of the literature, and especially of the ASTM X-ray diffraction files, listed data for the compounds Ni_8Ta and Ni_3Ta. There was only one source of data for the Ni_8Ta compound (ASTM file number 23-438) but there were three for Ni_3Ta (ASTM file numbers 18-893, 17-699, 19-855). Only the appropriate strong peaks (as indicated above), as tabulated in Table 6, were used. The lattice parameter used in calculating the FCC structure was taken to be 3.853 $\mathring{A}$ from Figure 4a for both binary and ternary alloys due to the lack of information of lattice parameter for the ternary alloy. Also, the 2θ values of the FCC peaks for a given {hkl} agreed within 0.1 degree for both alloys. Tables 7 and 8 show the original d-spacings and the relative intensity listed in the computer files which are connected with the Rigaku X-ray diffractometer. Tables 9. through 12 are the original X-ray diffraction data which are the sources for the ASTM X-ray data files. By examining the ASTM file data we find that some of the listed relative intensity values are referred to by letters only (e.g., s+, s, ss, mst), not numbers. A peak might be listed to be medium strong (e.g., 50% out of 100%) in the ASTM file while in the source article being indicated to be a weak peak as 10% out of 100%. All these deviations will influence the accuracy of the reference traces.

Table 6. 2θ and relative intensities of FCC, Ni_8Ta (#23-438) and three types of Ni_3Ta (#17-699, #18-893, and #19-855).

FCC	Ni_8Ta (23-438)		Ni_3Ta (17-699)		Ni_3Ta (18-893)		Ni_3Ta (19-855)	
2θ	2θ	I	2θ	I	2θ	I	2θ	I
43.76	16.53	20	27.38	25	27.48	60	27.48	20
50.98	43.75	60	40.70	55	35.20	50	40.51	20
74.98	50.94	20	43.14	70	43.00	100	41.08	30
90.99	74.80	100	45.65	70	44.40	50	42.97	70
96.38	91.90	60	46.14	100	50.50	50	44.26	100
118.80	119.4	20	60.60	40	73.00	80	47.29	30
			73.50	70	74.30	50	48.33	80
			74.87	40	87.20	50		
			80.10	40	89.70	80		
			80.90	70	94.00	50		
			88.00	100	117.30	25		
			90.20	85	120.54	25		
			92.40	85				
			93.40	55				
			99.70	40				
			101.50	40				

* wavelength of Cu ($K\alpha_1$) = 1.540562Å
Cu ($K\alpha_2$) = 1.544390Å

Table 7. The d-spacings and relative intensity of Ni_8Ta (#23-438) listed in the computer file.

23 438 (NIB TA) NICKEL TANTALUM					
5.371	20	1.236	5	0.842	5
3.791	5	1.203	5	0.839	5
3.241	5	1.184	5	0.821	60
2.696	5	1.148	5	0.820	5
2.473	5	1.129	5	0.810	5
2.403	5	* 1.074	60	0.804	5
* 2.072	60	1.071	5	0.801	30
1.901	5	1.050	5	0.793	20
1.820	5	1.036	5	0.786	20
* 1.795	20	1.031	5		
1.718	5	1.000	5		
1.645	5	0.995	5		
1.624	5	0.948	5		
1.493	5	0.920	5		
1.438	5	0.910	5		
1.400	5	* 0.894	20		
1.352	5	0.883	5		
1.315	5	0.871	5		
1.307	5	0.863	5		
* 1.271	100	0.849	5		

* - Used to compared with the experimental diffractometer traces.

Table 8. The d-spacings and relative intensity of three types of Ni_3Ta (B.C.T., monoclinic, and orthorhombic) listed in the computer file.

18 893 (NI3 TA) NICKEL TANTALUM			
3.700	20	* 1.119	50
* 3.250	60	* 1.095	80
* 2.557	50	* 1.055	50
2.210	20	1.021	20
* 2.108	100	0.994	20
* 2.044	50	0.975	20
1.879	10	* 0.931	25
1.862	20	* 0.904	25
* 1.810	50	0.889	25
1.630	20	0.872	20
1.584	25	0.853	10
1.506	20	0.842	80
1.377	10		
1.359	25		
* 1.298	80		
* 1.278	50		
1.243	10		
1.211	20		
1.191	10		
1.145	10		

19 855 (NI3 TA) NICKEL TANTALUM			
4.271	5	1.631	10
3.371	10	1.603	10
* 3.250	20	1.600	5
2.959	10	1.583	10
2.822	10	1.506	15
2.564	10	1.464	5
2.259	5	1.429	5
* 2.230	20	1.411	10
* 2.200	30	1.400	5
2.134	10	1.374	10
* 2.108	70	1.361	10
2.067	10		
* 2.049	100		
1.973	5		
* 1.925	30		
1.886	80		
1.825	10		
1.698	5		
1.680	5		
1.666	10		

17 699 (NI3 TA) NICKEL TANTALUM			
3.401	25	* 1.290	70
3.261	25	* 1.270	40
3.110	25	1.230	10
2.641	25	* 1.200	40
2.560	25	* 1.190	70
2.270	25	1.180	10
* 2.220	55	1.140	10
* 2.100	70	1.130	10
2.060	10	* 1.110	100
* 1.990	70	* 1.090	85
* 1.970	100	1.080	10
1.790	10	* 1.070	85
1.630	10	* 1.060	55
1.570	25	* 1.010	40
1.540	10	* 0.997	40
* 1.530	40		
1.470	25		
1.370	25		
1.350	10		
1.340	10		

* -

Used to compared with the experiemntal diffractometer traces.

Table 9. X-ray diffraction data of Ni_8Ta which is the source listed as #23-438 in the ASTM file.

θ Values for Ni_8X				
	$(h\ k\ l)$		θ, deg. Ni_8Ta	θ, deg. Ni_8Nb
2 0 0			8.24	8.18
2 2 0			11.72	11.70
1 1 1			13.75	13.70
4 0 0			16.60	16.56
3 1 1			18.15	18.12
4 2 0			18.70	18.62
*3 3 1			21.82	21.78
4 4 0			23.90	23.84
5 1 1			25.04	24.98
*6 0 0	0 0 2		25.41	25.36
6 2 0	0 2 2		26.64	
5 3 1			27.92	
6 4 0	2 2 2		28.32	
0 4 2			31.05	31.00
4 2 2			32.38	32.25
5 5 1	1 7 1		33.38	33.20
8 0 0			34.72	
3 7 1			35.85	35.72
8 2 0	4 4 2		36.12	
*6 6 0	0 6 2		37.32	37.20
6 2 2			38.55	38.18
8 4 0			39.82	
7 5 1	1 1 3		40.60	40.52
6 4 2			42.15	
9 1 1	1 3 3		43.04	42.86
*3 3 3	9 3 1		45.82	45.72
10 0 0	8 6 0	0 8 2	46.00	
10 2 0	8 2 2		47.20	
7 7 1	5 1 3		48.02	
*6 6 2			48.35	48.28
5 3 3	9 5 1		50.38	
10 4 0	8 4 2		50.72	50.58
8 8 0			54.35	
11 1 1	7 1 3	5 5 3	55.28	55.22
8 6 2	10 0 2	10 6 0	56.88	56.84
11 3 1	9 7 1	7 3 3	57.80	57.75
*12 0 0	0 0 4		59.45	59.35
12 2 0	0 2 4		60.78	
10 4 2	2 2 4		62.15	62.08
11 5 1	7 5 3		63.25	63.14
12 4 0	0 4 4		65.08	65.02
9 1 3			66.28	66.12
10 8 0	2 4 4	8 8 2	66.65	
*9 9 1	9 3 3		69.60	69.40
10 6 2			70.02	
4 4 4			70.70	
11 7 1	13 1 1	7 7 3	73.45	73.25
*12 6 0	0 6 4		73.92	73.78
12 2 2	6 2 4		76.32	76.12
13 3 1	9 5 3		78.40	78.12

*Fundamental x-ray diffraction lines $(h\ k\ l)$ fct = $(3h, 3k, l)$ fcc.

Table 10. The calculated and observed $\sin^2\theta$ and intensity of β-Ni_3Ta published by Nowotny et al. (2) in 1964. This is identified to be B.C.T. structure and #18-893 listed in the ASTM file.

(hkl)	$10^3 \cdot \sin^2\theta$ beobachtet	$10^3 \cdot \sin^2\theta$ berechnet	Intensität beobachtet	Intensität berechnet
(002)	43,2	42,8	s	6,1
(101)	56,1	56,0	mst	17,6
(110)	90,8	90,6	m	4,8
—	121,5	—	s	Fremdlinie
(112)	133,5	133,4	sst	54,6
(103)	142,0	141,5	m K	5,1
—	168,0	—	ss	Fremdlinie
(004)	171,2	171,1	s	9,2
(200)	181,0	181,2	m	16,8
(202)	223,3	224,0	s	2,6
(211)	236,5	237,2	s+	4,7
(114)	261,6	261,7	s	2,0
(105)	312,7	312,6	ss	1,5
(213)	321,5	322.7	s+	2,9
(204)	352,1	352,3	st	11,1
(220)	363,0	362,4	m	5,3
(006)	384,1	384,9	ss	0,3
(222)	404,6	405,2	s	1,0
(301)	418,3	418,4	ss	1,0
(310)	452,9	453,0	ss	0,9
(116)	474,2	475,5	m	7,1
(215)	494,8	493,8	st	1,6
(312)		495,8		13,5
(303)	—	503,9	—	0,8
(224)	533,1	533,5	m	6,3
(206)	569,6	566,1	s	0,7
(107)		569,2		0,7
(321)	600,5	599,6	s	1,4
(314)	624,3	624,1	s	1,4
(305)	—	675,0	—	0,7
(323)	684,1	685,1	s+	1,4
(400)	725,4	724,8	s+	2,9
(226)	750,0	747,3	s+	0,8
(217)		750,4		1,5
(402)	—	767,6	—	0,8
(118)	—	774,9	—	0,8
(411)	779,6	780,8	s	1,6
(330)	814,7	815,4	ss	0,4
(316)	837,2	837,9	st	14,3

Table 11. X-Ray diffraction data of monoclinic Ni_3Ta which is the source of #19-855 listed in the ASTM file (12).

$a_o = 5.12_8$ Å; $b_o = 4.52_2$ Å; $c_o = 25.37$ Å; $\alpha = 90°50'$
(only lines with calculated intensity >0.1 are presented)

hkl	$\sin^2\theta$ obs.	$\sin^2\theta$ calc.	Intensity est.	Intensity calc.
001	—	0.0301	—	0.26
012	0.0326	0.0324	~½	0.91
014	—	0.0444	—	0.21
01$\bar{5}$	0.0524	0.0514	1	1.97
111		0.0527		3.42
1$\bar{1}$2	0.0561	0.0550	2	0.32
106		0.0558		5.09
114	0.0679	0.0670	1	0.76
1$\bar{1}$5	0.746	0.0740	<1	0.17
017		0.0754		1.22
200	0.0904	0.0905	1	1.37
117	—	0.0980	—	0.12
1$\bar{1}$8	—	0.1095	—	0.39
021	0.1165	0.1168	~½	0.48
022	~0.1190	0.1205	2	1.72
211		0.1206		0.92
01, 10	~0.1226	0.1229	3	0.17
2$\bar{1}$2		0.1229		3.34
024	0.1305	0.1298	1	0.51
00, 12	0.1337	0.1330	7	7.89
214		0.1349		0.96
121	0.1391	0.1395	~1	1.03
025	0.1415	0.1408	10	5.05
2$\bar{1}$5		0.1418		10.00
124	0.1527	0.1524	<½	0.24
027	0.1603	0.1594	3	4.16
1$\bar{1}$, 11		0.1618		0.84
217	0.1670	0.1658	8	7.82
2$\bar{1}$8	0.1785	0.1774	1	0.62
028		0.1777		0.31
128	—	0.2003	—	0.16
02, 10	0.2061	0.2055	½	0.74
11, 13	~0.2105	0.2097	½	0.57
222		0.2110		0.15
21, 10	0.2140	0.2134	1	1.39
20, 12	0.2235	0.2234	1	0.74
2$\bar{1}$, 11	—	0.2296	—	0.33
02, 11	0.2313	0.2312	<1	0.16
225		0.2312		0.49
311	~0.2330	0.2337	~½	0.48
306	0.2371	0.2368	1	0.67
314	—	0.2480	—	0.11
227	—	0.2498	—	0.43
12, 11	—	0.2539	—	0.42
030	0.2620	0.2615	1.5 (texture)	0.29
02, 13	—	0.2684	—	0.12
21, 13	0.2773	0.2775	<½	0.24
12, 13	0.2910	0.2910	½	0.34
0$\bar{1}$, 17	—	0.2934	—	0.17
2$\bar{1}$, 14	0.2984	0.2984	1	0.79
02, 14	~0.3010	0.3014	½	0.39
136	0.3150	0.3146	1	0.43
136	0.3208	0.3200	1	0.42

Table 12. X-ray diffraction data of orthorhombic Ni_3Ta which is the source of #17-699 listed in the computer file (3).

Ni_3Ta

$\sin^2\theta$ observed	$\sin^2\theta$ calculated	I° observed	Type β-$TiCu_3$ hkl°°°	I°° calculated
Does not exist	0.036	0	100	0
•	0.046	0	001	3.4
•	0.052	0	010	0
0.082	0.082	2	101	19.5
0.088	0.088	2	110	26.0
0.098	0.098	2	011	19.6
0.145	0.131	2	111	12.1
0.144	0.144	2	200	12.0
0.181	0.181	2	002	29.0
0.191	0.190	4	201	53.5
Does not exist	0.196	0	210	0
0.212	0.209	3	020	103.6
0.220	0.219	1	102	17.0
0.236	0.236	5	012	152.0
0.253	0.242	7	211	301.0
Does not exist	0.245	0	120	0
•	0.255	0	021	5.4
•	0.272	0	112	10.4
0.291	0.291	1	121	31.2
Does not exist	0.321	0	202	0
•	0.327	0	202	4.9
0.351	0.351	1	220	18.5
0.372	0.369	1	301	11.8
0.381	0.376	2	310	17.9
	0.380		212	26.8
0.395	0.392	1	022	39.8
0.401	0.399	3	221	77.5
Does not exist	0.412	0	311	8.8
•	0.422	0	311	8.7
0.430	0.428	2	122	26.0
Does not exist	0.438	0	103	0
•	0.465	0	013	0

Ni_3Ta

$\sin^2\theta$ observed	$\sin^2\theta$ calculated	I° observed	Type β-$TiCu_3$ hkl°°°	I°° calculated
Does not exist	0.470	0	103	0
0.500	0.501	2	113	31.4
0.510	0.507	1	302	11.8
	0.509		130	15.7
0.519	0.517	1	031	11.8
Does not exist	0.533	0	320	0
•	0.536	0	222	7.7
•	0.553	0	131	7.7
0.557	0.556	5	203	131.0
Does not exist	0.559	0	312	7.5
0.576	0.576	3	400	65.6
Does not exist	0.579	0	321	22.4
•	0.609	0	213	0
•	0.615	0	230	0
0.621	0.621	1	023	14.1
	0.621		401	14.1
Does not exist	0.628	0	410	0
0.654	0.654	3	032	80.0
Does not exist	0.658	0	123	0
0.663	0.661	5	231	180.0
0.676	0.675	1	411	20.2
Does not exist	0.681	0	132	6.7
0.717	0.717	1	322	20.2
0.733	0.733	1	004	14.4
Does not exist	0.736	0	303	0
0.768	0.760	1	402	28.8
	0.765		223	220.0
Does not exist	0.769	0	104	0.5
0.785	0.785	6	014	81.5
	0.785		420	107.5
	0.789		313	25.2
0.840	0.795	1	330	12.4
	0.799		232	18.6

Ni_3Ta

$\sin^2\theta$ observed	$\sin^2\theta$ calculated	I° observed	Type β-$TiCu_3$ hkl°°°	I°° calculated
0.812	0.811	6	412	156.0
Does not exist	0.820	0	114	8.2
•	0.821	0	421	8.2
0.838	0.839	4	040	52.0
Does not exist	0.840	0	331	8.2
•	0.874	0	140	0
•	0.877	0	204	3.1
•	0.894	0	041	3.1
•	0.894	0	033	0
•	0.900	0	340	0
0.919	0.920	3	133	23.2
	0.920		141	17.6
Does not exist	0.939	0	214	17.6
0.942	0.942	3	024	25.0
Does not exist	0.945	0	323	0
•	0.945	0	501	8.8
•	0.950	0	510	11.8

The reference traces are sketched in Figure 44, and these traces are used in the following figures for visual comparison to the experimental traces.

(a) Ni-Ta alloy

The observed 2θ and relative intensities of Ni-Ta alloys are listed in Table 13. Figures 45a-f show the comparisons between the experimental results and the reference FCC and Ni_8Ta traces.

For the solution treated condition, as shown in Figure 45a the observed peaks are at 2θ =43.5° (strongest), 50.9° (medium strong), 74.1° (medium), 91.0°(medium), and 96.8° (strong). Although there is no peak at 119.0°, it may be missing due to the factors mentioned earlier (e.g., preferred orientation). After aging at 600°C for 1000 hrs, as shown in Figure 45b the strongest peak is still at 2θ = 43.8°. The other peaks show very well, including the one at 119.0°. After aging at 900°C for 500 hrs, the peak at 50.9° becomes the strongest one (so does the trace of 1000°C for 500 hrs as shown in Fig. 45e) and the peaks at 74.0°, 91.0° and 119.0° are relatively strong (Fig. 45c).

A very low scanning speed was also applied for several specimens to examine in more detail the peaks. The results are shown in Table 14 and Figures 46a-d. The low-scanning diffraction patterns show that peaks are located at : 2θ = 43.94°, 51.06°, 75.06°, 91.10°, 96.32° after aging at 600°C

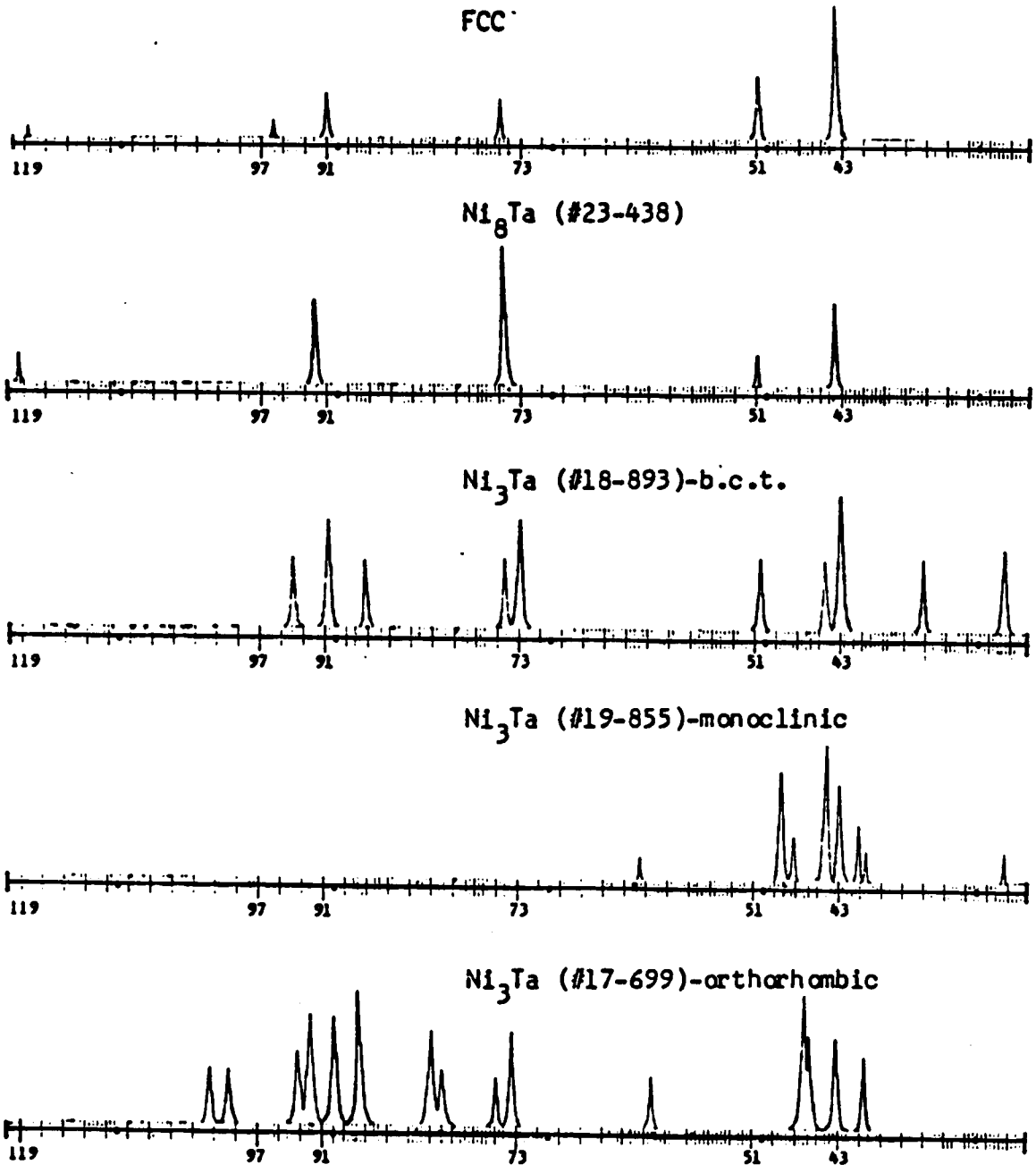

Figure 44. Diffractometer traces of FCC, Ni_8Ta (#23-438), and three types of Ni_3Ta (#18-893, #17-699 and #19-855) which are listed in the computer file.

Table 13. Experimental 2θ values and relative intensities of Ni-Ta alloy (solution treated condition and aging at 600°C, 900°C, 1000°C for 1000 hours).

Sample treated condition	1250°C, 7 days. (Fig. 45a)	600°C 1000 hrs (Fig. 45b)	900°C 1000 hrs (Fig. 45d)	1000°C 1000 hrs (Fig.45f)
2θ	44.15	43.90	43.80	43.90
relative I	100	> 100	100	43
2θ	51.20	51.05	50.94	51.05
relative I	28	100	25	100
2θ	75.20	75.05	74.80	75.10
relative I	5	27	19	72
2θ	91.40	91.09	90.90	118.00
relative I	9	42	16	10
2θ		96.31	96.20	
relative I		48	18	

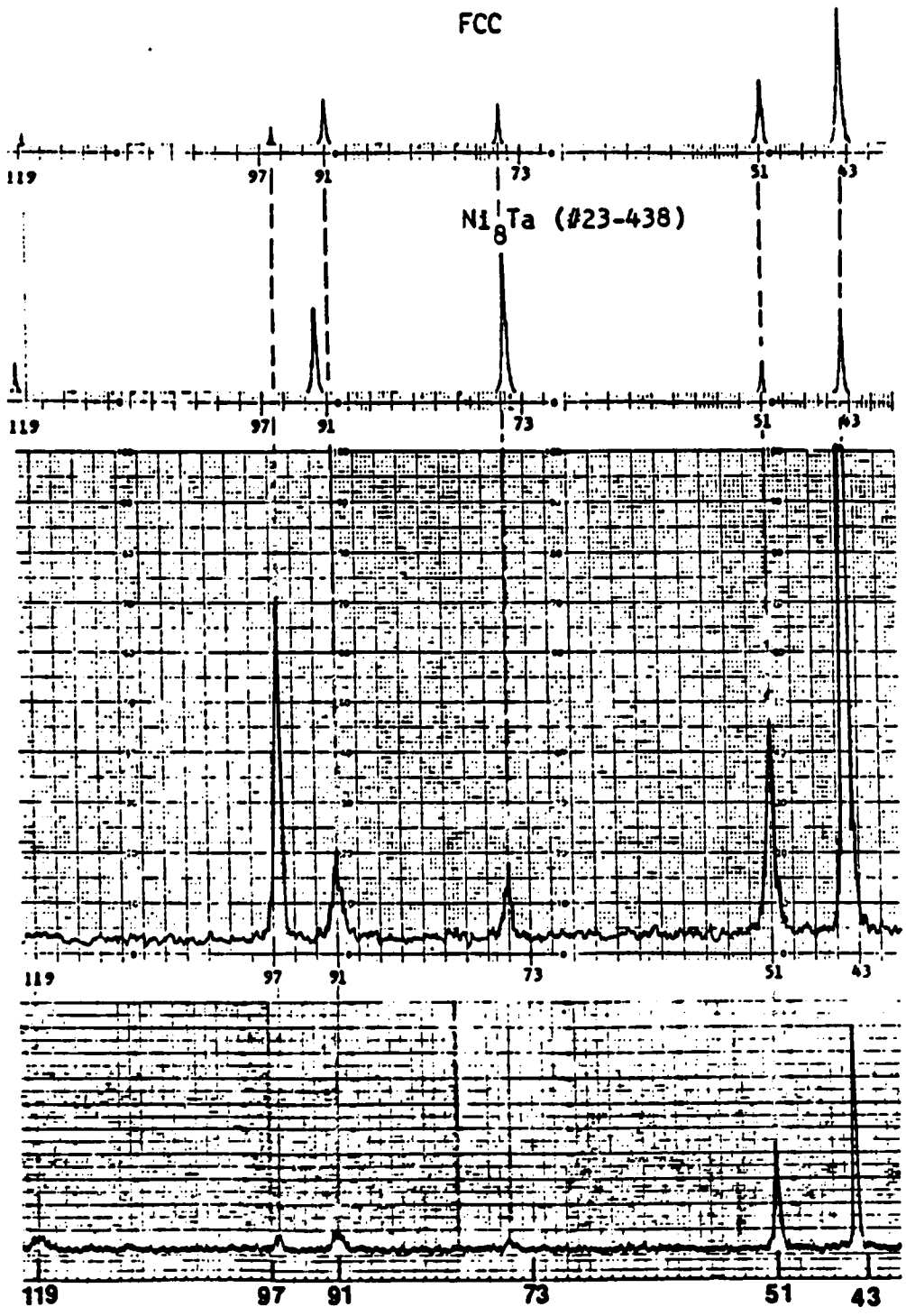

45a. Diffractometer trace of as-quenched Ni-Ta alloy.

Figure 45. Diffractometer trace of the Ni-Ta alloy after solution treatment and aging.

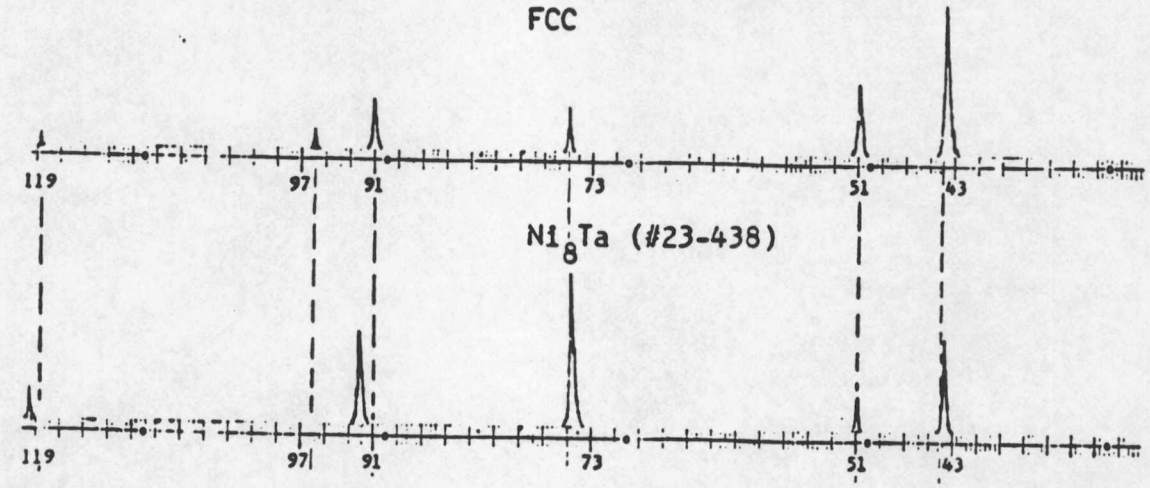

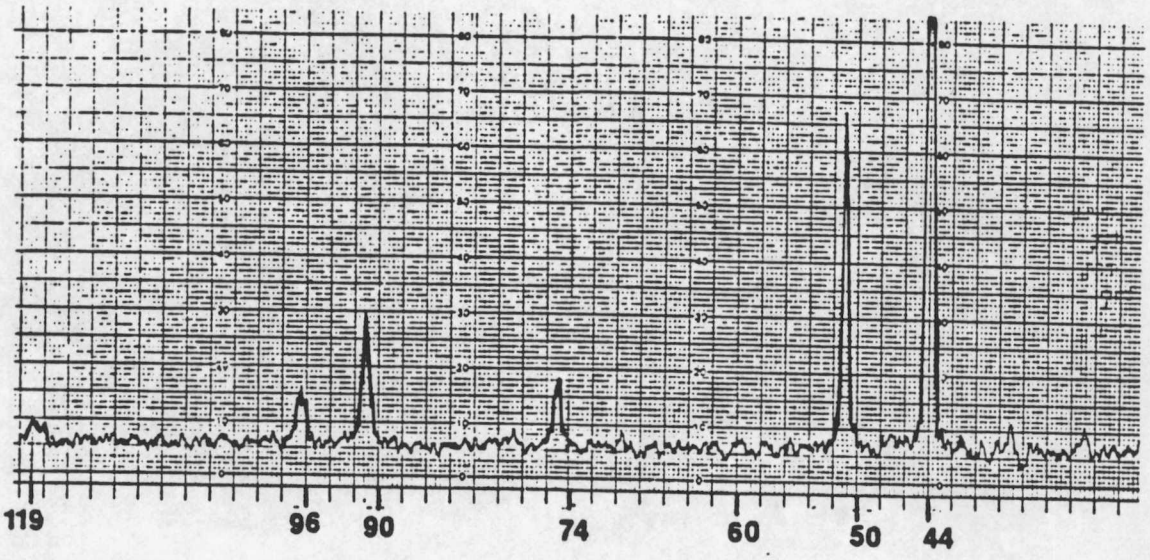

45b. Diffractometer trace of Ni-Ta alloy aged at 600°C for 1000 hrs.

Figure 45. (Continued)

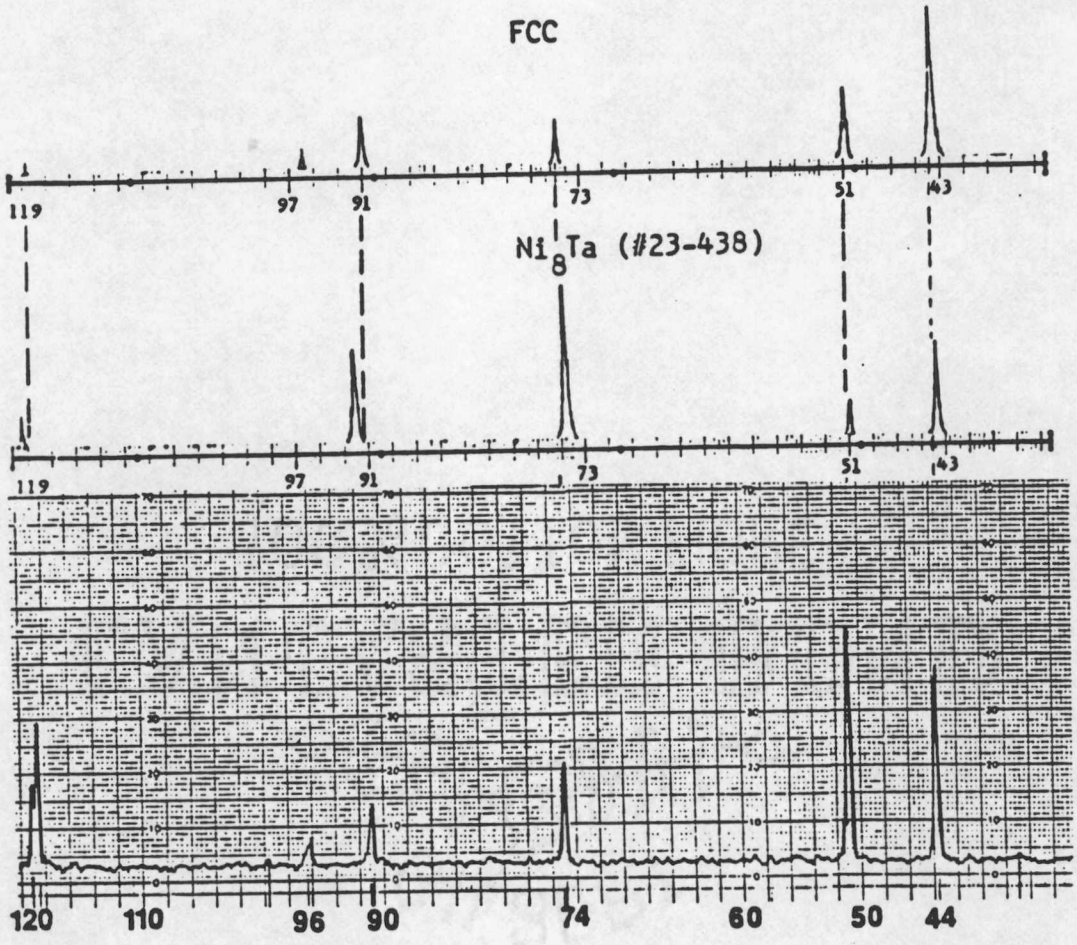

45c. Diffractometer trace of Ni-Ta alloy aged at 900°C for 500 hrs.

Figure 45. (Continued)

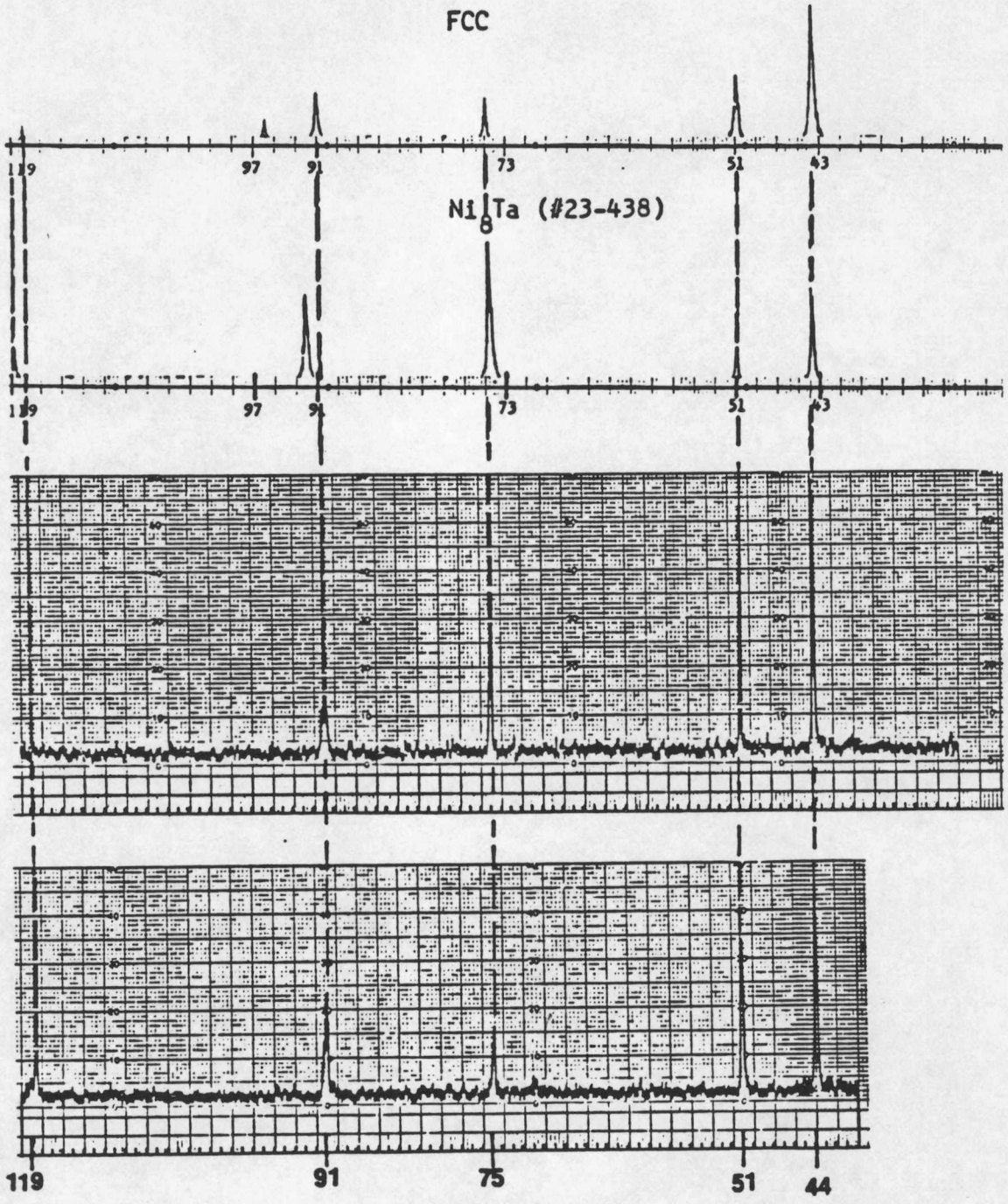

45d. Diffractometer trace of Ni-Ta alloy aged at 900° C for 1000 hrs.

Figure 45. (Continued)

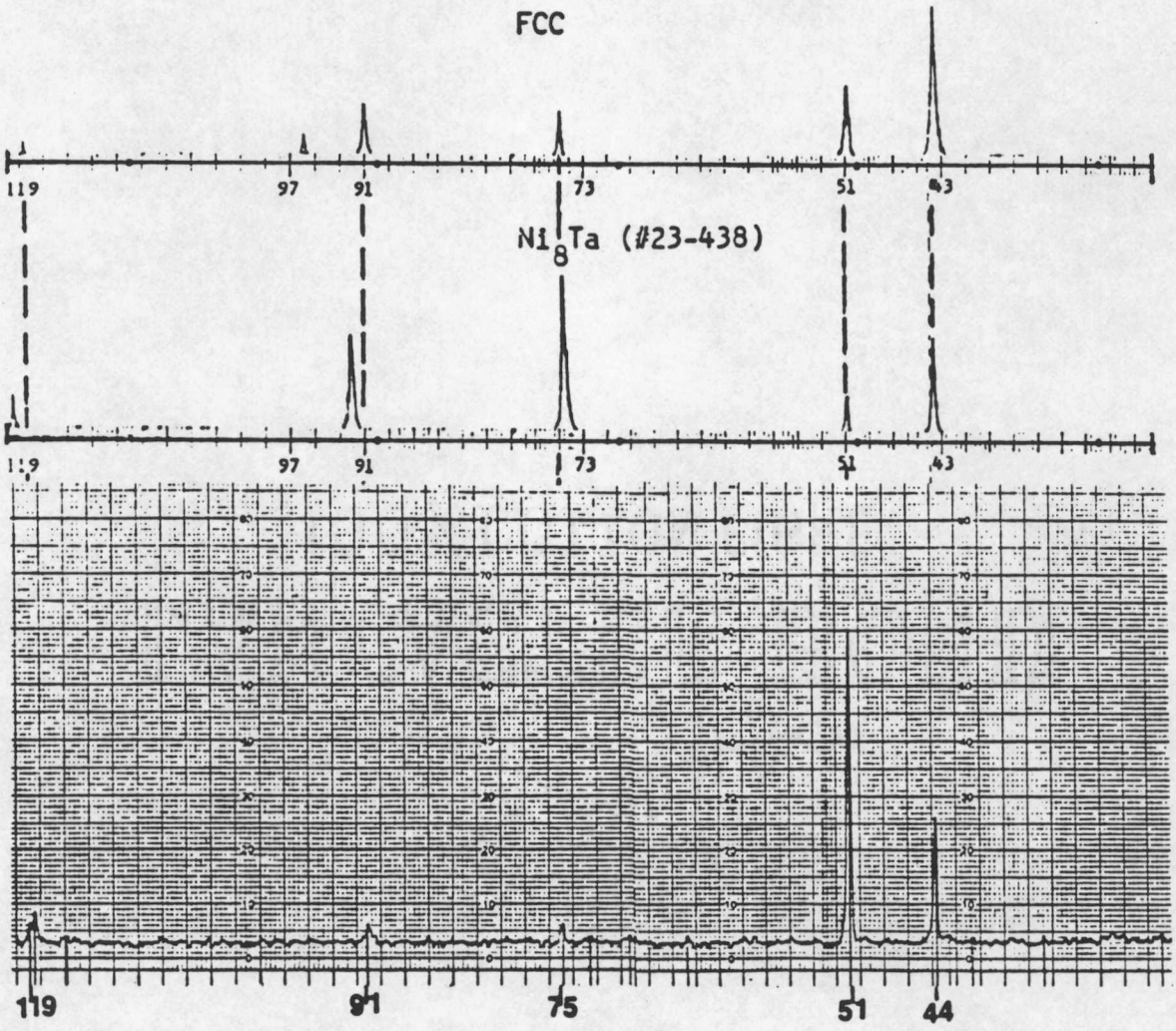

45e. Diffractometer trace of Ni-Ta alloy aged at 1000°C for 500 hrs.

Figure 45. (Continued)

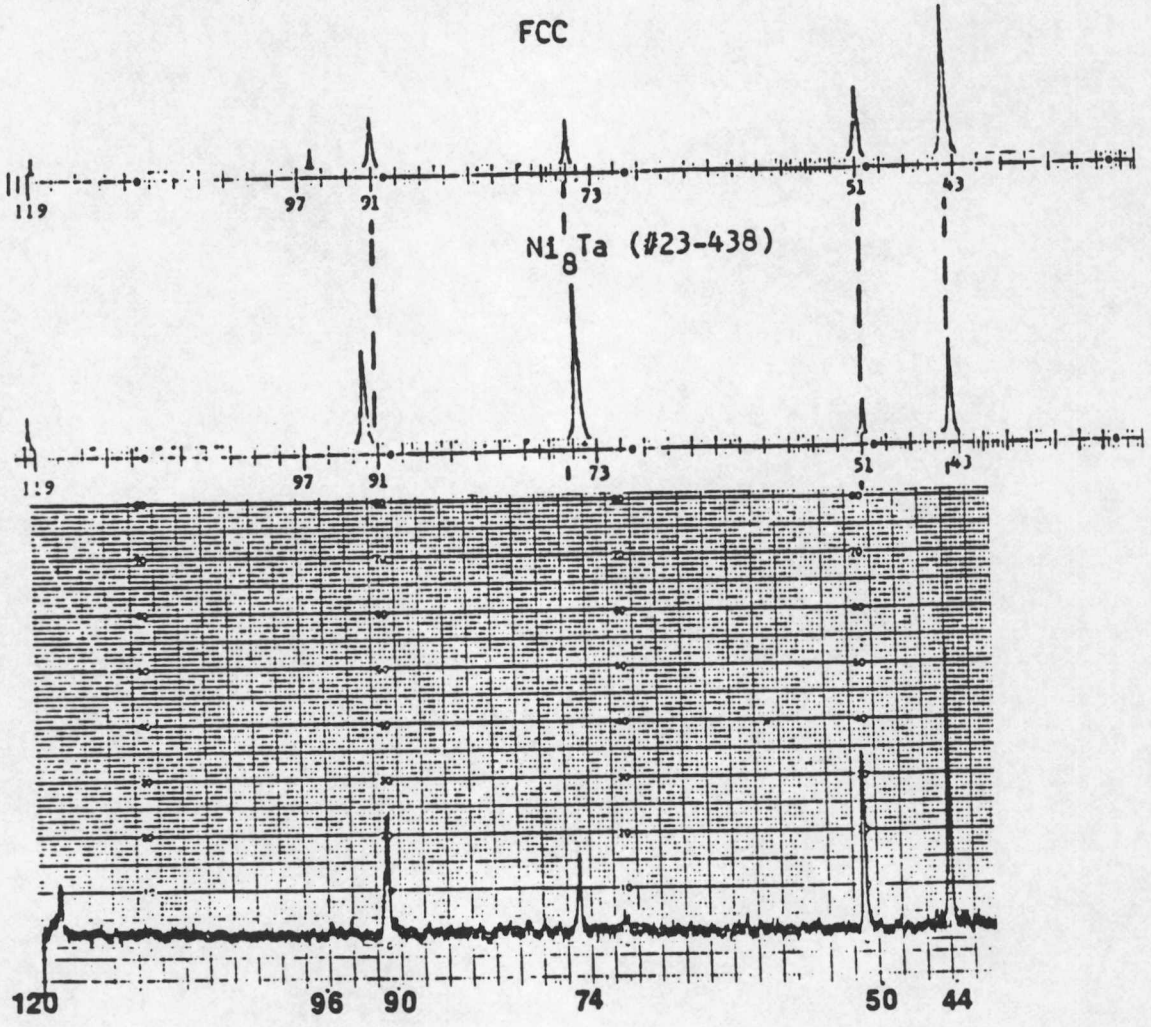

45f. Diffractometer trace of Ni-Ta alloy aged at 1000° C for 1000 hrs.

Figure 45. (Continued)

Table 14. The observed diffractometer traces by slowly scanning which are compared with FCC and Ni_8Ta traces.

(hkl)	FCC		Ni_8Ta	1000 hrs		
	*$K\alpha_1$	$K\alpha_2$		600°C	900°C	1000°C
111	43.74	43.85	43.64	43.94	*43.75 43.80	43.93
200	50.95	51.08	50.82	51.06	*50.90 51.20 51.35	51.00 *51.15 51.30
220	74.92	75.14	74.64	75.06	*74.90 75.15	*74.85 75.10
311	90.90	91.28	91.64	91.11	*90.95 91.20	---
222	96.31	96.62	96.70	96.32	*96.40 96.70	*95.90 96.25
400	118.67	119.15	118.90	---	*118.60 119.14	118.42 *118.94 119.52

* indicates stronger peak

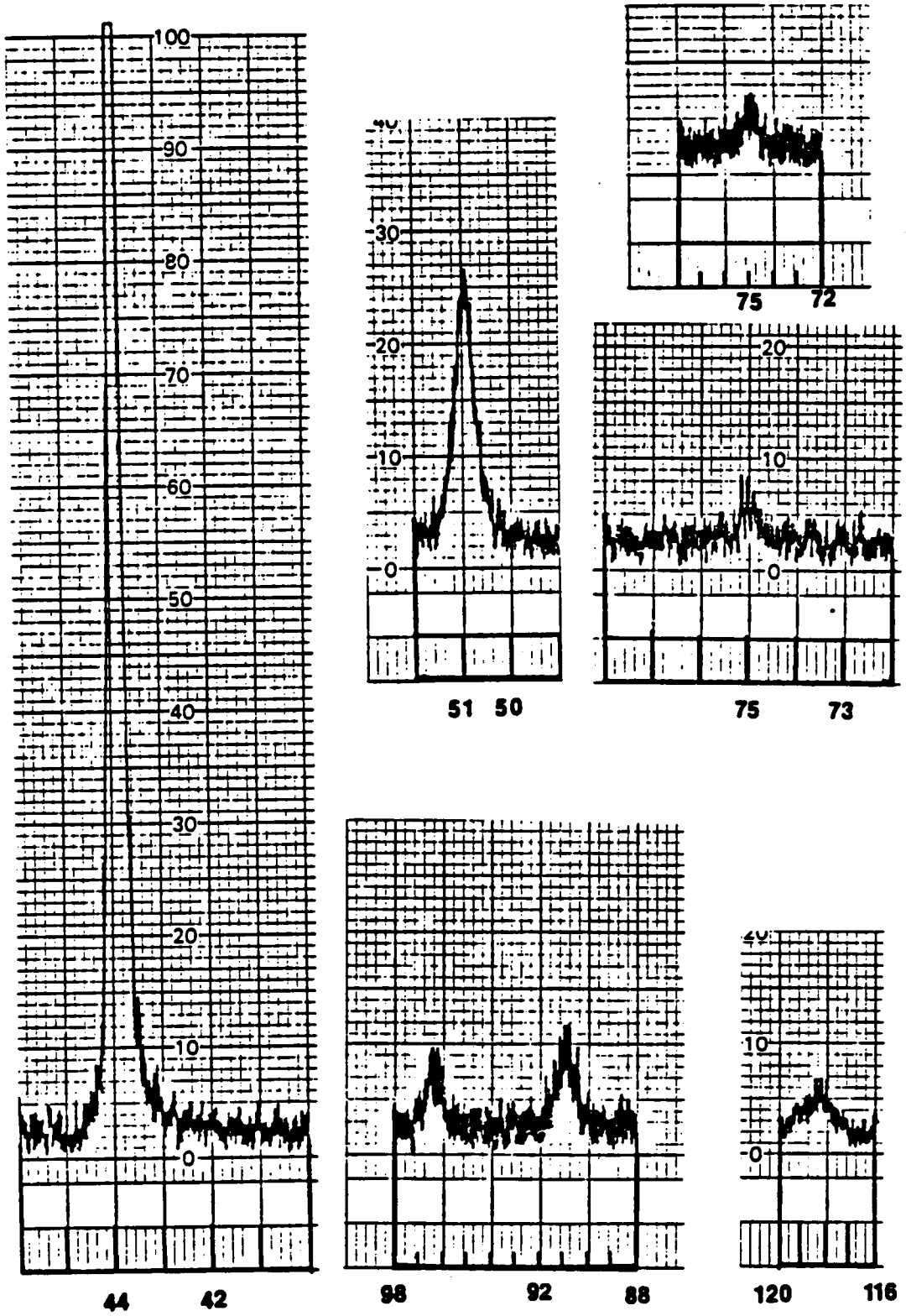

46a. Diffractometer trace of as-quenched Ni-Ta alloy with low scanning speed.

Figure 46. Diffractometer trace of the Ni-Ta alloy with low sacnning speed.

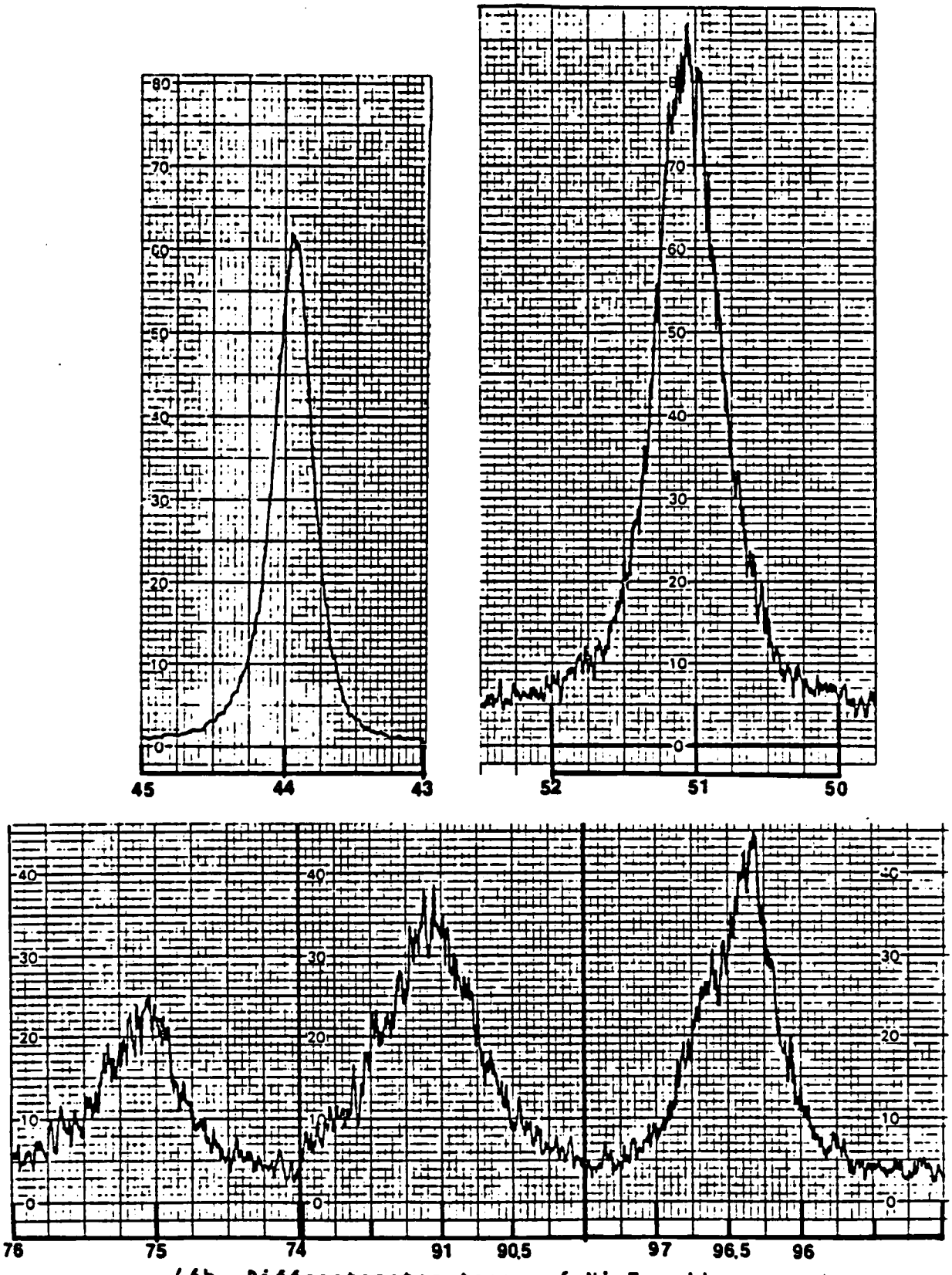

46b. Diffractometer trace of Ni-Ta alloy, aged at 600°C for 1000 hrs, by using low scanning speed.

Figure 46. (Continued)

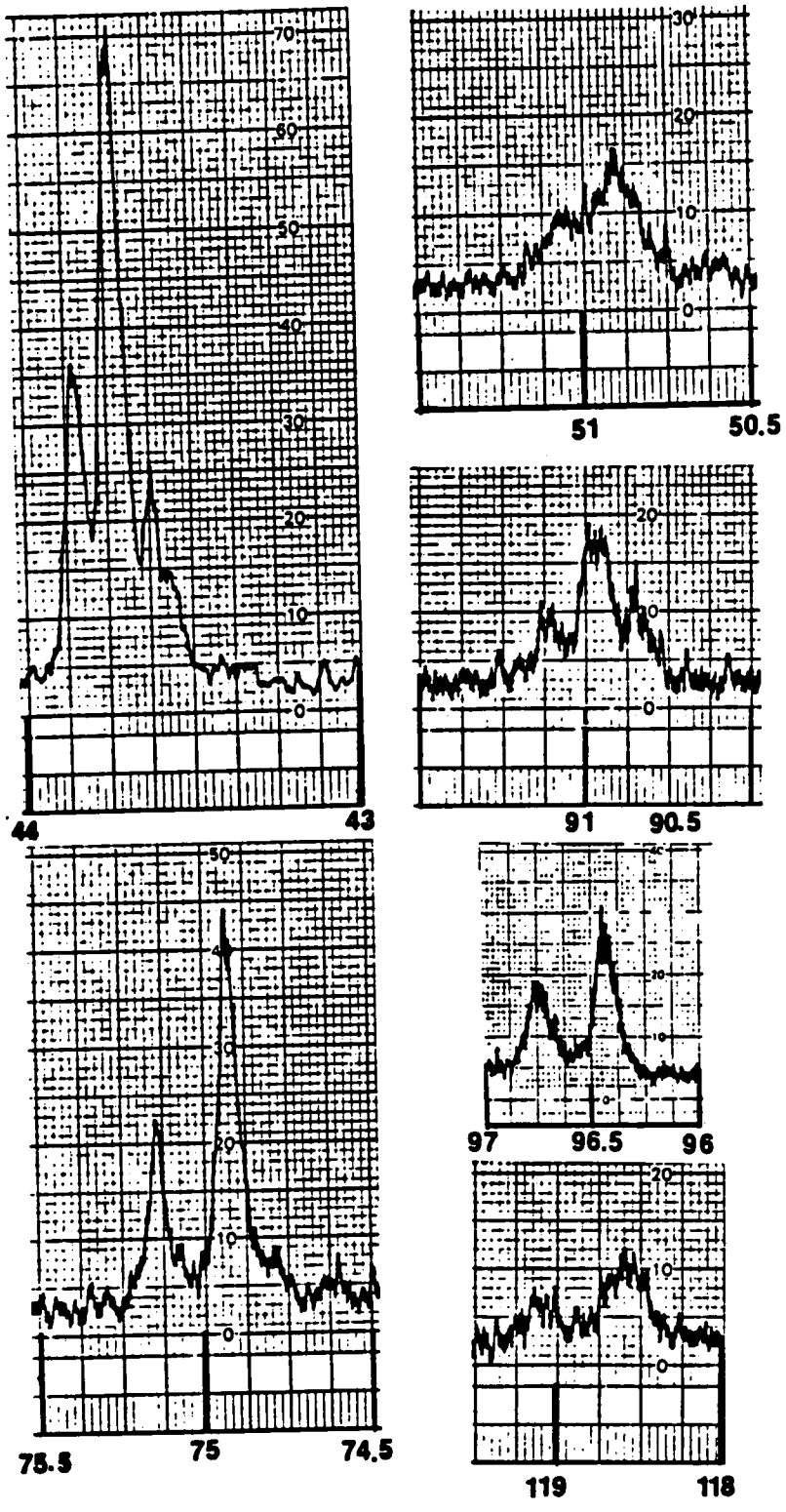

46c. Diffractometer trace of Ni-Ta alloy aged at 900°C for 1000 hrs, by using low scanning speed.

Figure 46. (Continued)

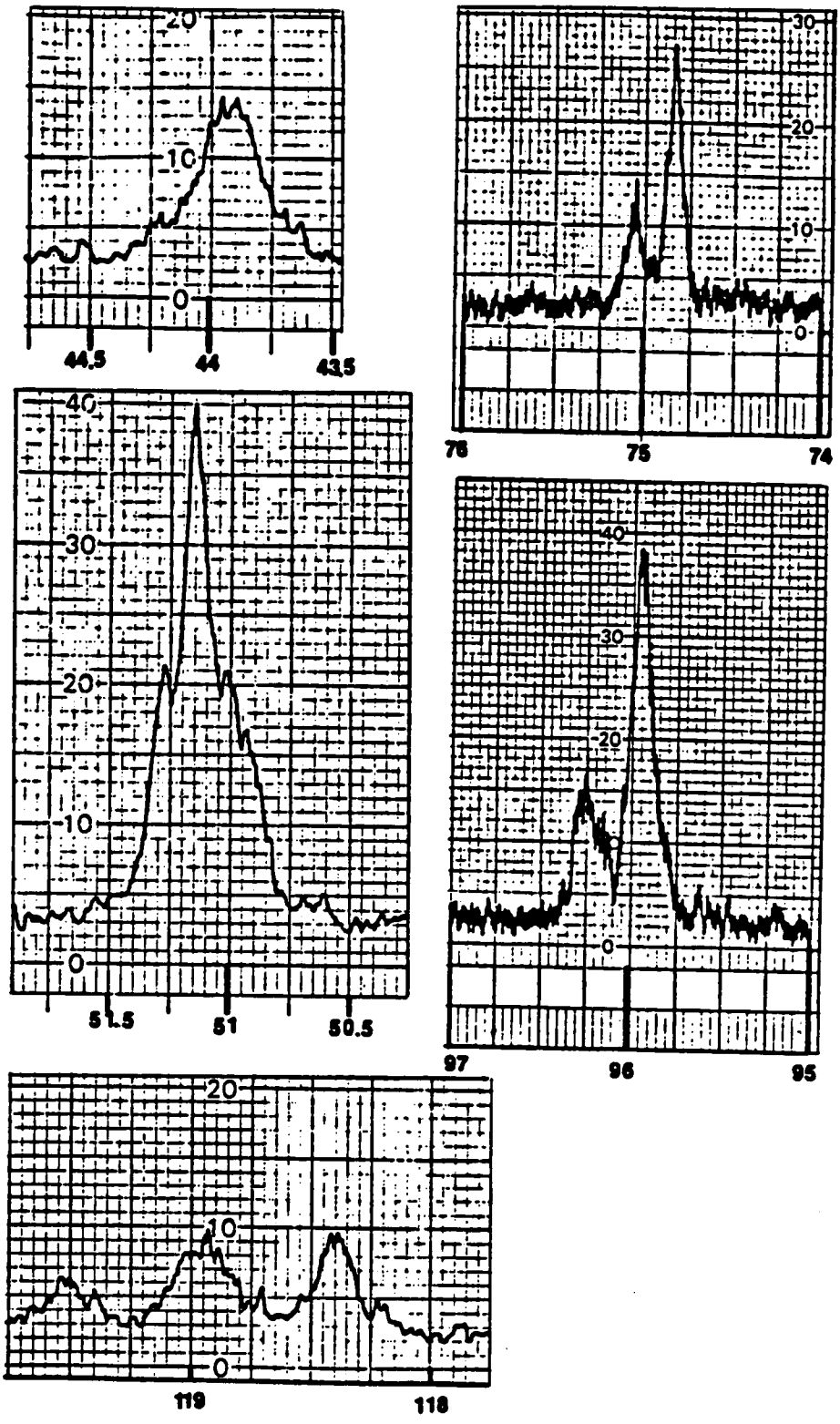

46d. Diffractometer trace of Ni-Ta alloy aged at 1000°C for 1000 hrs, by using low scanning speed.

Figure 46. (Continued)

for 1000 hrs; at 2θ = 44.00°(stronger), 44.06°, 51.13°, 51.20° (stronger), 51.35°, 75.02° (stronger), 75.23°, 91.15° (stronger), 91.41°, 96.45° (stronger), 96.75° after aging at 900°C for 1000 hrs; at 2θ = 43.93°, 51.00°, 51.15° (stronger), 51.30°, 118.42°, 118.94° after aging at 1000°C for 1000 hrs. Comparing the experimental traces to the reference FCC and Ni_8Ta traces, the peak observed at 2θ = 91.1° always agreed with the FCC peak at 91.2°, but never with the Ni_8Ta peak at 91.6°. Thus, it is concluded that all these traces have good agreement with that of FCC, not Ni_8Ta.

It is concluded that only FCC Ni-rich solid solution is present in the binary Ni-Ta alloy whether in solution treated condition or aged at 600°C to 1000°C for times up to 1000 hours.

For Ni_2Ta, two groups of reference values are listed in the computer files. One group (14) is : (a) 2θ = 29.5°, medium peak, (b) 2θ = 30.9°, medium, (c) 2θ = 40.6°, strong, (d) 2θ = 49.3°, the strongest peak, (e) 2θ = 58.7°, medium, (f) 2θ = 76.8°, strong. The other group (13) is : (a) 2θ = 30.6°, medium peak, (b) 2θ = 40.5°, medium peak, (c) 2θ = 44.9°, the strongest one, (d) 2θ = 76.8°, strong peak. Table 15 shows the original computer data file for these two groups for Ni_2Ta. The Ni_2Ta structure, which is present in this material as shown in TEM diffraction patterns (described later), was not observed by X-ray diffraction. This is

Table 15. The d-spacings and relative intensity of two types of Ni_2Ta (#17-563 and # 18-894) listed in the computer file.

17 563	(NI2 TA) NICKEL TANTALUM		
3.941	20	1.052	30
2.930	40	1.043	5
2.439	10	1.011	60
2.229	50	0.998	40
2.143	5	0.988	5
2.020	100	0.977	30
1.978	5	0.972	5
1.942	10	0.967	20
1.577	40	0.903	20
1.482	20	0.890	30
1.465	20	0.881	40
1.414	40	0.875	15
1.390	40	0.869	30
1.320	30	0.851	50
1.243	70	0.846	60
1.232	5	0.837	20
1.135	40	0.830	80
1.114	15	0.795	100
1.073	10	0.791	5
1.063	20	0.789	20

18 894	(TA NI2) NICKEL TANTALUM		
3.931	40	1.011	45
2.902	60	0.998	45
2.227	80	0.972	40
2.021	100	0.904	10
1.975	20	0.891	20
1.940	25	0.882	20
1.574	60	0.876	10
1.478	20	0.870	20
1.464	20	0.852	60
1.412	20	0.847	60
1.388	25	0.838	10
1.320	25	0.831	80
1.243	80	0.796	85
1.232	10	0.789	40
1.136	60		
1.115	25		
1.074	10		
1.064	10		
1.053	20		
1.043	10		

probably due to the low percentage in volume (less than 5%) of Ni_2Ta.

(b) Ni-Ta-Cr alloy

The structure of the Ni-Ta-Cr alloy is complicated. After being solution treated at 1250°C for one week, the material contained two phases (different morphologies). After reheating to 1280°C for four hours and water quenching, the matrix contained about 10% of only a single second phase (Figures 22a-b). Figure 47a is the diffractometer trace for the first solution treated condition , and Figure 47b, for the reheated condition (1280°C, four hrs). The optical microstructure of the material aged at 600°C is similar to the reheated material (1280°C), and the diffractometer traces are similar, too (Figures 47b and 48). In Figure 48 (600°C, 1000 hrs), the weak peak at $2\theta = 74.5^{\circ}$ is not observed in Figure 47b (1280°C, 4 hrs), while the weak peak at $2\theta = 90.5^{\circ}$ (Figure 48) is strong in the reheated condition (Figure 47b). All these solution treated and aged specimens were scanned again at very low speed to get a better resolution, and the results are shown in Figures 53-62. Thus 2θ values and the intensities could be more accurately compared. Tables 9a-b list the measurements of experimental 2θ and relative intensities.

In Figures 47-52, the experimental curves are compared with the trace of FCC, one Ni_8Ta reference trace (ASTM card

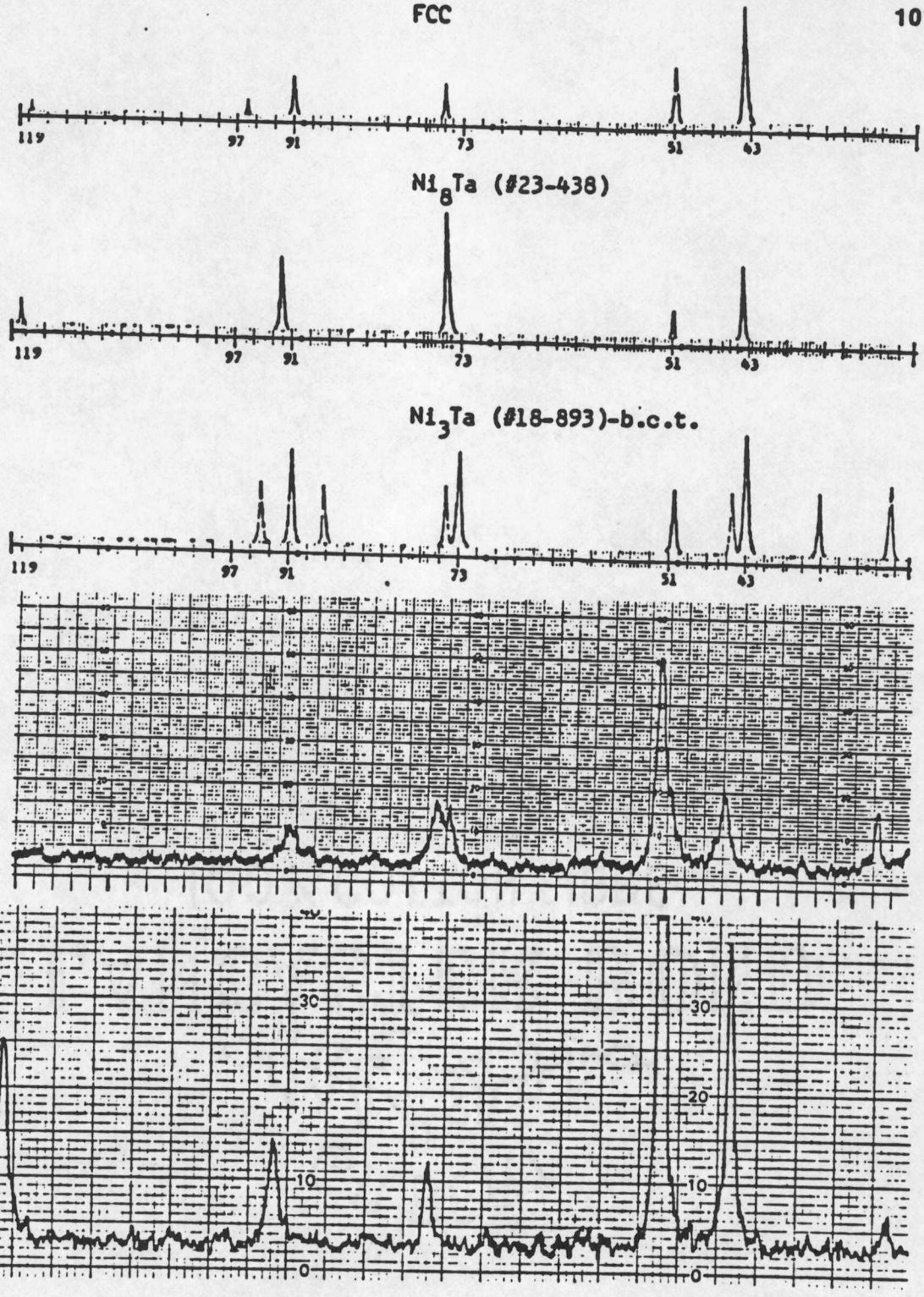

47a. Diffractometer trace of solution treated Ni-Ta-Cr alloy with two second phases present in the matrix.

Figure 47. Diffractometer trace of the Ni-Ta-Cr alloy after solution treatment.

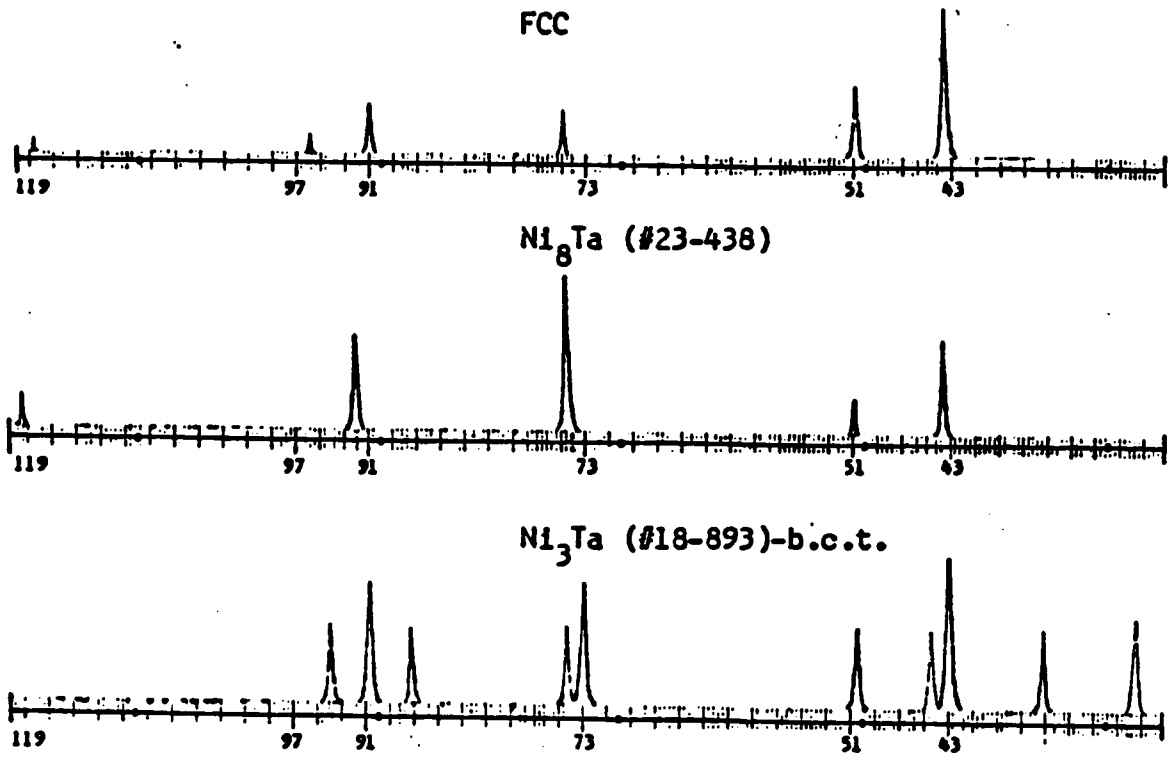

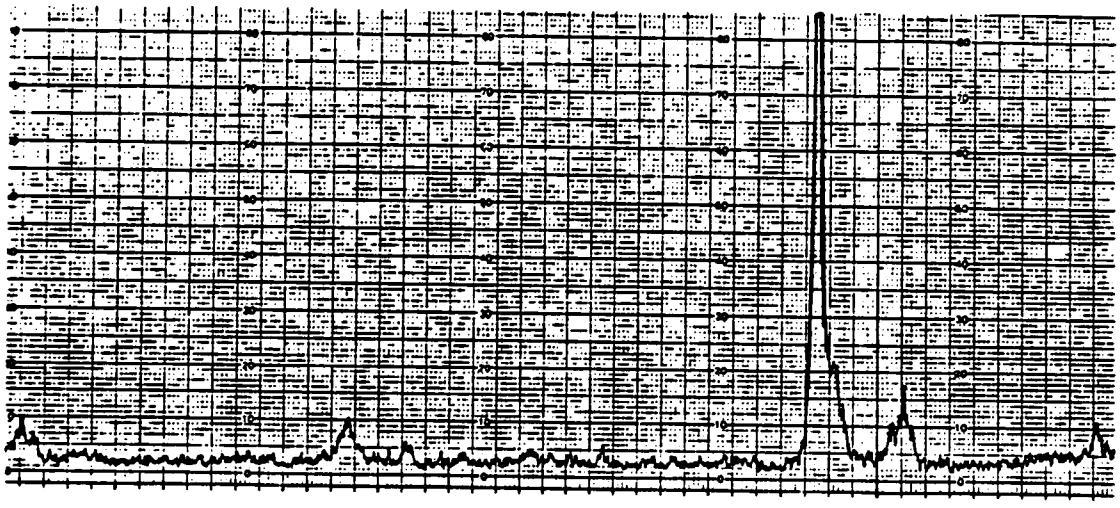

47b. Diffractometer trace of Ni-Ta-Cr alloy, heated to 1280°C for 4 hrs after first solution treatment.

Figure 47. (Continued)

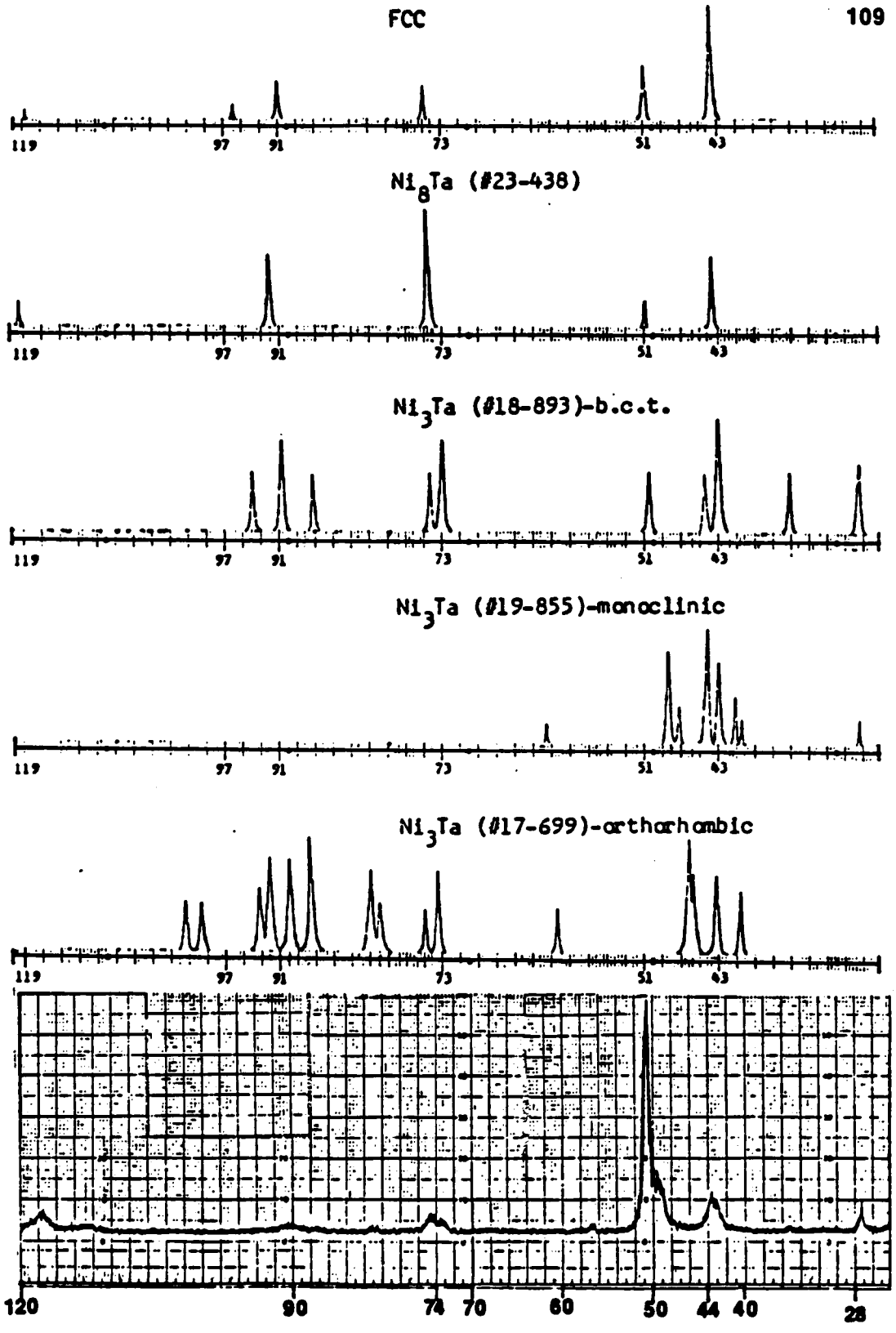

Figure 48. Diffractometer trace of Ni-Ta-Cr alloy, aged at 600°C for 1000 hrs.

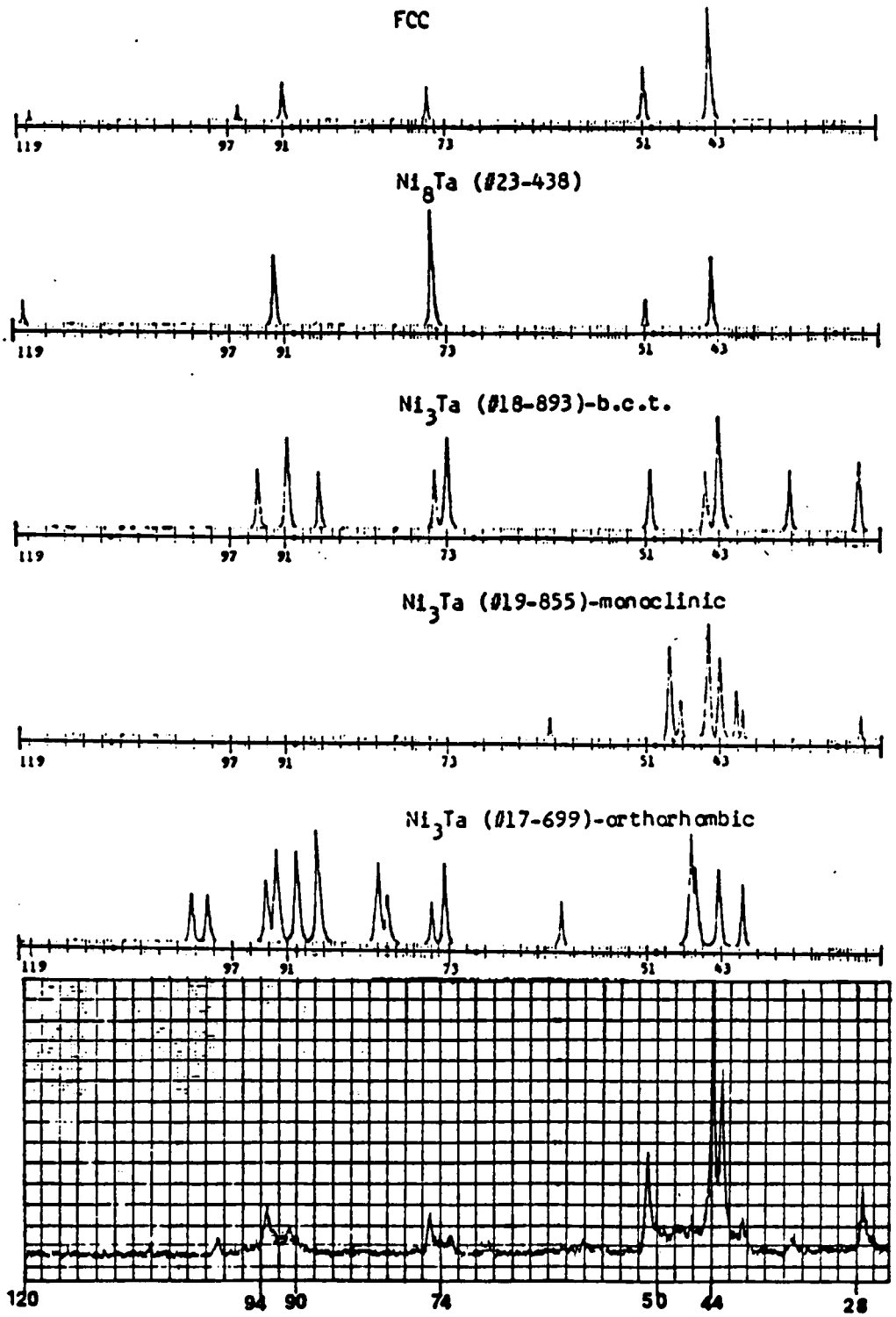

49a. Diffractometer trace of Ni-Ta-Cr alloy, aged at 700°C for 500 hrs.

Figure 49. Diffractometer traces of the Ni-Ta-Cr alloy after aging at 700°.

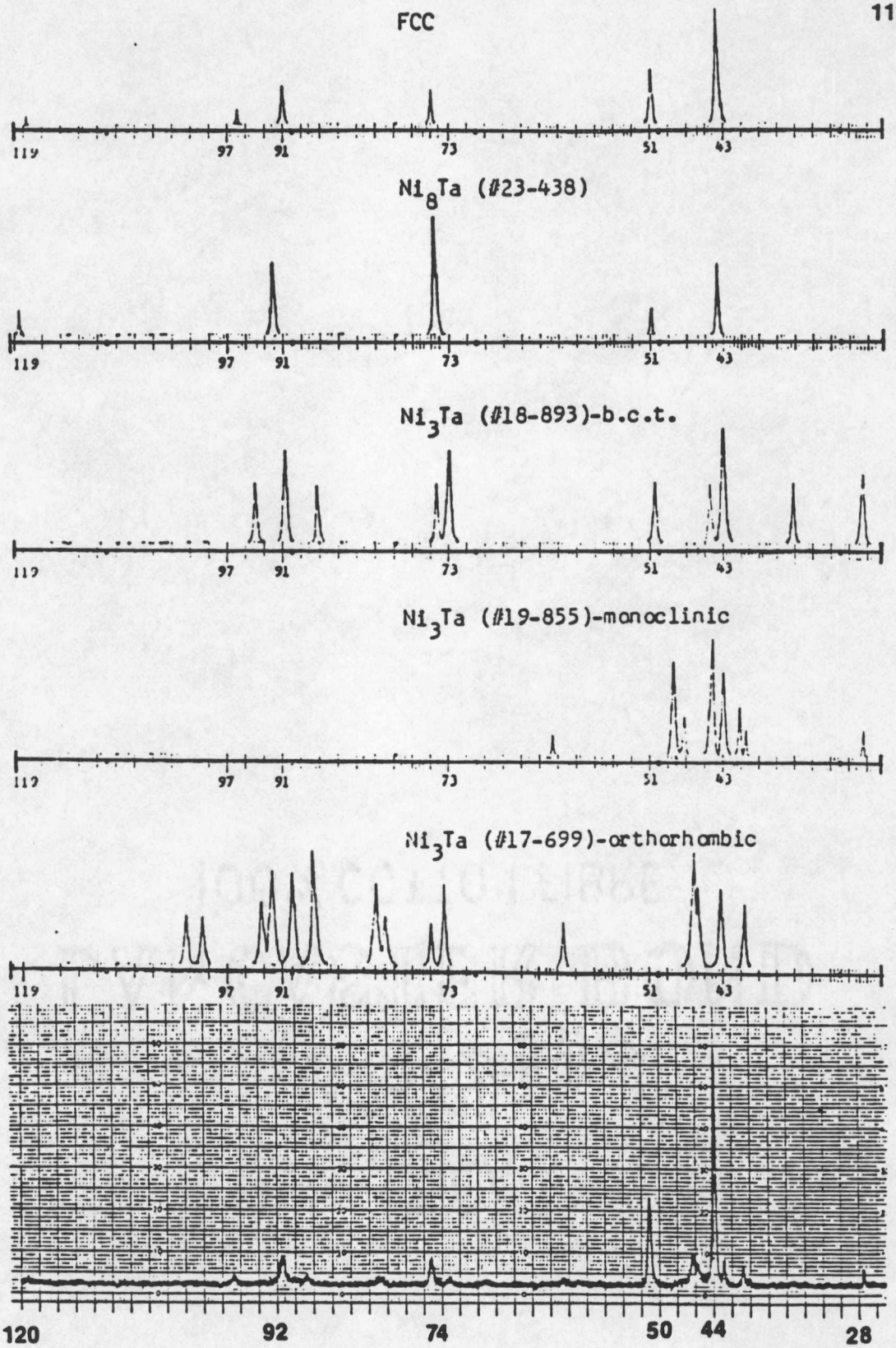

49b. Diffractometer trace of Ni-Ta-Cr alloy, aged at 700°C for 1000 hrs.

Figure 49. (Continued)

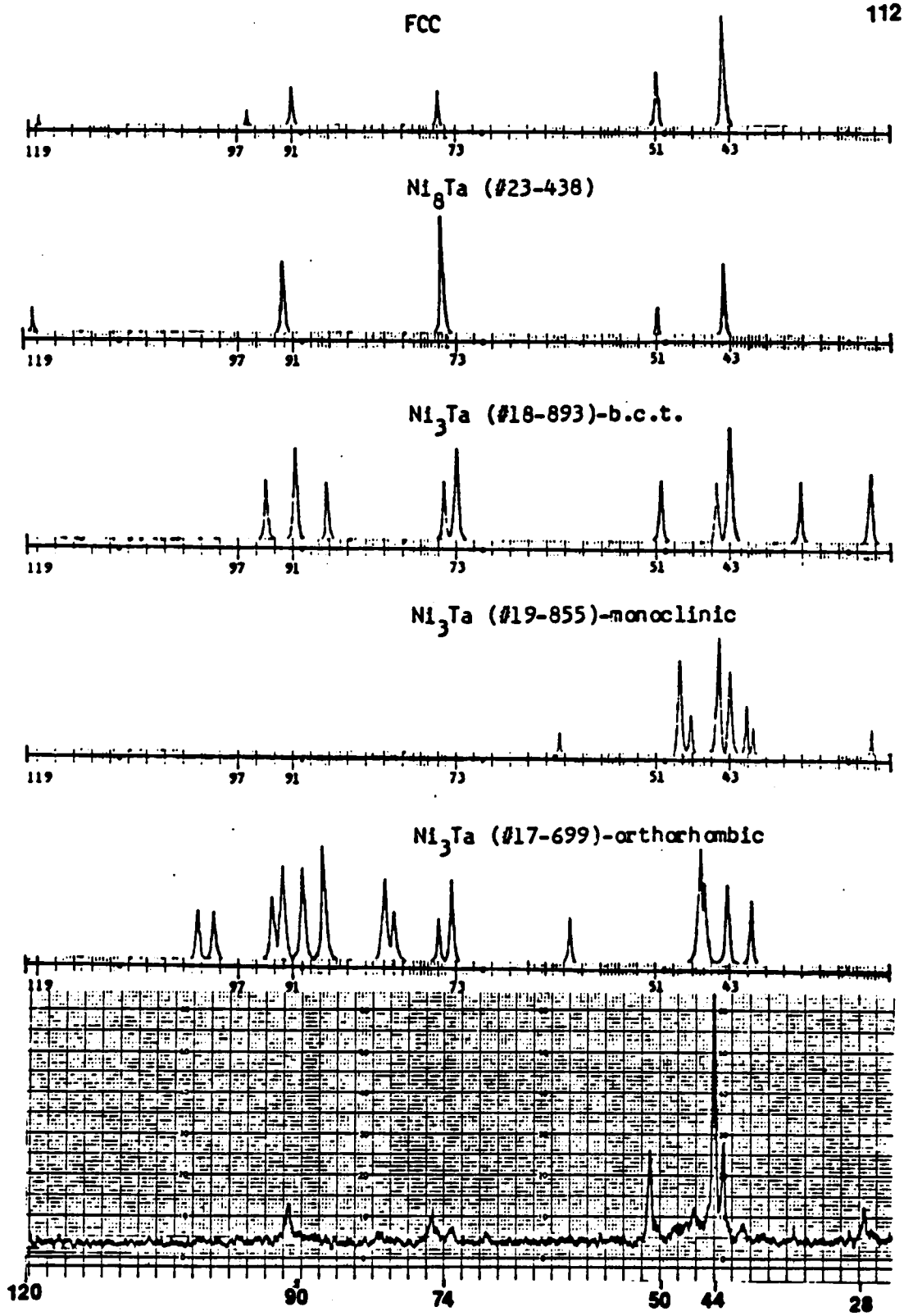

Figure 50. Diffractometer trace of Ni-Ta-Cr alloy, aged at 800°C for 1000 hrs.

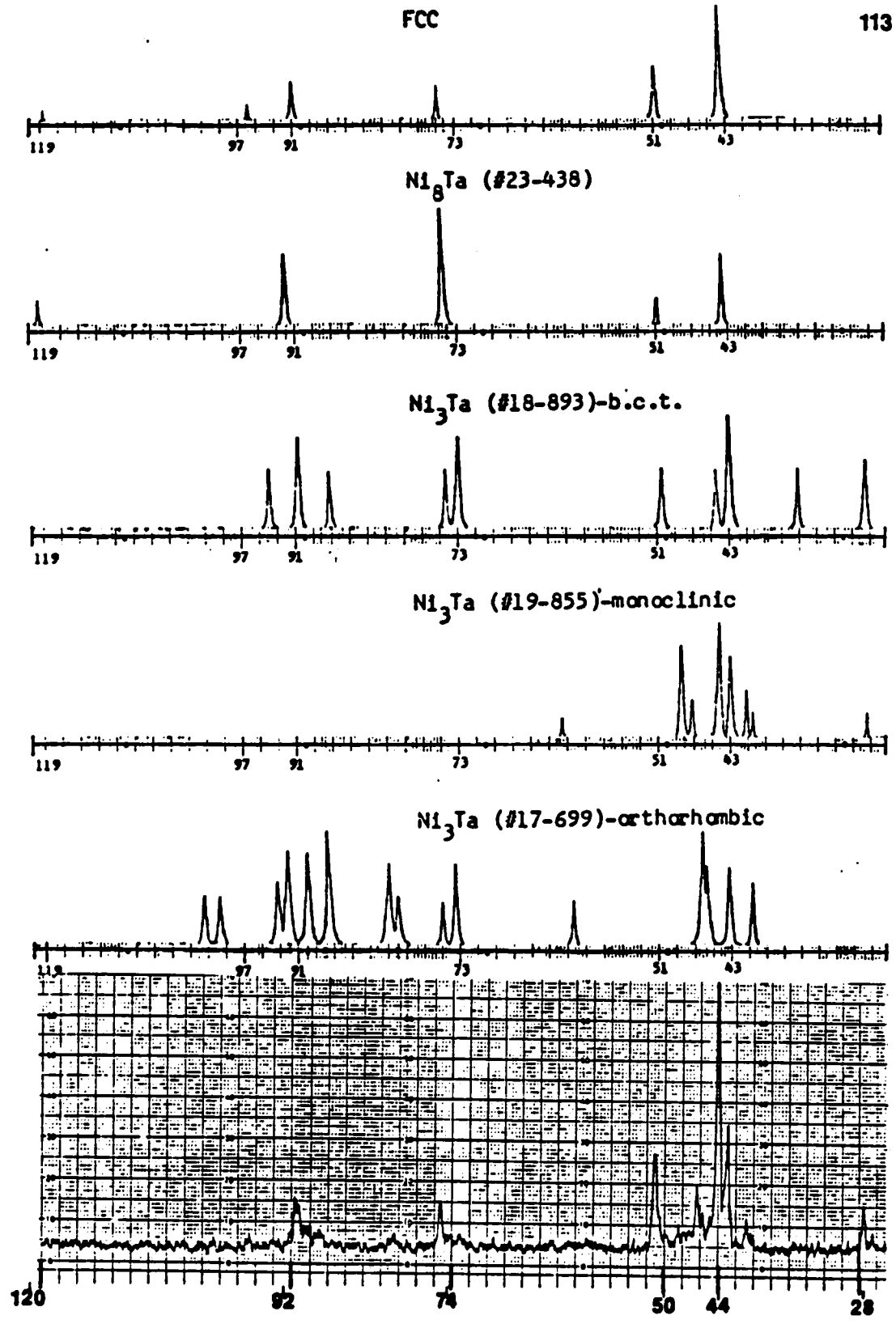

Figure 51. Diffractometer trace of Ni-Ta-Cr alloy, aged at 900°C for 1000 hrs.

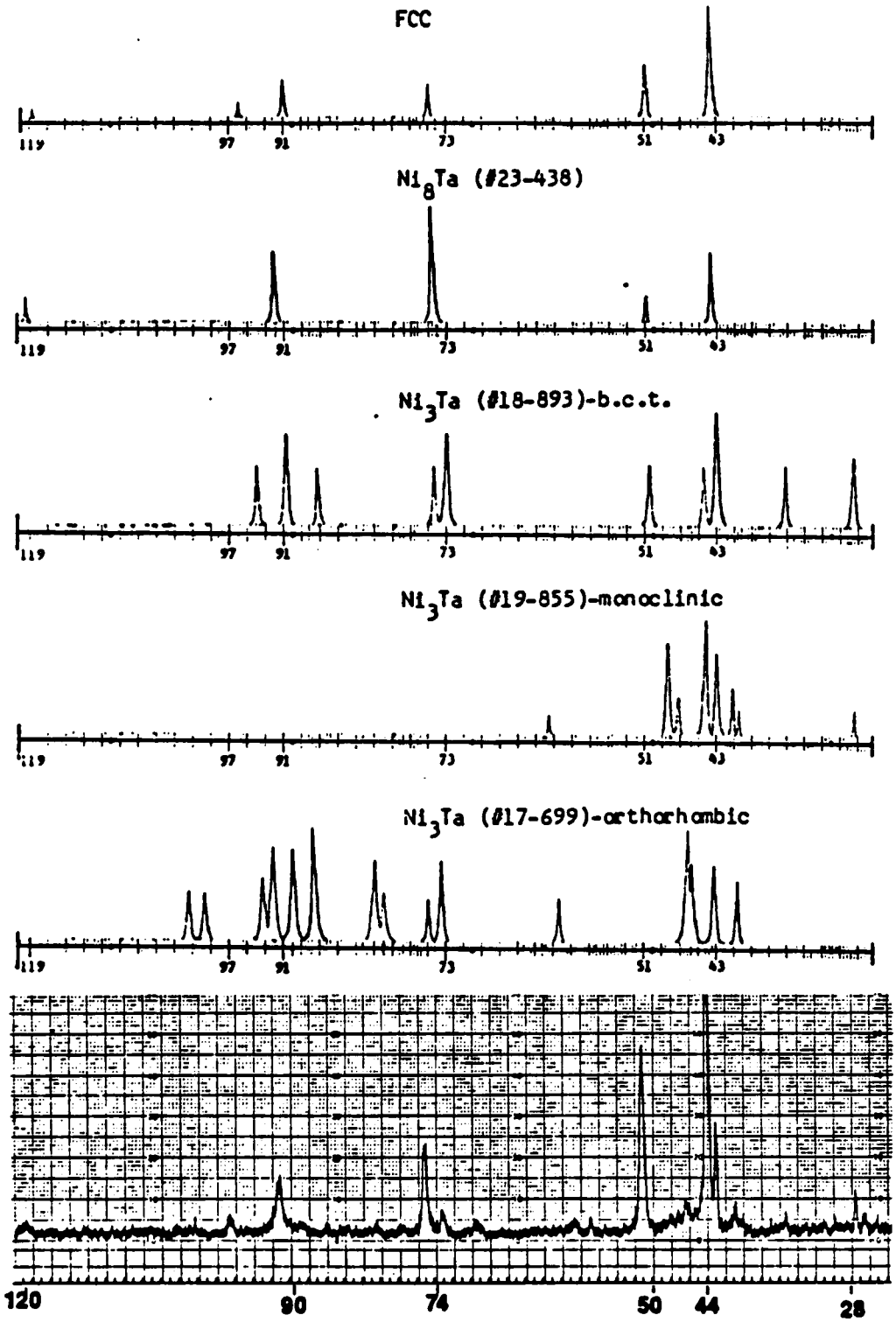

Figure 52. Diffractometer trace of Ni-Ta-Cr alloy, aged at 1000°C for 1000 hrs.

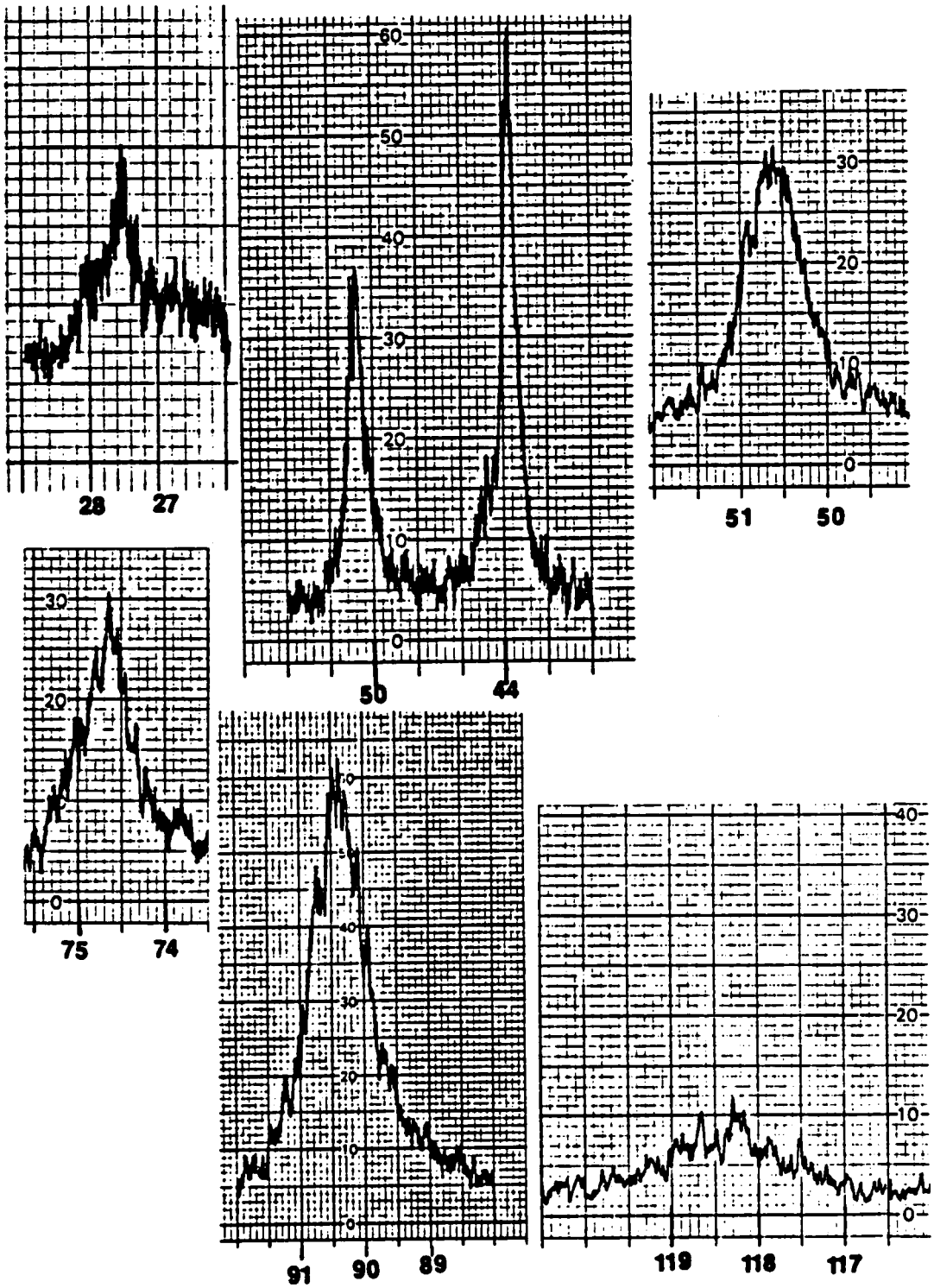

Figure 53. Diffractometer traces of Ni-Ta-Cr alloy, solution treated condition at 1250°C for 7 days, by using low scanning speed.

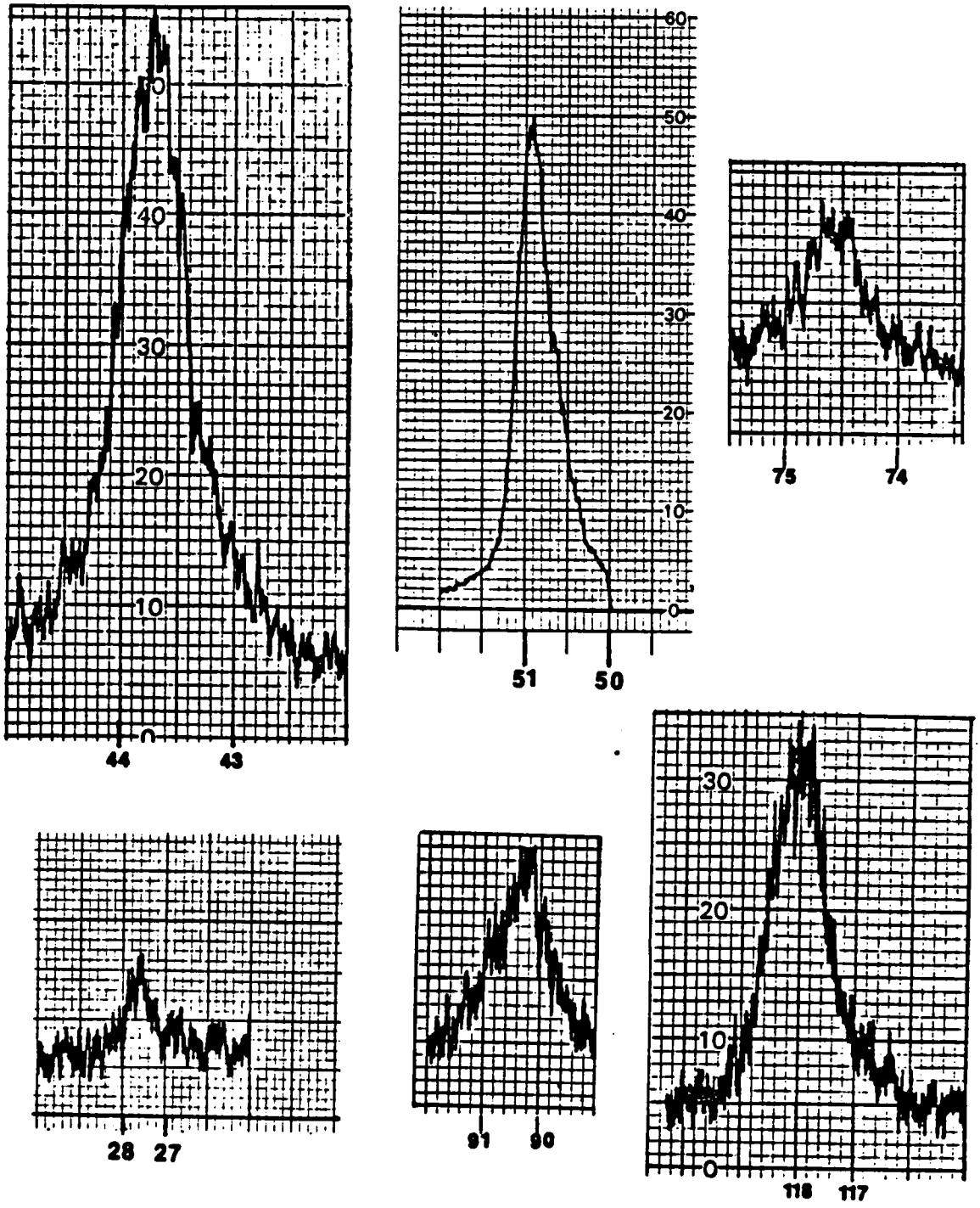

Figure 54. Diffractometer traces of Ni-Ta-Cr alloy, heated to 1280°C for 4 hrs after first solution treated, scanned in low speed.

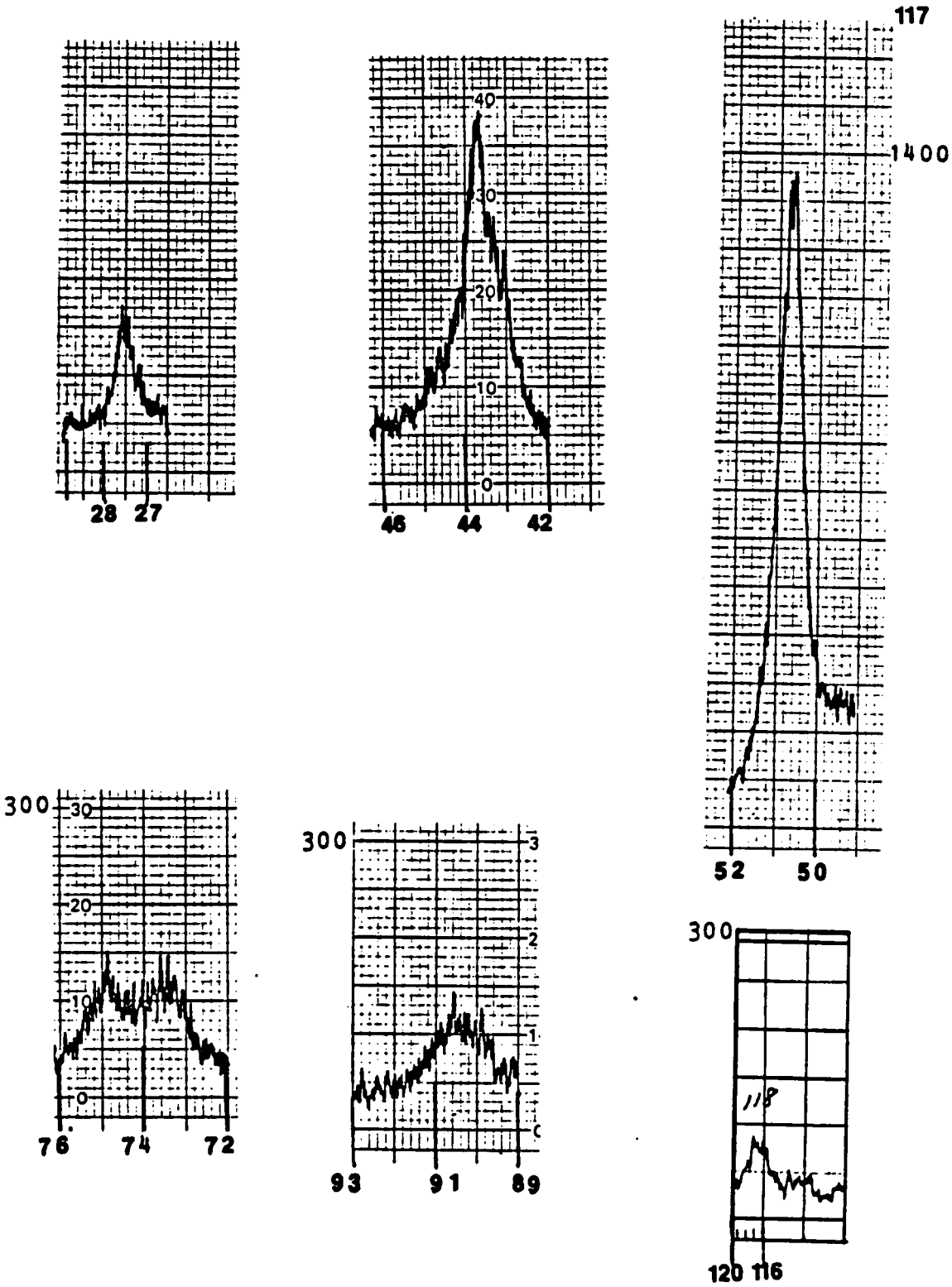

Figure 55. Diffractometer traces of Ni-Ta-Cr alloy, aged at 600°C for 100 hrs, scanned in low speed.

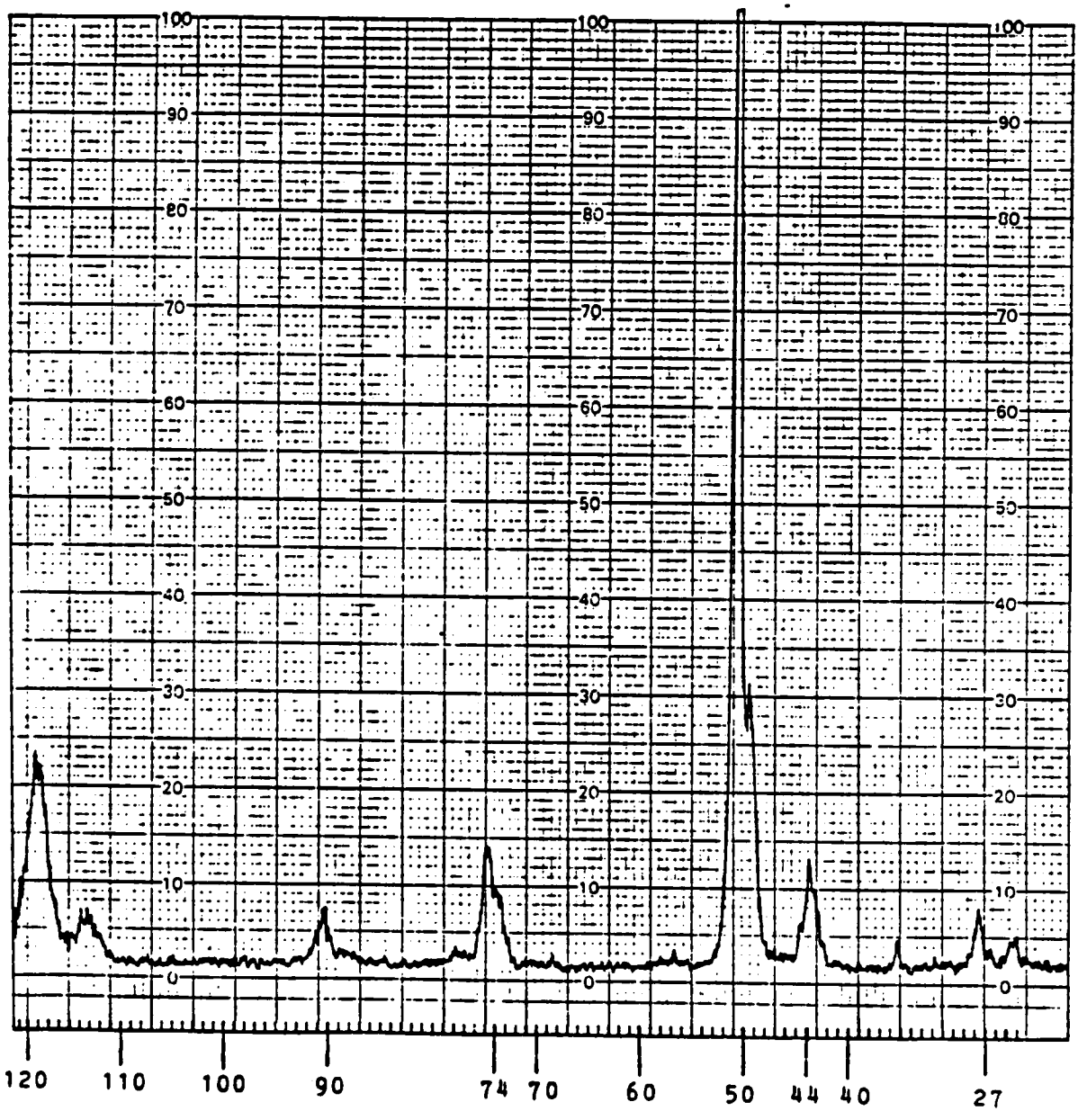

Figure 56. Diffractometer traces of Ni-Ta-Cr alloy, aged at 600°C for 500 hrs.

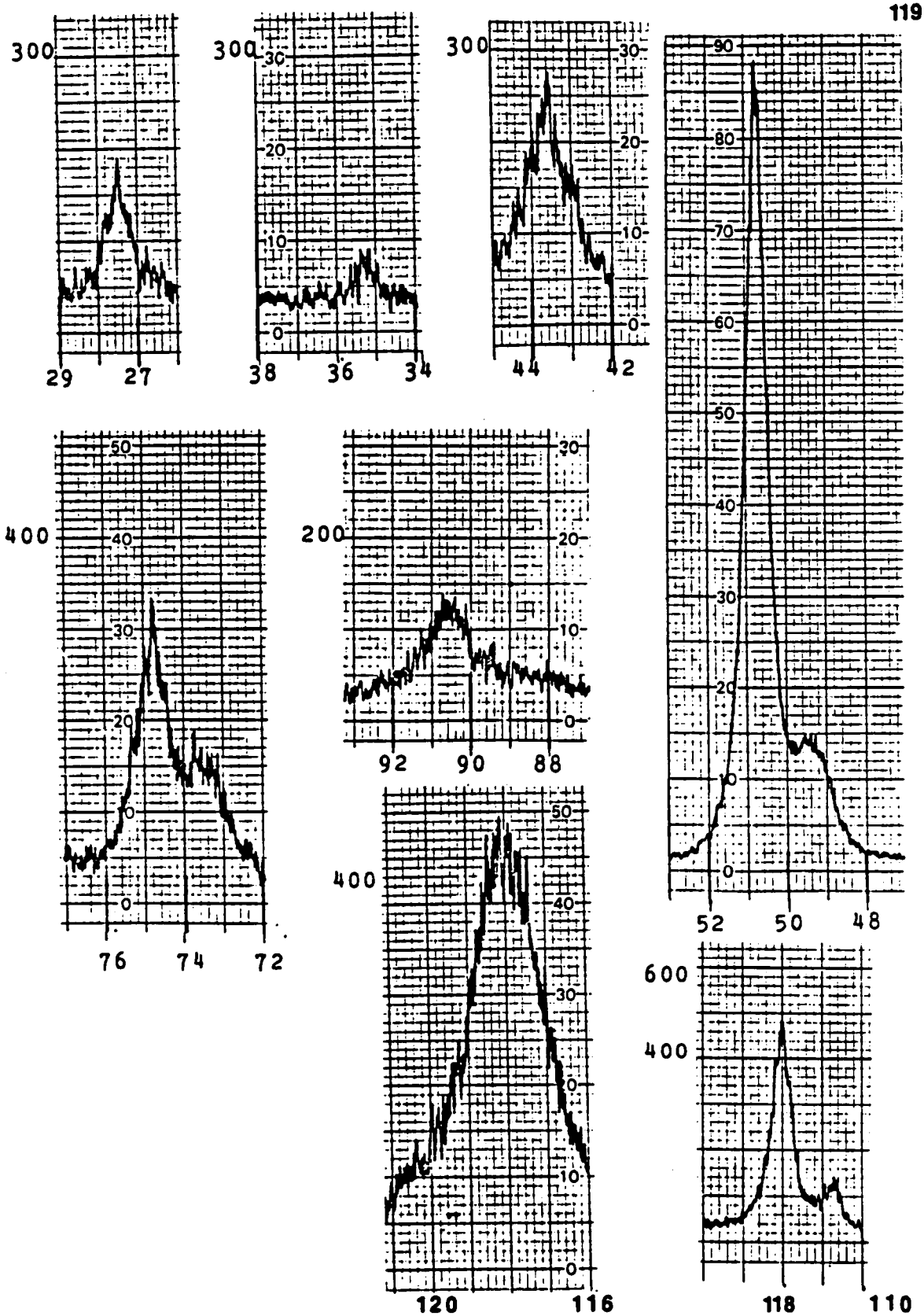

Figure 57. Diffractometer traces of Ni-Ta-Cr alloy, aged at 600°C for 500 hrs, scanned in low speed.

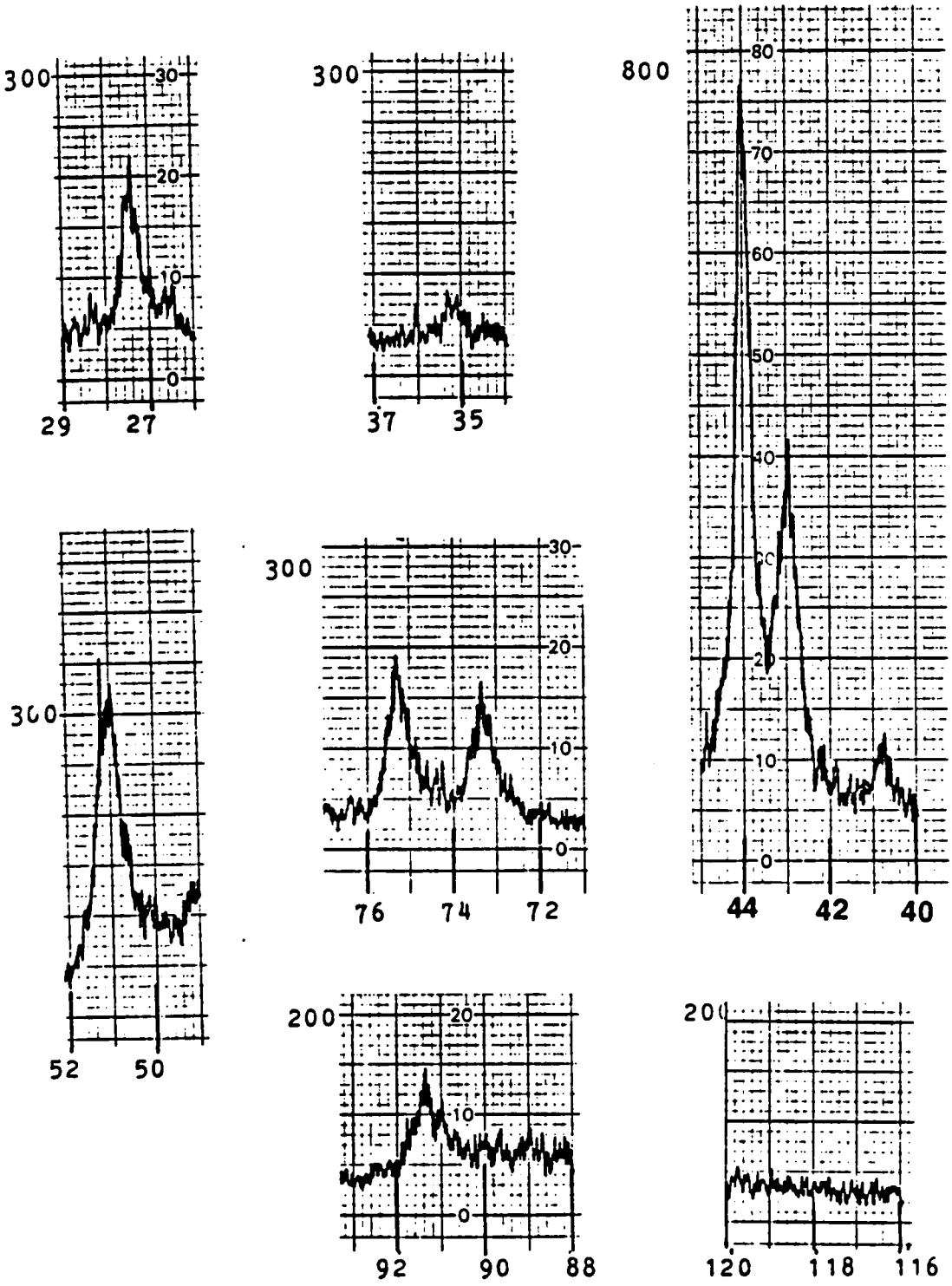

Figure 58. Diffractometer traces of Ni-Ta-Cr alloy, aged at 700°C for 100 hrs, scanned in low speed.

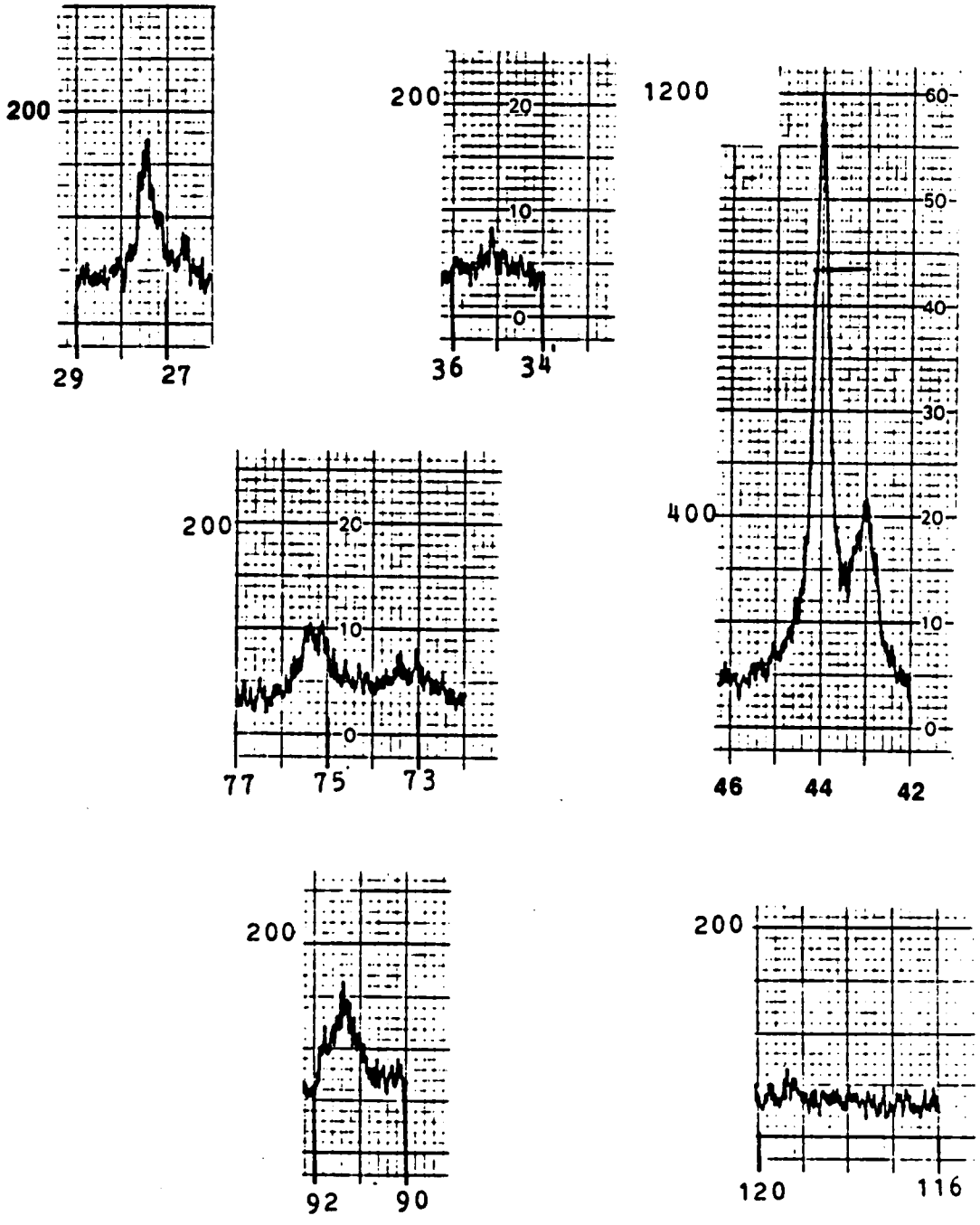

Figure 59. Diffractometer traces of Ni-Ta-Cr alloy, aged at 800°C for 100 hrs, scanned in low speed.

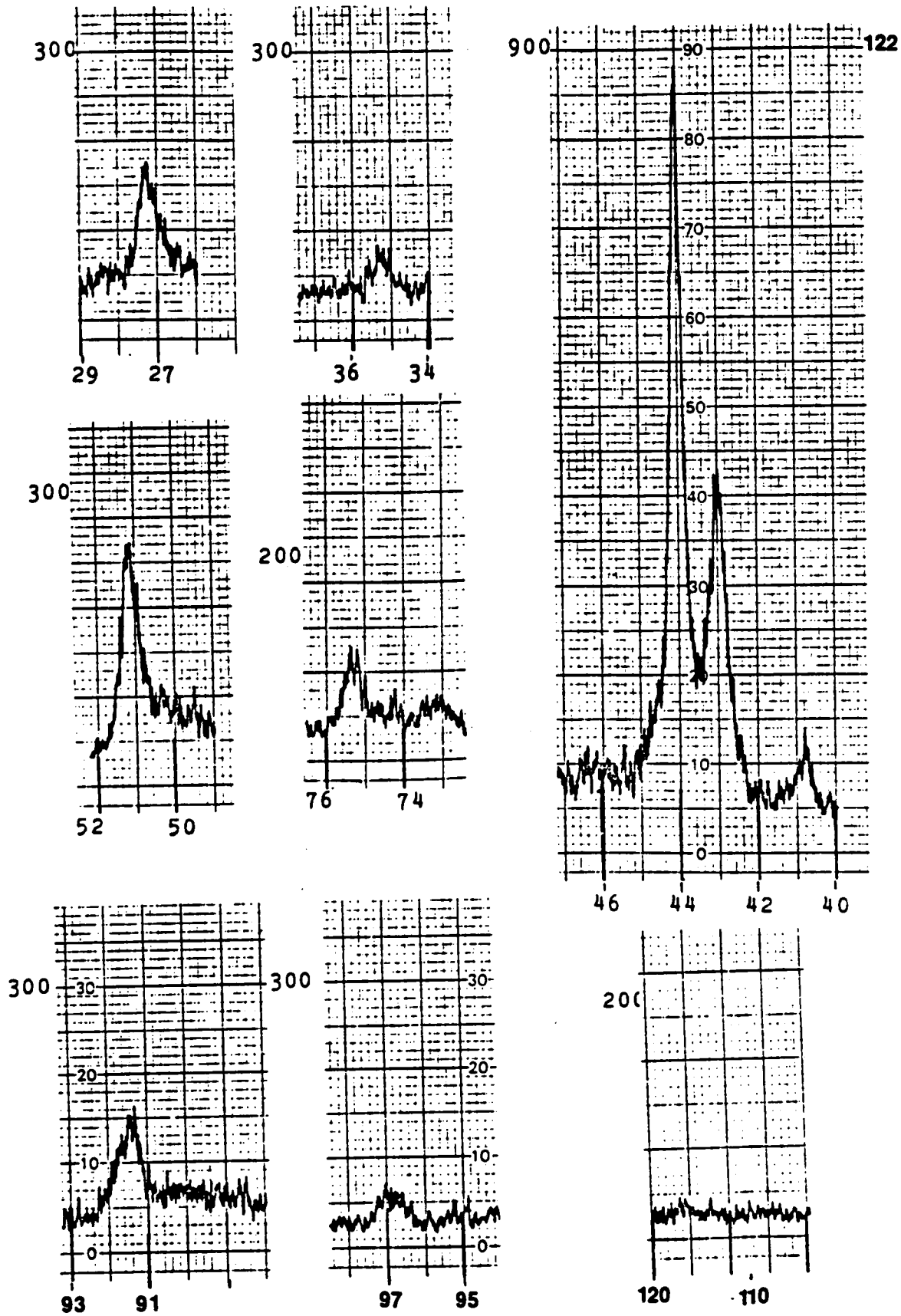

Figure 60. Diffractometer traces of Ni-Ta-Cr alloy, aged at 700°C for 500 hrs, scanned in low speed.

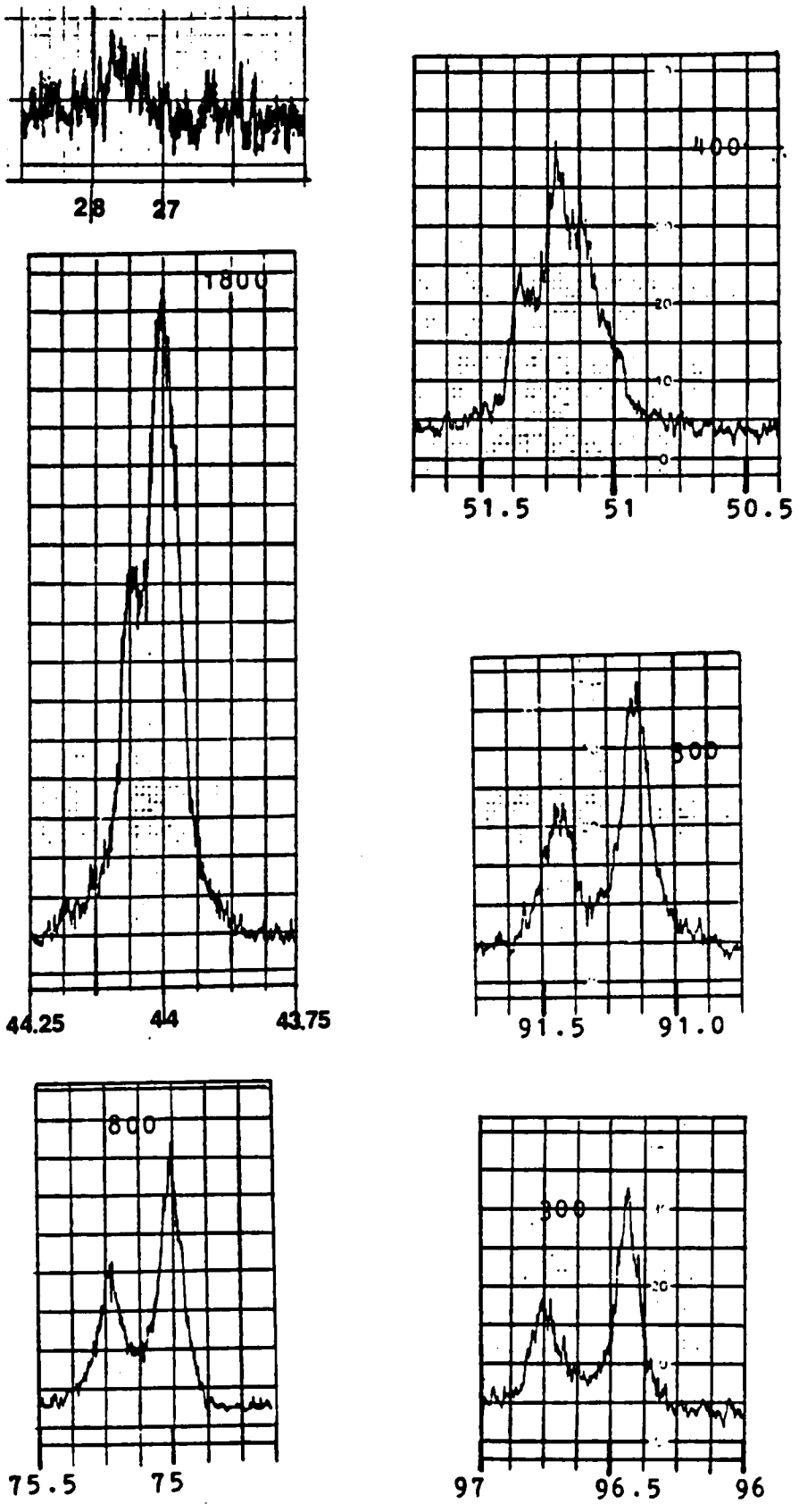

Figure 61. Diffractometer traces of Ni-Ta-Cr alloy, aged at 900°C for 1000 hrs, scanned in low speed.

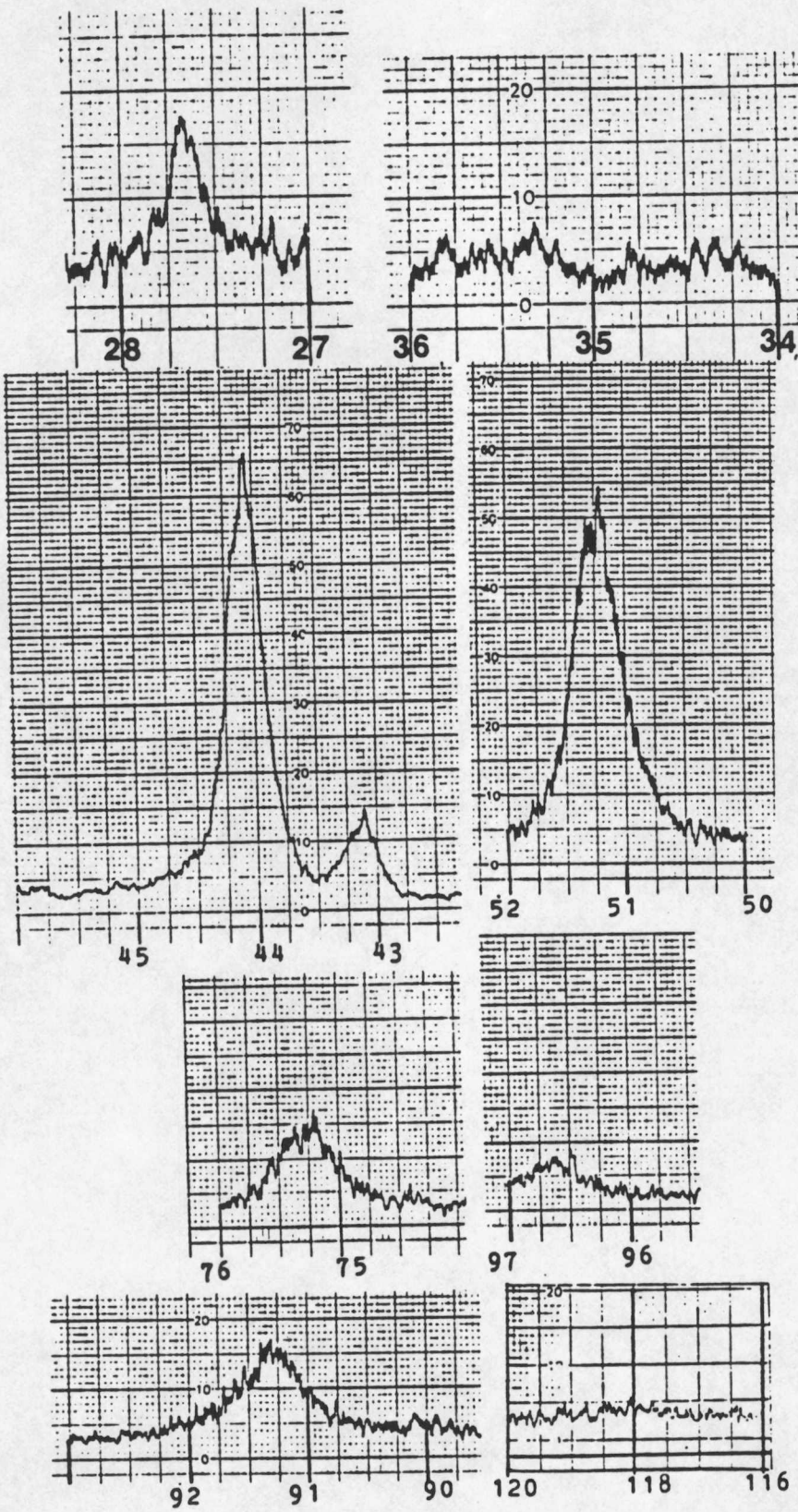

Figure 62. Diffractometer traces of Ni-Ta-Cr alloy, aged at 1000°C for 1000 hrs, scanned in low speed.

Table 16. Experimental 2θ values and relative intensities of Ni-Ta-Cr alloy.

Heat treated condition	1280°C, 4 hours	600°C 100 hrs	600°C 500 hrs	700°C 100 hrs
Figure number	54	55	57	58
2θ	27.75	27.55	27.48	27.41
I	184	170	200	220
2θ	44.10	43.80	35.30	35.30
I	144	388	90	85
2θ	*51.05	*50.60	43.60	42.90
I	1380	1360	278	418
2θ	75.35	74.90	*50.78	*44.00
I	192	150	1765	768
2θ	90.90	90.60	73.80	51.00
I	104	145	188	330
2θ		118.30	74.60	73.30
I		80	334	170
2θ			90.60	75.30
I			140	193
2θ			113.00	91.38
I			140	148
2θ			118.00	
I			490	

* indicates strongest peak

Table 17. Experimental 2θ and intensities of Ni-Ta-Cr alloy.

Heat treated condition	800°C 100 hrs	700°C 500 hrs	900°C 1000 hrs	1000°C 1000 hrs
Figure number	59	60	61	62
2θ	27.43	27.25	*44.00	27.65
I	170	170	1760	150
2θ	35.18	35.40	51.23	43.20
I	84	85	410	280
2θ	43.00	43.00	75.02	*44.08
I	440	430	745	1340
2θ	*44.00	*44.00	75.21	51.21
I	1200	880	425	540
2θ	75.10	51.10	91.13	75.20
I	108	270	385	170
2θ	91.39	91.40	91.45	91.30
I	165	160	230	171
2θ	-	96.90	96.44	96.50
I		70	330	90
2θ			96.75	
I			190	

* indicates strongest peak

number 23-438), and three Ni_3Ta reference traces (ASTM file #17-699, #18-893, and #19-855). These three types of Ni_3Ta are referred to as b.c.t (#18-893), monoclinic (#19-855), and orthorhombic (#17-699).

The observed diffractometer traces of the second solution treated condition (1280°C for four hrs, then water quenching) and of the aging at 600°C for 1000 hrs are similar which is consistent with the optical microscopic observation. Although the microstructure of the first solution treated condition shows two second phases present in the matrix (Figure 22a), its diffrcatometer trace is similar to that of the second solution treated condition which contains only one second phase. It seems that the two second phases present in the first solution treated condition have the same structure, but with different orientation.

According to the comparisons between the observed traces and the reference ones (Figures 47a-b and Figure 48), it is concluded that the ternary alloy after the first and the second solution treatments has only Ni_3Ta and FCC Ni-rich solid solution present. This structure doesn't change after aging at 600°C for up to 1000 hrs.

From the optical microstructures, about 60% of the matrix was transformed after aging at 700°C for 500 hrs (Figure 25a). The amount of the plate-like particles remained the same after agings. The intensity of the FCC

peaks reduced, as can be seen by examining the peak at 2θ = 118.5° (Figures 49-52). The matrix was almost 100% transformed after aging at 800°C to 1000°C for 500 hrs and 700°C to 1000°C for 1000 hours (Figures 25b-27d). The FCC peak at 2θ = 118.5° has almost disappeared in Figures 49b-52 which corresponds to these microstructural observations.

It is concluded that the matrix of the reheated (1280°C, 4 hrs) and then aged at 600°C materials is FCC structure, and the plate-like particles are body-centered tetragonal Ni_3Ta (#18-893).

During and after the transformation of the matrix, the diffractometer traces at 2θ = 43.0°, 44.0°, and 50.5° changed obviously (compare Figures 47-48 with Figures 49-52) and the comparison is shown in Table 18. The intensity of the peak located at 2θ = 44.0° is always observed to be the strongest one after aging from 700°to 1000°C for long time, which is associated with the formation of a new structure in considerable quantity. This transformation can be written as γ (90% of structure) + BCT Ni_3Ta (10% of structure)→ γ (5 %) + BCT Ni_3Ta (10 %) + newly formed structure (85 %). The trace of the orthorhombic Ni_3Ta does not have good agreement with the experimentally observed traces (after aging at 700 to 1000°C) due to the following reasons. (a) No strong (not even a weak) peak is located at 2θ = 44.0° for orthorhombic Ni_3Ta in the ASTM data file and (b) several medium strong or strong peaks, while listed for the orthorhombic Ni_3Ta, such

Table 18. List of some chosen 2θ values and relative intensity of Ni-Ta-Cr alloy to show the differences between Figures 47-48 and Figures 49-52.

Figures / 2θ	47-48 FCC + Ni_3Ta (BCT)	49-52 Ni_3Ta(BCT) + Ni_3Ta(newly formed)
43.8°	I = medium	I = medium strong
44.0°	I = none	I = strongest
50.9°	I = strongest	I = medium strong

as $2\theta = 46.1^{o}$, 80.9^{o}, 92.4^{o}, and 93.4^{o}, are not observed in the present work. The observed traces after the formation of the new structure have better agreement with that of the monoclinic Ni_3Ta (100% intensity at $2\theta = 44.0^{o}$) than that of the orthorhombic Ni_3Ta, although the strong peak (80% intensity) listed at 48.0^{o} for monoclinic is not observed in the present work.

Unfortunately there is no monoclinic Ni_3Ta micrograph available in the previous articles for comparison. However, the newly formed structure is identified to be more like orthorhombic Ni_3Ta by comparing with a micrograph shown in the literature and the behavior of the microhardness (31). In the present research, the hardness of the Ni-Ta-Cr alloy decreased after long time aging, and Aballe et al. (31) found a similar effect which they report is due to the presence of this orthorhombic Ni_3Ta (31).

The diffractometer traces obtained from the present work do not match the reference traces of orthorhombic Ni_3Ta well, but this may due to the influence of preferred orientation. However, the newly formed structure is taken to be orthorhombic Ni_3Ta and will be described in the COMPARISON section.

EDS ANALYSIS

The chemical analyses reported here are based on fluorescent X-ray detection in the SEM using an energy dispersive analyzer; such a method is now referred to as EDS (energy dispersive spectrometry). It is emphasized that the analysis is qualitative, and the results are presented in terms of the highest X-ray peak intensity for the elements Ni, Ta, and Cr. These intensity values cannot be converted into quantitative analysis without precautions and corrections, none of which were applied here. Instead, the ratio of the peaks was examined, then corrected based on the ratios obtained from a spectrum at low magnification (e.g., 100 X) and using the known chemical analysis of the alloy. This is described in detail in Appendix 1. Thus, conclusions regarding agreement or differences in chemical composition must be tempered with the uncertainity in the method used.

For the Ni-Ta-Cr alloy, EDS analysis was done to examine the chemical content of different areas. In the following, the results are presented with the data normalized to the Ni peak at 100. The EDS analyses of Figures 63-66 were obtained by setting 2000 counts for Ni. Figure 63 shows the chemical analysis at four areas of the sample aged 500 hours at 700^{o}C. Area A is located at the platelike particle, B the matrix, C one of the pearlite-like component, and D the etched out, deeper area parallel to C. Figure 64 shows another EDS analysis result of the sample

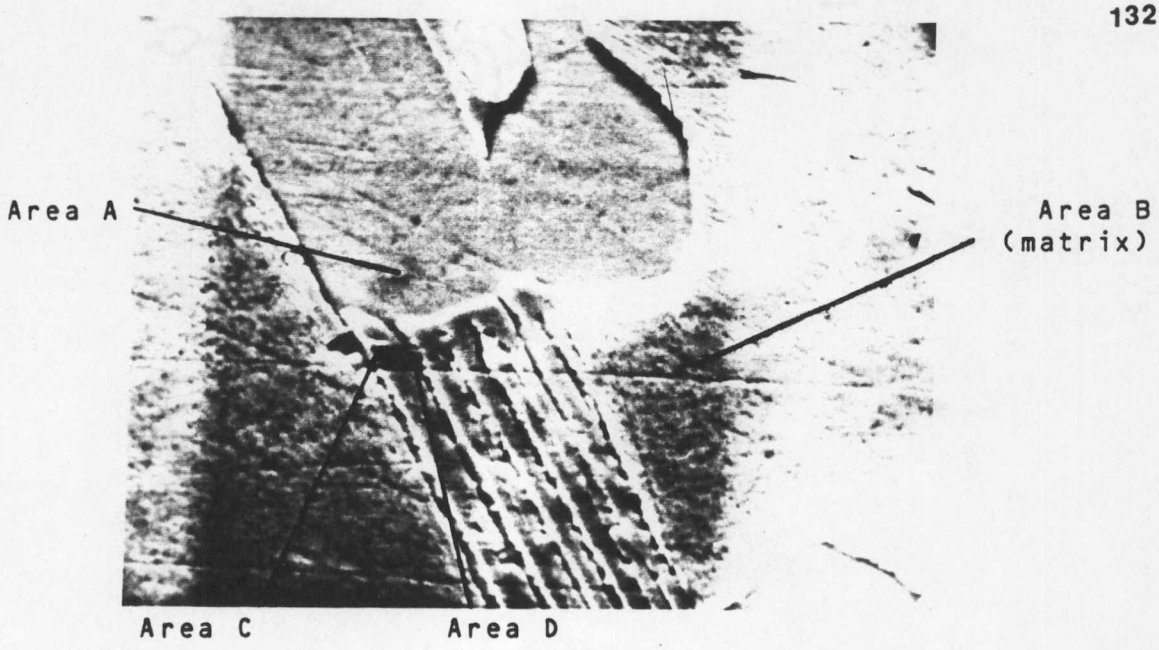

	Ni	Ta	Cr	
Area A	100	64	13	Ta-rich
Area B	100	27	42	Cr-rich
Area C	100	19	49	Cr-rich
Area D	100	36	43	

Figure 63. EDS analysis of Ni-Ta-Cr alloy, aged at 700°C for 500 hrs, SEM, 5000 X.

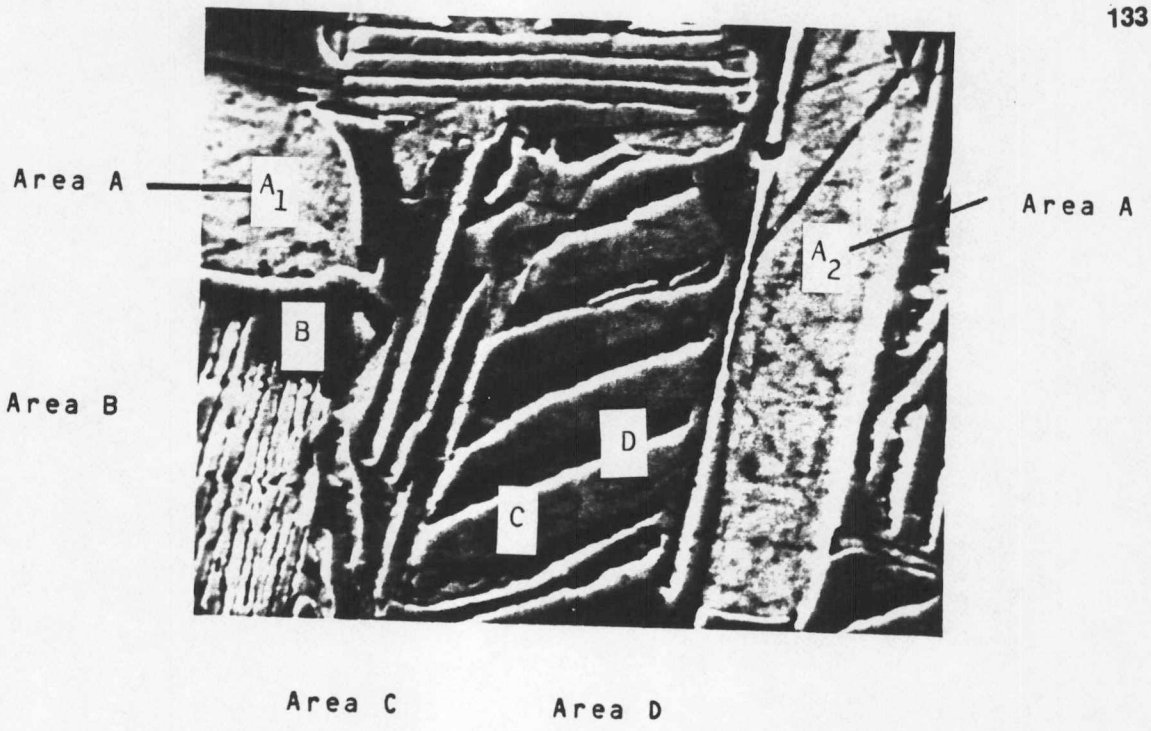

	Ni	Ta	Cr	
Area A	100	44	19	Ta-rich
Area A	100	50	13	Ta-rich
Area B	100	9	57	Cr-rich
Area C	100	14	44	Cr-rich
Area D	100	21	41	

Figure 64. EDS analysis of Ni-Ta-Cr alloy, aged at 900°C for 500 hrs, SEM, 5000 X.

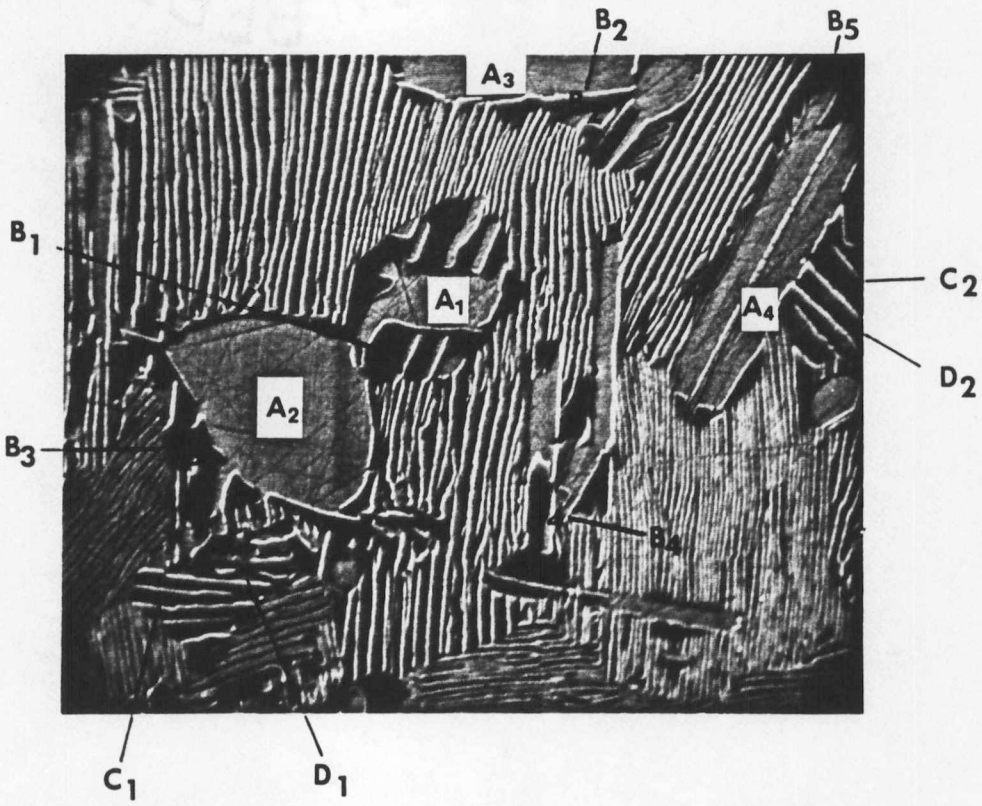

	Ni	Ta	Cr	
Area A	100	72	16	Average from A_1 through A_4
Area B	100	21	53	Average from B_1 through B_5
Area C	100	27	45	Average of C_1 and C_2
Area D	100	34	46	Average of D_1 and D_2

Figure 65. EDS analysis of Ni-Ta-Cr alloy, aged at 900°C for 500 hrs, SEM, 2000 X.

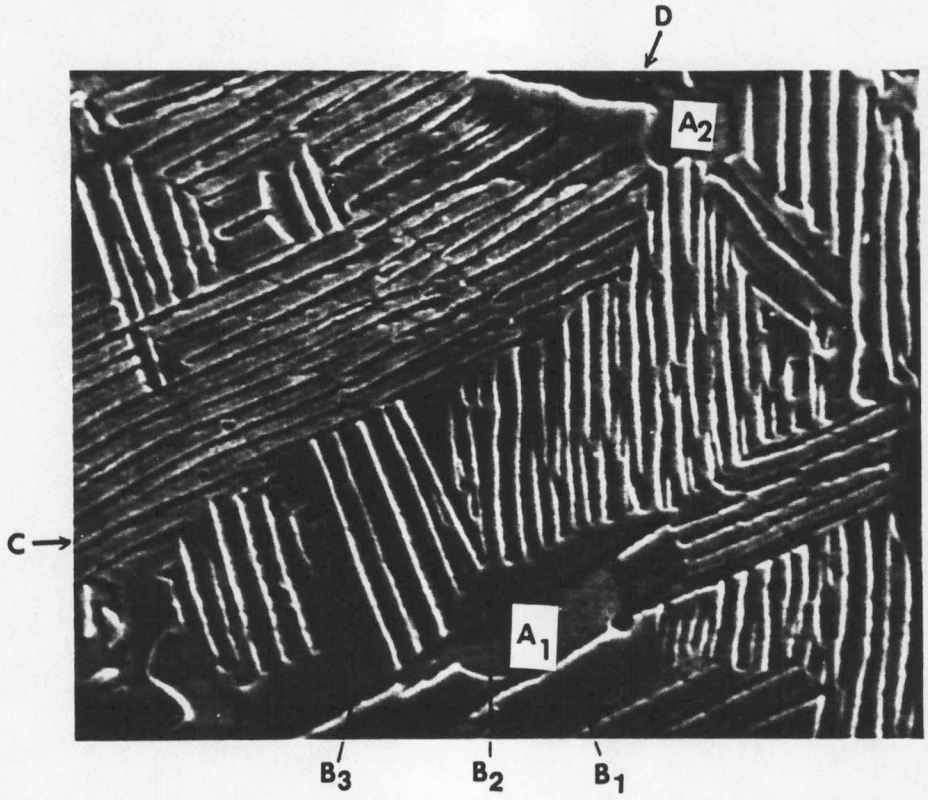

	Ni	Ta	Cr	
Area A_1	100	66	18	Ta-rich
Area A_2	100	60	22	Ta-rich
Area B_1	100	15	56	Cr-rich
Area B_2	100	14	54	Cr-rich
Area B_3	100	13	58	Cr-rich
Area C	100	23	49	
Area D	100	28	47	

Figure 66. EDS analysis of Ni-Ta-Cr alloy, aged at 900°C for 1000 hrs, SEM, 5000 X.

aged at 900°C for 500 hrs. Again, A1 and A2 are particles, B the matrix, C one component of the pearlite-like material, and D the etched out, other component. If we compare the analyses of Figure 63 and 64, good agreement is obtained at particle areas (which are Ta-rich) and the unetched regions of pearlite-like material (Cr-rich). Area D was so small that it is possible to detect the neighboring material at the same time.

Let's look at two more EDS analyses to examine the transformation in this material. In Figure 65, area A1 through A4 are as the previous A, B1 through B5 are B, C1 and C2 are C, and D1 and D2 are D. For Figure 66, detected areas are denoted as A1, A2, B1, B2, B3, C, and D.

From all these EDS analysis data we can get several conclusions :

(a) The particles are Ta-rich, with Cr/Ta ratio from 0.21 to 0.33.

(b) The original matrix is high in Ni, with a Cr/Ta ratio from 2.0 to 4.5.

(c) One of the pearlite-like components is high in Ni. The Cr content is a little higher than Ta, where Cr/Ta is 1.2 to 2.5.

(d) The etched out, deeper area parallel to C is high in Ni and Cr/Ta ratio is about one.

To determine the composition of the plate-like particles present in the ternary alloy, an un-etched sample

reheated to 1280°C, 4 hrs) was examined by EDS analysis as shown in Figure 67. The particle is assumed to be a $Ni_XTa_YCr_Z$ type compound, and the ratios of Cr/Ta, Ta/Ni and Cr/Ni are obtained as follows (after calibration, see Appendix 1):

$$Y/X = 0.27, \qquad Z/X = 0.09, \qquad Z/Y = 0.27,$$

and let X + Y + Z = 1. Solving the above equations we get X : Y : Z = 0.73 : 0.21 : 0.06, or X : (Y + Z) = 3 : 1 which indicates that the particle has $Ni_3(Ta_ACr_B)$ type. From the above calculation A : B = 3.7 : 1 and A + B = 1, then A = 0.79, B = 0.21. It is concluded that the structure of the particle is $Ni_3(Ta_{0.79}Cr_{0.21})$.

The effect of Cr on the lattice parameters of Ni_3Ta depends on the extent to which it substitutes for Ni and for Ta; substitution for Ta will decrease the parameters and hence the mismatch. Cr induces copious matrix nucleation of b.c.t. precipitate. One possible factor is a reduction in the nucleation energy resulting from a decrease in lattice mismatch. Quist et al. (23) observed that the additions of iron and aluminum assisted nucleation of Ni_3Nb in Ni-Nb alloys which was attributed to the partitioning of Fe and Al between matrix and precipitate, expanding the matrix lattice and reducing the precipitate lattice parameter, leading to a smaller mismatch.

The reduction in the lattice mismatch due to the presence of Cr in Ni-Ta-Cr alloys is an important factor in aiding precipitation.

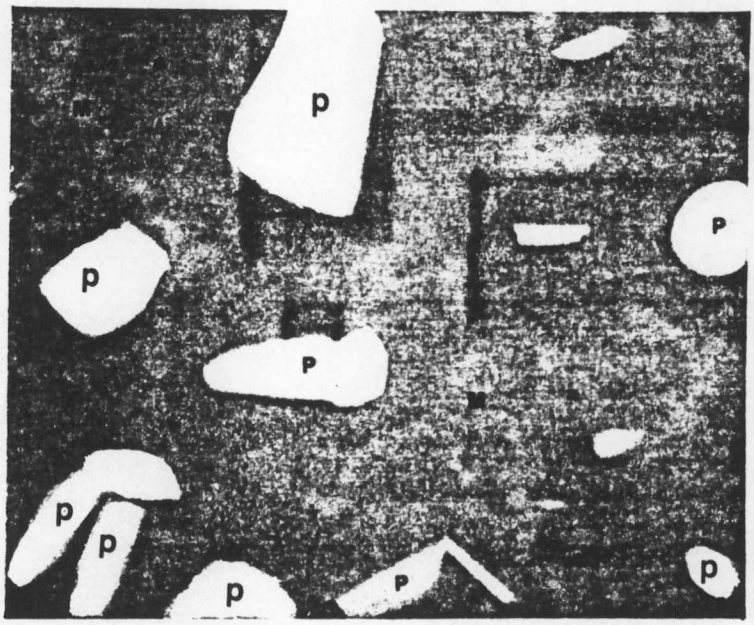

	Ni	Ta	Cr	
Particle	100	67	14	Average, Ta-rich
Matrix	100	37	45	Average

Figure 67. EDS analysis of un-etched Ni-Ta-Cr alloy, which was reheated to 1280°C for 4 hrs after the first solution treatment (1250°C, 7 days).

TRANSMISSION ELECTRON MICROSCOPY EXAMINATION

The TEM work has been done on the Ni-Ta alloy to examine the fine structure. TEM samples were prepared from material aged at 600°C and 1000°C for 1000 hrs and several electron diffraction patterns were obtained as shown in the following pictures. Electron diffraction patterns of Ni_2Mo (Ni_2Ta), DO_{22} structure and FCC fundamental spots are shown in Figure 68. The Ni_2Ta spots are present at the one-third positions of the diagonals for either the <011> or the <112> zone axis. The electron diffraction patterns of aged Ni_8V alloys (shown in Figure 9), Ni_8Ta electron diffraction patterns (shown in Figure 13), and the calculated R (camera length / d spacing) values and the corresponding (hkl) were used to check the experimentally observed diffraction patterns.

The calculation of R values was made as follows :

$R = L\lambda / d$,

$L\lambda$ = camera constant = 53.7×10^{-8} cm Å,

L = 1452 mm = camera length,

= 0.037 Å for 100 KV.

$R = L\lambda / d = L\lambda \sqrt{h^2 + k^2 + l^2} / a_o$,

a_o = 3.58 Å (20).

Table 19 lists the calculated R values and the corresponding (hkl) for FCC fundamental spots.

Figures 69 through 71d show the patterns of Ni-Ta alloy where the zone axis, DO_{22} spots, Ni_2Ta spots and fundamental FCC positions are indicated in the accompanying diagram.

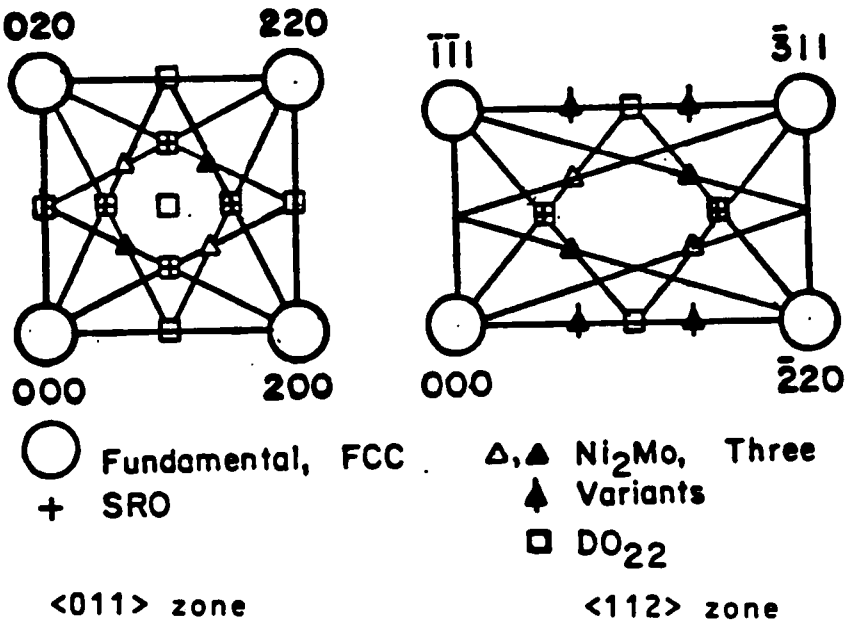

Figure 68. Electron diffraction patterns of Ni_2Mo (Ni_2Ta), DO_{22} structure and FCC fundamental spots. There are three variants for Ni_2Mo (34).

Table 19. The R values and the corresponding (hkl) of FCC fundamental spots.

(hkl)	R (cm)
111	1.26
200	1.45
220	2.05
311	2.40
222	2.51
400	2.81
331	3.16
420	3.24
422	3.55
511	3.77
531	4.29

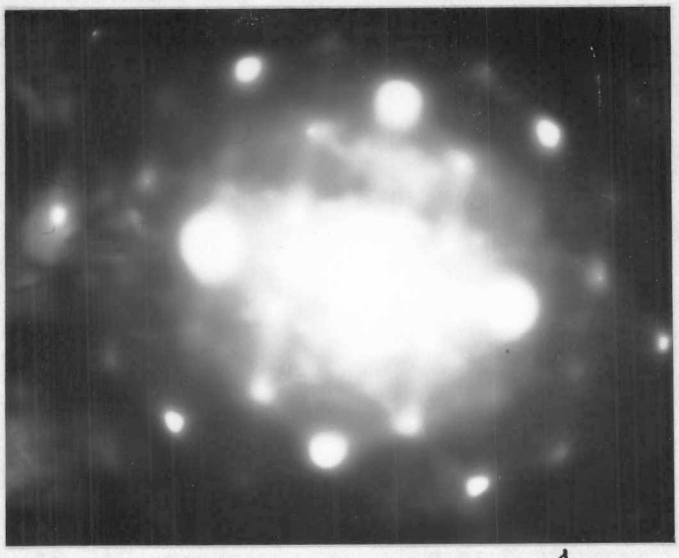

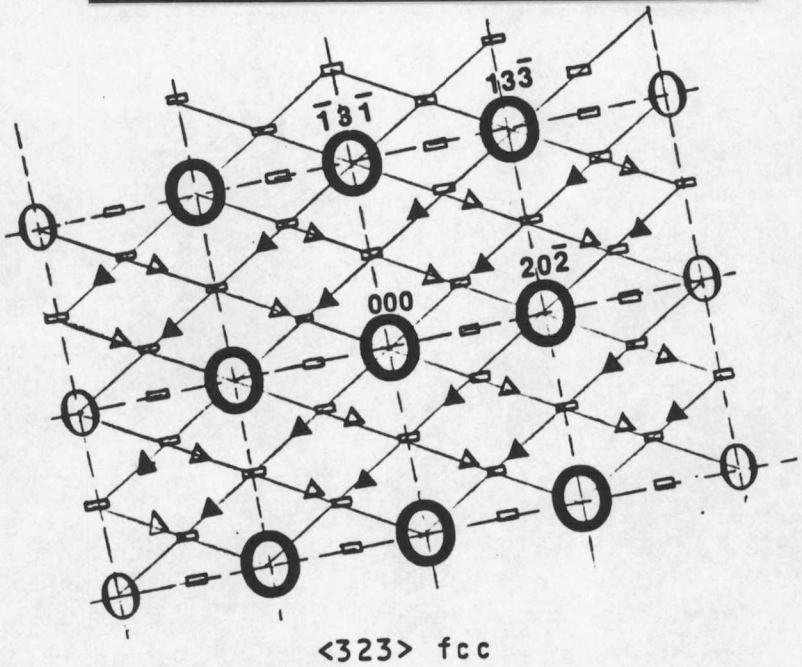

<323> fcc

O --------- FCC, fundamental

▭ --------- DO_{22}

△,▲--------- Ni_2Ta, two variants

Figure 69. Diffraction patterns of Ni-Ta alloy, aged at 600°C for 1000 hrs, showing DO_{22}, Ni_2Ta, and FCC fundamental spots.

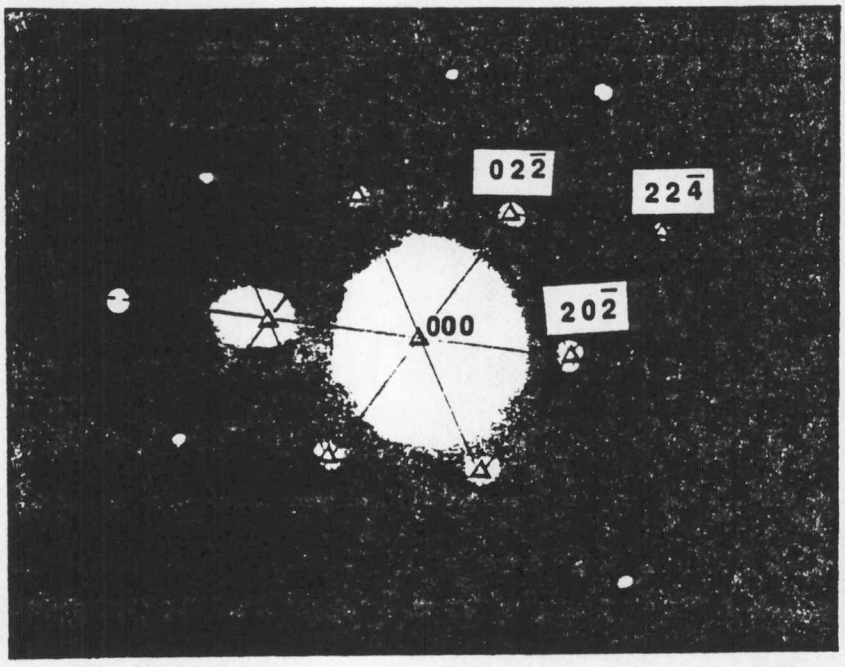

<111> fcc

Δ---------- FCC fundamental spots

Figure 70. Diffraction pattern of Ni-Ta alloy which shows FCC spots only (600°C, 1000 hrs).

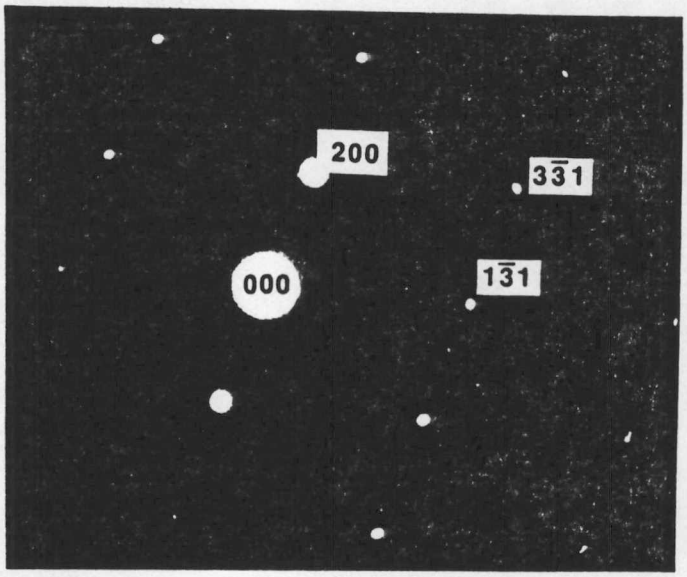

71a. Diffraction patterns of Ni-Ta alloy, aged at 600^{o}C for 1000 hrs; <013>zone.

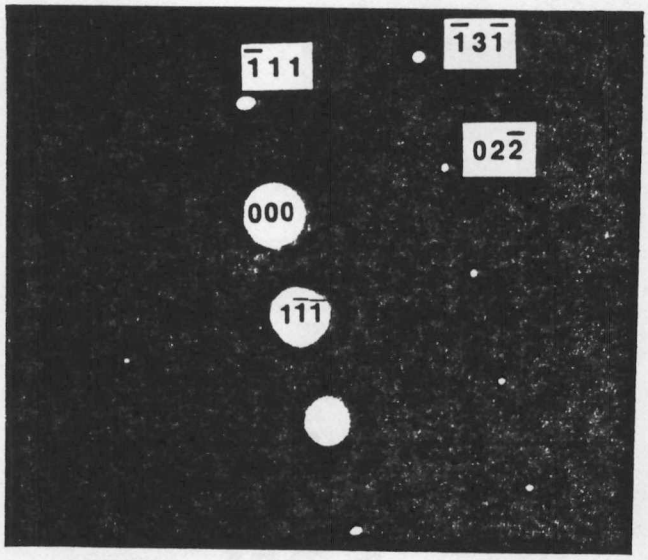

71b. Diffraction pattern of Ni-Ta alloy, aged at 600^{o}C for 1000 hrs; <112>zone .

Figure 71. Electron diffraction pattern of the Ni-Ta alloy.

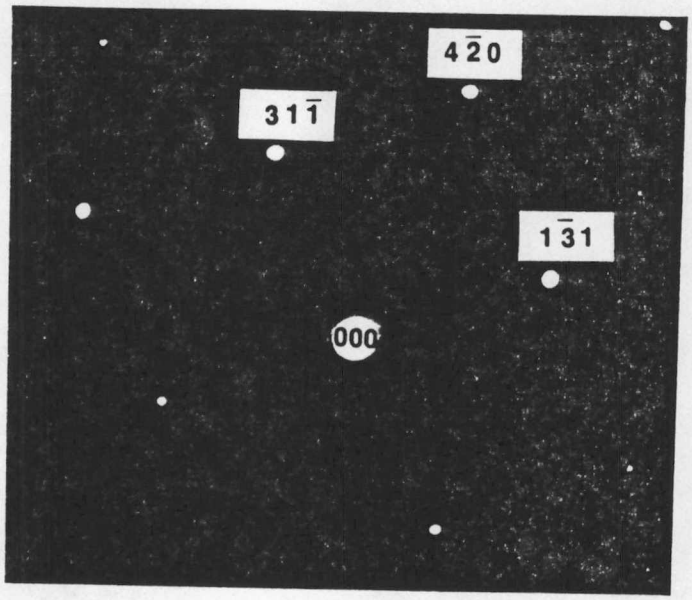

71c. Diffraction patterns of Ni-Ta alloy, aged at 1000°C for 1000 hrs; <125>zone.

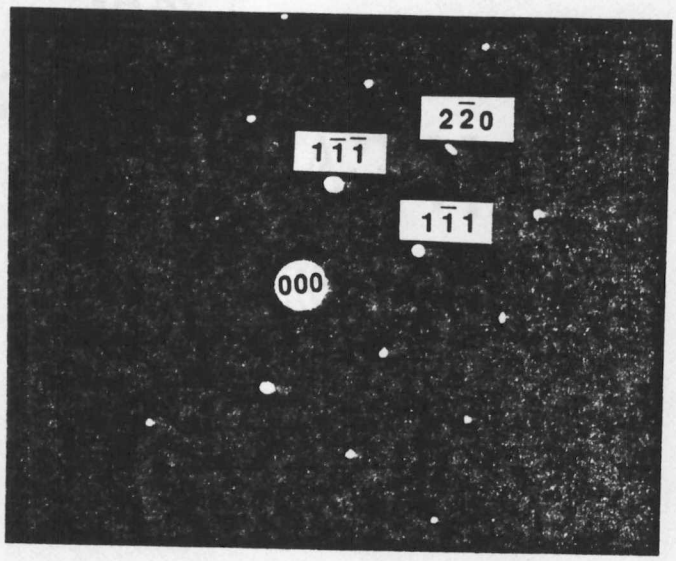

71d. Diffraction pattern of Ni-Ta alloy, aged at 1000°C for 1000 hrs; <011>zone.

Figure 71. (Continued)

From the observation of these pictures, Ni_2Ta and DO_{22} structures are present in the aged Ni-Ta alloy. The reason why they can not be detected by X-ray diffraction analysis might be due to the small amount in volume (less than 5%) they are present in the materials.

In Figure 69, the electron diffraction pattern shows the DO_{22}, Ni_2Ta (two variants), and FCC fundamental spots. In the schematic diagram, the open circles denote FCC fundamental spots, the open rectangles denote DO_{22} structure and the open and closed triangles denote two Ni_2Ta variants. This sample was aged at 600°C for 1000 hrs. Figure 70 (also 600°C for 1000 hrs) shows fundamental FCC spots. In Figures 71a-d, only FCC fundamental spots are observed, which indicates that these samples have a disordered FCC Ni-rich solid solution due to the rapid cooling after aging. All the aging temperatures were higher than the reported order-disorder critical temperature 843 K (570°C). One possible reason why some of the aged materials contained an ordered structure is the lack of fast cooling (quartz tube was not broken within 15 seconds after taken out of the furnace). It is possible that the samples with a lower cooling rate contain both the ordered and disordered structures.

Due to time limitation, no further work was done on the Ni-Ta alloy to study its structure, especially the order-disorder transformation. This alloy needs further TEM work to study its characteristics and structure.

COMPARISON

Several comparisons between the present work and previously published papers are shown as follows.

(a) Microstucture

Figures 72a-b are the optical microstructures of the as-cast Ni-Ta-Cr alloy. Figure 72c shows the primary Ni_3Ta in γ matrix for a Ni-20 at.% Ta alloy in the as-cast condition (Nash and West) (16). The dark areas (Fig. 72a-b) were developed by heavy etching. Upon etching the sample of Figures 72a-b slightly, the platelike crystals of Ni_3Ta are observed as shown in Figure 73 (high magnification SEM picture). The matrix appears to be two phases, but the x-ray diffraction data only indicated γ and Ni_3Ta present in this sample. However, EDS shows the long thin particles to be Ta rich.

The platelike crystals of Ni_3Ta in γ matrix shown in Chakravorty and West's paper published in 1983 (33) (Figure 74b) were designated to be orthorhombic $Ni_3(Ta,Mo)$ or δ . Their pictures are similar to the present work, as shown in Figure 74a (Ni-Ta-Cr alloy, solution treated at 1250°C, 7 days, water quenched, OM, 500X) where the plate-like particles have been taken to be BCT $Ni_3(Ta,Cr)$ compound from the observed diffractometer traces. In Chakravorty and West's experiments, X-ray diffractometry was carried out on bulk polished samples in deciding the structure. The ASTM

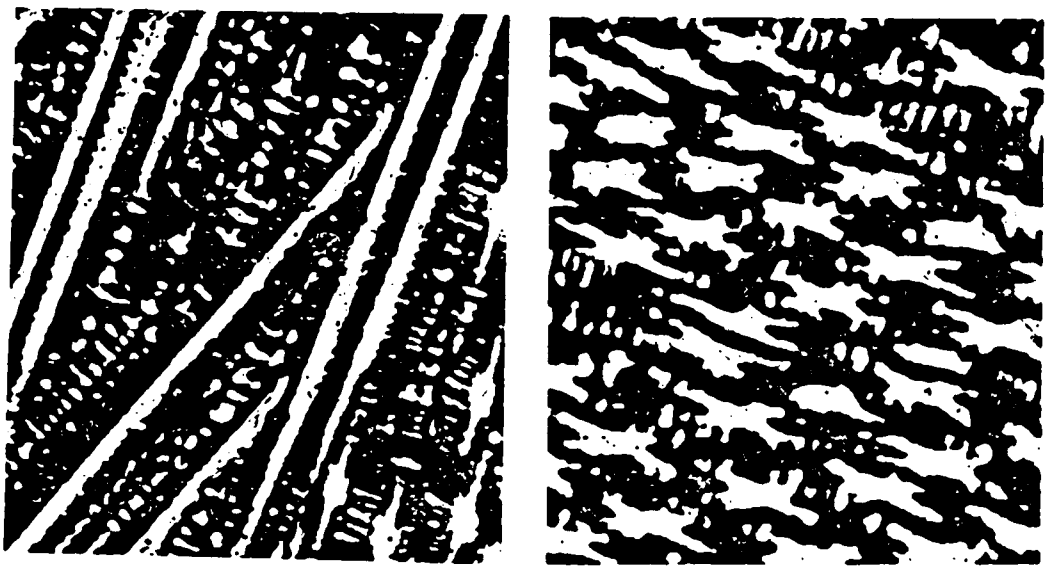

72a and b. Optical microstructure of as-cast Ni-Ta-Cr alloy, OM, 200 X.

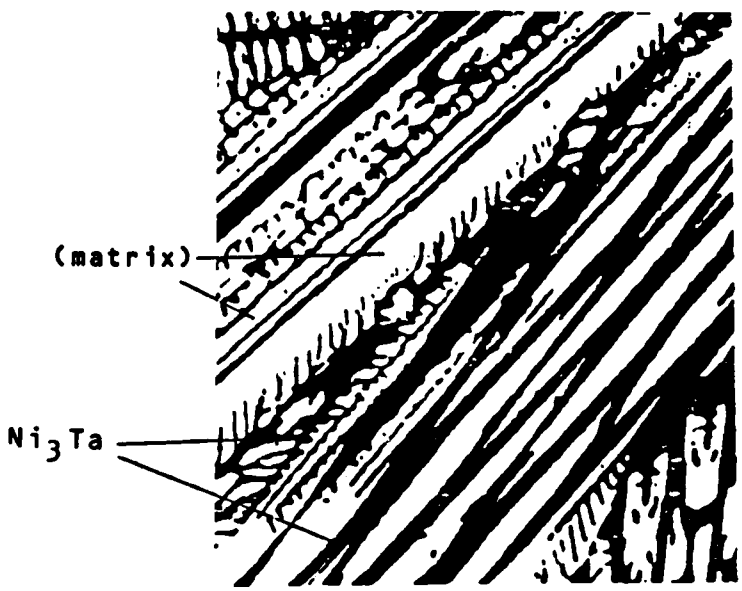

72c. Ni-20 at.% Ta alloy; "as-cast" showing primary lamellae of Ni_3Ta in matrix, OM, 250 X (16).

Figure 72. Optical microstructures of the as-cast Ni-Ta-Cr alloy.

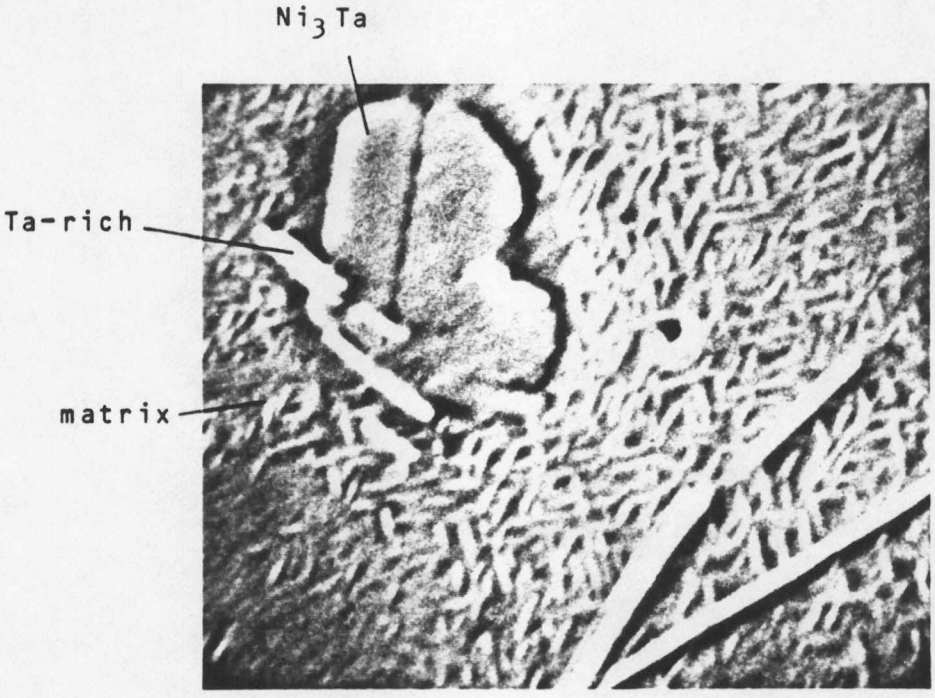

Figure 73. Ni-9.6 at.% Ta-16.6 at.% Cr alloy, "as-cast" showing primary particles of Ni_3Ta without over-etching, SEM, 10,000 X.

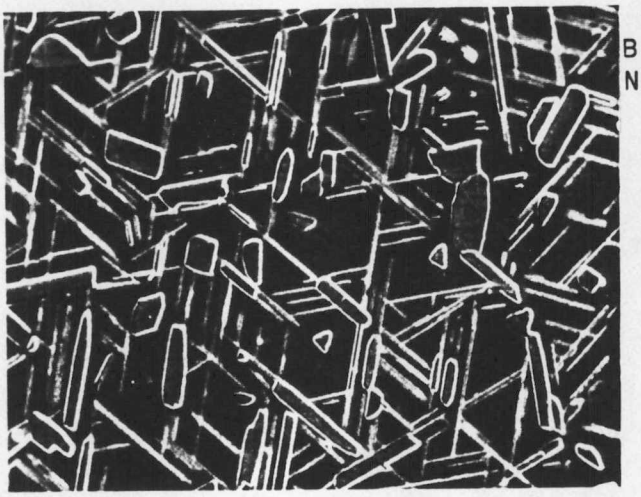

74a. Ni-25Ta-12.5Cr alloy, solution treated at 1250°C for one week; plate-like particles of BCT $Ni_3(Ta_{0.79}Cr_{0.21})$ in γ matrix (FCC) (present work).

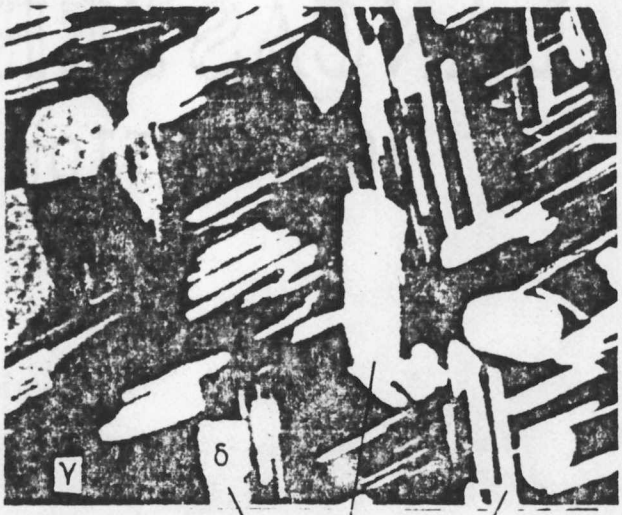

74b. Ni-9Mo-11Ta alloy, annealed at 1250°C for one week; plate-like crystals of orthorhombic $Ni_3(Ta,Mo)$ or δ in γ matrix (33).

Figure 74. Scanning electron microstructures of the Ni-Ta-Cr alloy which show $Ni_3(Ta,X)$.

data file was not mentioned in their phase identification. The material shown in Figure 74b is Ni-9Mo-11Ta alloy annealed at 1523 K (1250°C) for one week. This microstructure is similar to that of the alloy of the present work, as shown in Figure 74a. The contradiction between the results of theirs and mine might be due to the different characteristics of Mo and Cr. In the work of Aballe, Ramaswamy, and West published in 1975 (31), an alloy Ni-25 wt.% Ta-10 wt.% Cr was studied by applying two solution-treatment temperatures, 1250°C and 1270°C. After quenching from 1250°C the structure was found to be two-phase consisting of "large, plate-like particles" in a matrix. The particles were given to be orthorhombic Ni_3Ta by X-ray diffraction examination. On aging in the range 650°C to 800°C, substantial hardening occurred, associated with the formation of a fine dispersion of precipitate apparently homogeneously nucleated in the matrix regions between the large orthorhombic Ni_3Ta plates. The newly formed harder precipitate was identified to be BCT Ni_3Ta structure having a habit plane as (001) matrix by selected area diffraction examination. On over-aging, "larger", plate-shaped orthorhombic Ni_3Ta particles formed. In the over-aged condition, they did not mention what happened to the finely dispersed BCT Ni_3Ta precipitate. In the present work, the plate-like particles were identified in the Ni-25 Ta-12.5 Cr alloy to be BCT Ni_3Ta after solution treating at 1250°C for

one week. The structure found by Aballe et al. (31) after quenching from 1270°C was reported to have the presence of a very fine BCT precipitate dispersed in a matrix. On aging at 800°C the hardness was slightly greater than that in the alloy aged at 800°C after quenching from 1250°C. In the over-aged condition after quenching from 1270°C, a coarser dispersion formed which was given to be orthorhombic Ni_3Ta. The result of this treatment was similar to that observed in the present work (after a second solution treatment at 1280°C for four hours, then aged at 700°C to 1000°C). Table 20 shows the comparison in phase identification between their result and those of the present work. Figure 75a and 75b are scanning electron micrographs (35) showing the so-called "plate-like" particles of orthorhombic Ni_3Ta designated by West et al.

Figure 76 is a scanning electron micrograph showing coarse dispersion of orthorhombic Ni_3Ta which Aballe et al. (30) report to be softer than BCT Ni_3Ta. This microstructure is similar to the newly formed material present in the ternary Ni-Ta-Cr alloy after aging. Figure 77 (36) shows a lamellar microstructure which Abelle et al. identify as containing orthorhombic Ni_3Nb (which has the same structure as Ni_3Ta); they do not indicate what the other phase is, but it is presumed to be the FCC structure.

Table 20. A comparison in phase identificstion between the work of Aballe et al. and the present work.

Material	source	solution treatment temperature	phases present after solution treatment	phases present after aging	phases present after over-aging
Ni-25Ta-10Cr	Aballe et al. (31)	1250°C, water quenched	γ(matrix) + large, plate-like orthorhombic Ni_3Ta particles	γ(matrix) + orthorhombic Ni_3Ta + fine dispersion of BCT Ni_3Ta (650-800°C)	γ(matrix) + large, plate-like orthorhombic Ni_3Ta + BCT Ni_3Ta
Ni-25Ta-12.5Cr	present work	1250°C, 7 days, water quenched	γ(matrix) + unknown second phase (5%) + BCT Ni_3Ta particles (10%)	--------	--------
Ni-25Ta-10Cr	Aballe et al.	1270°C, water quenched	γ(matrix) + fine dispersion of BCT Ni_3Ta precipitate	remained the same	γ(matrix) + BCT Ni_3Ta + coarser orthorhombic Ni_3Ta
Ni-25Ta-12.5Cr	present work	1250°C, 7 days, water quenched then heated to 1280°C, 4 hrs, water quenched	γ(matrix) (90%) + BCT Ni_3Ta particles (10%)	γ(matrix) (5%) + BCT Ni_3Ta (10%) + orthorhombic Ni_3Ta (85%) (700-1000°C)	γ(matrix) (15%) + BCT Ni_3Ta (10%) + coarser orthorhombic Ni_3Ta (75%) (1000°C, 1000 hrs)

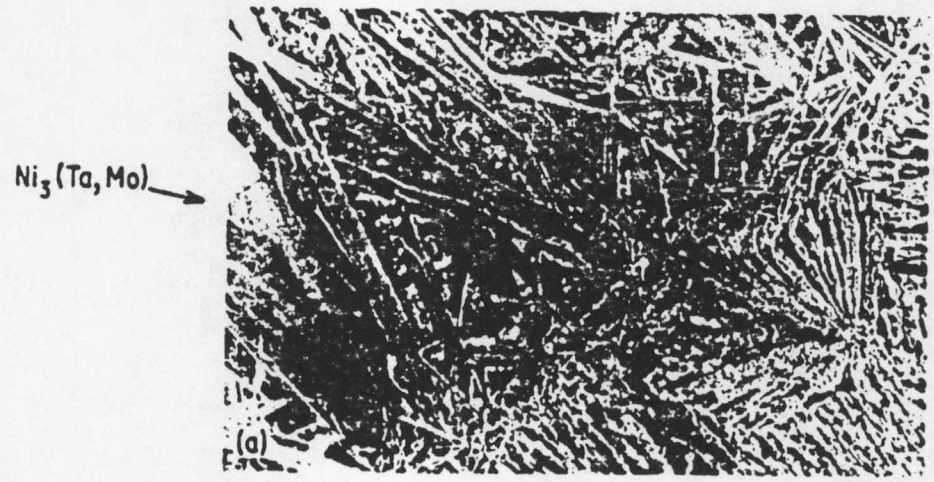

75a. As-cast structure of Ni-12.5Mo-12.5Ta (at.%) alloy showing "plate-like" crystals of $Ni_3(Ta,Mo)$, 275 X (35).

75b. Structure of Ni-12.5Mo-12.5Ta (at.%) alloy after annealing at 1250°C for one week showing orthorhombic $Ni_3(Ta,Mo)$ together with a small portion of γ, 700 X (35).

Figure 75. Scanning electron micrographs of the Ni-Mo-Ta alloy which show $Ni_3(Ta,Mo)$.

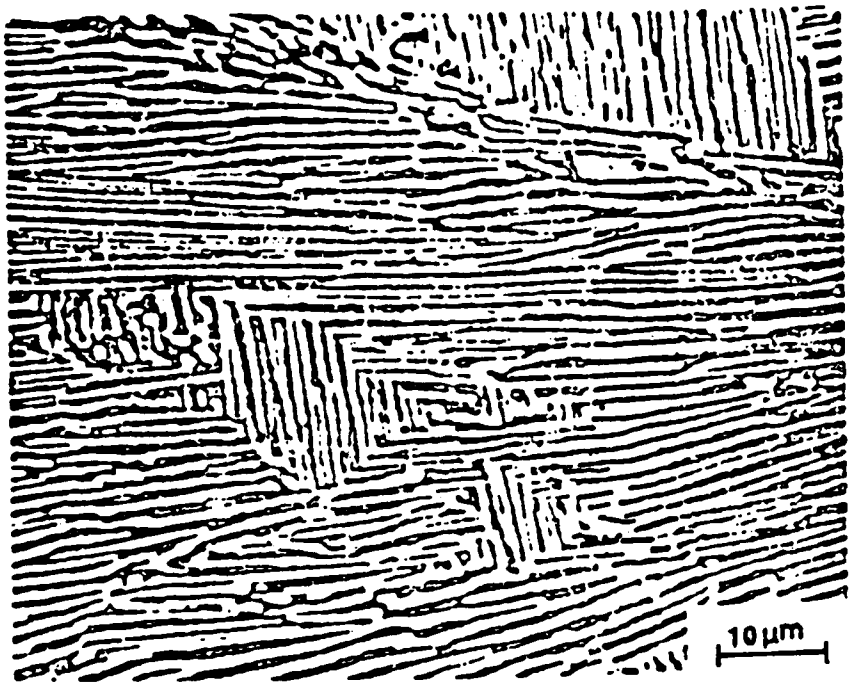

Figure 76. Ni-25 wt.% Ta-10 wt.% Cr alloy, solution treated at 1270°C, water quenched and then aged at 900°C for 30 hrs. Scanning electron micrograph shows coarse dispersion of orthorhombic Ni_3Ta, which is reported to be softer than BCT Ni_3Ta, in FCC γ (31).

Figure 77. TEM micrograph shows Ni_3Nb (Ni_3Ta) orthorhombic precipitates which was annealed at 700°C for 350 hrs (36).

(b) Microhardness Results

Figure 17 shows the hardness vs. aging time data for a Ni-25 wt.% Ta-10 wt.% Cr alloy (31). The microhardness data of the present work are compared to these in Figure 78. The chemical composition of the Ni-Ta-Cr alloy of the present work was a little higher in Cr and Ta than their (Aballe et al.) material (0.75% Ta higher, 2.46% Cr higher). Good agreement is found for aging at 600°C and 650°C. The deviation is quite large for 700°C; for 800°C, the difference is less than that aging at 700°C.

Figure 79a-c shows the relationship between the phases present in the material and the changes in microhardness. Figure 79a is the ternary alloy water quenched from 1250°C after one week, which contains about 15% of "two" second phases. The average microhardness for this material is 335 DPH . In Figure 79b only one second phase (10%) is present in the matrix (90%) after reheating to 1280°C for four hrs, then water quenching. For this treatment, the alloy had a higher hardness of 530 DPH which might be associated with the absence of the dissolved thin second phase (denoted 2 in Figure 39a) and the increase of Ta and Cr in solid solution. Most of the matrix transformed to a new structure after aging from 700°C to 1000°C and caused the decrease in hardness (from 530 to 335 DPH). The aged materials contained

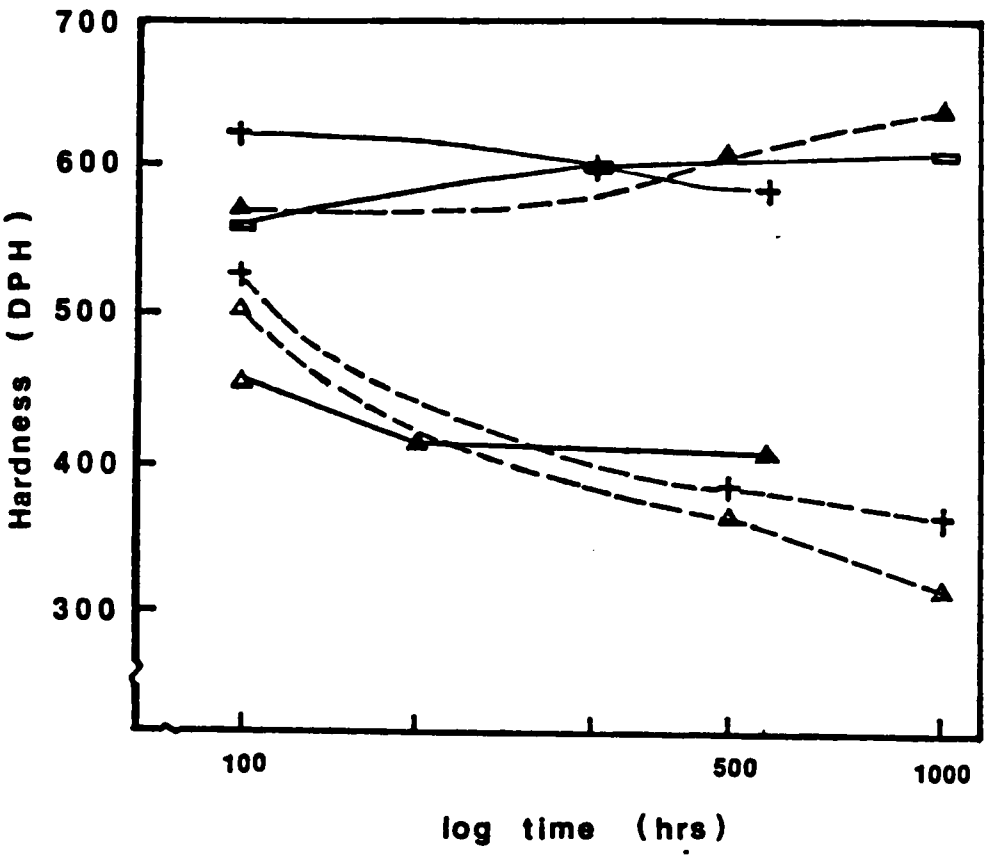

△ — Solution treated 1250°C, aged at 800°C;

\+ — Solution treated 1250°C, aged at 700°C;

▭ — Solution treated 1250°C, aged at 800°C;

▲ — Solution treated 1250°C, aged at 700°C;

-------- present work

——— Reference 31

Figure 78. Comparison between the hardness values of the present work and the data published in reference 31.

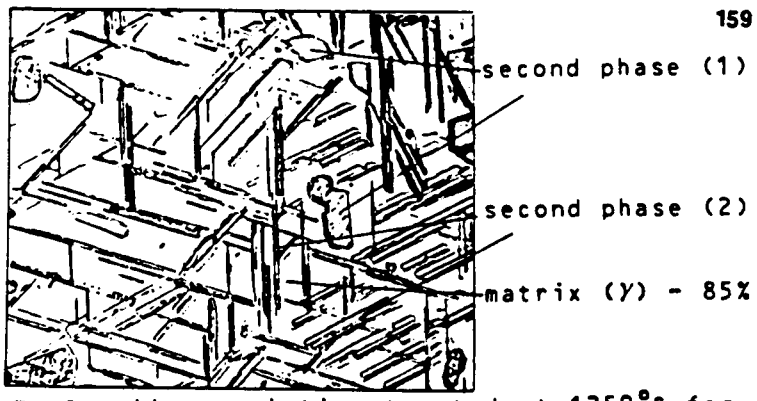

79a. Ni-Ta-Cr alloy, solution treated at 1250°C for one week, then water quenched, SEM, 500 X; the microhardness is 335 DPH.

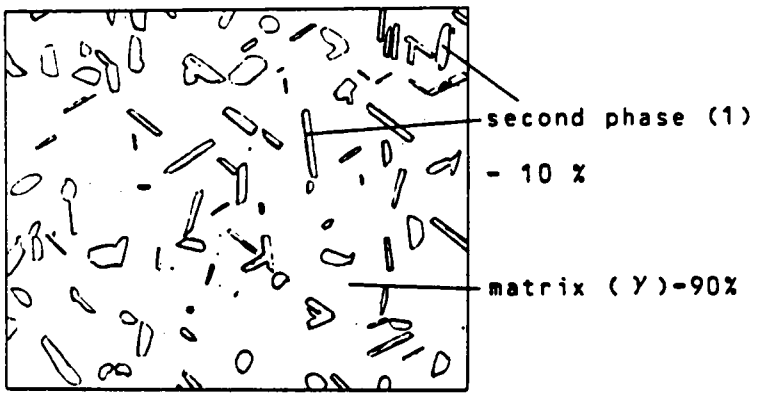

79b. Ni-Ta-Cr alloy, reheated to 1280°C for 4 hrs., then water quenched after the first solution treatment as Figure 79a, OM, 200 X; microhardness is 530 DPH.

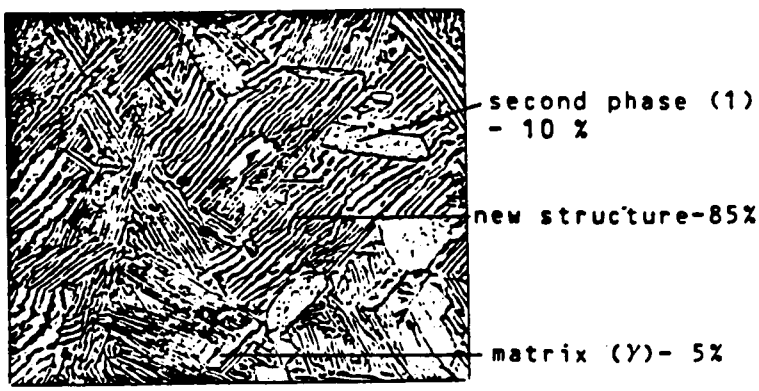

79c. Ni-Ta-Cr alloy, aged at 900°C for 1000 hrs, then water quenched after the second solution treatment, SEM, 500 X; the microhardness is 330 DPH.

Figure 79. The microstructures of the Ni-Ta-Cr alloy which show the change in structure between solution treatment and aging.

the original second phase (10%), the newly formed structure (85%), and the matrix (5%). It is concluded that the newly formed structure (taken to be orthorhombic Ni_3Ta) is associated with the decrease in hardness and is softer than the original second phase (taken to be BCT Ni_3Ta).

(c) Phase diagram

In Figures 1 and 2, Ni_8Ta was not present in those phase diagrams. Figure 3 showed Ni_8Ta to range from 10.5 to 13.0 at.% Ta, but the lower limit was not sure for Ta below 10 at.% (Nash and West, 1983) (18). The present work has been on a Ni-10 at.% Ta alloy. The results indicate that Ni_8Ta is not present at this region (at temperatures from 873 K to 1273 K) which is consistent with the work of Larson et al. (17) published in 1970, but is contradictory to the phase diagram suggested by Nash and West in 1983 (Figure 3). It is very difficult to modify the partial phase diagram for the Ni-Ta system at Ta < 10 at.% to give agreement simultaneously with the results of Larson et al., Nash and West, Moreen et al., and the present work. To decide the structure present in this region, it is recommended that alloys containing 5, 7.5, 9, 10, and 12 at.% Ta be aged from 400^{o}to 1000^{o}C for time up to 1000 hrs. These samples should then be examined using TEM.

LIST OF REFERENCES

LIST OF REFERENCES

1. J. W. Martin, Precipitation Hardening, p.3, A. Weaton and Co., Great Britain, 1966.

2. H. Nowontny and H. Qeateneicher, "The crystal structures of β-$TaNi_3$, $Ta(Cu,Al)_2$, $Nb(Cu,Al)_2$ and $Ta_6(Cu,Al)_7$", Monatashefte fur Chemie, vol. 95, 1964, pp. 982-989.

3. E. N. Pylaeva, E. I. Gladyshevskii, and P. I. Kripyakevich, "Crystalline structure of Ni_3Nb and Ni_3Ta compounds", Journal of Inorganic Chemistry, vol. 3, 1958, pp. 1626-1631.

4. N. Karlsen, "An X-ray study of the phases in the copper-titanium system", Journal of Institute Metals, vol. 79, 1951, pp. 391-405.

5. V. Ramaswamy, P. R. Swann and D. R. F. West, unpublished work as given in M. Ablle, V. Ramaswamy and D. R. F. West, "Intermetallic compound precipitation from solid solution in some Ni-Ta and Ni-Ta-Cr alloys", Journal of the Less-Common Metals, vol. 39, 1975, pp. 287-292.

6. S. E. Axter and D. H. Polonis, "The influence of iron and aluminum on the kinetics of precipitation in Ni-Ta alloys", Materials Science and Engineering, vol. 36, 1978, pp. 71-79.

7. I. I. Kornilov and E. N. Pylaeva, "Equilibrium diagram of the Nickel-Tantalum system", Russian Journal of Inorganic Chemistry, vol. 7, 1962, pp.300-302.

8. M. Hansen, Constitution of Binary Alloys, p.1046, McGraw-Hill, New York, 1958.

9. F. A. Shunk, Constitution of Binary Alloys, 2nd supplement, 1958, McGraw-Hill, New York, p.557.

10. Metals Handbook, vol. 8, Metallography, Structures and Phase Digrams, 8th edition, American Society for Metals, Metals Park, Ohio, 1973, p.370.

11. O. Kubaschewski and H. Speidel, "Oxidation-resistance and some phase relationships in the system Cr-Ta-Ni", Journal of Institute of Metals, vol. 75, 1948, pp. 417-430.

12 B. C. Giessen and N. J. Grant, "The crystal structure of Ni_3Ta and its change on cold working", Acta Metallurgica vol. 15, 1967, pp. 871-877.

13. B. C. Giessen and N. J. Grant, "The crystal structure of Ni_2Ta", Transactions AIME, vol. 230, 1964, pp.1730-1731.

14. H. Oesterreicher and H. Nowotny, "The crystal structure of Ni_2Ta", Monatshefte fur Chemie, vol. 95, 1964, pp.1038-1039.

15. Metals Handbook, vol. 8, Metallography, Structures and Phase Diagrams, 8th edition, American Society for Metals Metals Park, Ohio, 1973, p.326.

16. P. Nash and D. R. F. West. "Phase diagram in the Ni-Ta-Al system", Metal Science, vol.13, 1979, pp. 670-675.

17. J. M. Larson, R. Taggart and D H. Polonis, "Ni_8Ta in nickel-rich Ni-Ta alloys", Metallurgical Transactions, vol. 1, 1970, pp. 485-489.

18. P. Nash and D. R. F. West, "Ni-Al and Ni-Ta phase diagram", Metal Science, vol. 17, 1983, pp. 99-100.

19. E. Therkelsen, paper published in Metals and Alloys, vol. 4, 1933, pp. 105-108, mentioned in Constitution of Binary Alloys, M. Hansen, 1958, MacGraw-Hill, New York, p.1047.

20. H. J. Wallbaum, "Die system der eisenmetalle mit titan, zirkon, niob und tantal", Archiv fur das Eisenhuttenwesen, vol. 14, 1940, pp. 521-526.

21. Hans-Gunter Baer, "Widerstandsanomalien im System Nickel-Tantal", Z. Metallkde., Bd.57, 1966, pp.392-395.

22. Metals Handbook, vol. 8, Metallography, Structures and Phase Diagrams, 8th edition, American Society for Metals, Metals Park, Ohio, 1973, p.237.

23. W. E. Quist, C. J. van der Wekken, R. Taggart, and D. H. Plonis, "Intermediate Compound Ni_8Nb(Cb) in Nickel-Rich Nickel-Niobium (Columbium) Alloys", Transactions AIME, vol. 245, 1969, p.345.

24. Metals Handbook, vol. 8, Metallography, Structures and Phase Diagrams, 8th edition, American Society for Metals, Metals Park, Ohio, 1973, p.352.

25. W. B. Pearson, "Handbook of Lattice Spacing and Structure of Metals and Alloys", Pergamon Press, New York, 1958.

26. P. S. Rudman, Atomic Size Difference as an Ordering and Driving Force, 1969 Bolton Landing (AIME) Conference on Ordered Alloys (Claitor, Baton Rouge, 1970).

27. H. A. Moreen, R. Taggart and D. H. Polonis, "Ni_8X Phases in the Systems Ni-V, Ni-V-Nb, and Ni-V-Ta", Journal of Materials Science, vol. 6, 1971, pp. 1425-1432.

28. J. Mayer and K. Urban, "Observation of Ni_8Mo Ordered Phase in Ni-Mo Alloys", Physica Status Solidi (a), vol. 90, 1985, pp. 469-475.

29. R. E. Reed-Hill, Physical Metallurgy Principles, Van Nostrand, Princeton, N. J., 1964.

30. W. E. Quist, R . Taggart and D. H. Polonis, "The influence of iron and aluminum on the precipitation of metastable Ni_3Nb phases in the Ni-Nb system", Metallurgical Transactions, vol. 2, 1971, pp. 825-832.

31. M. Aballe, V. Ramaswamy and D. R. F . West, "Intermetallic compound precipitation from solid solution in some Ni-Ta and Ni-Ta-Cr alloys", Journal of the Less-common Metals, vol. 39, 1975, pp. 287-288.

32. W. G. Moffatt, The Handbook of Binary Phase Diagram, Vol. 3, USA, General Electric Company, 1978.

33. S. Chakravorty and D. R. F. West, "Constitution of Ni-rich alloys in Ni-Mo-Ta system", Metal Science, Vol. 17, 1983, pp. 573-580.

34. Mentioned in K. Vasudevan's Ph.D. Dissertation, University of Tennessee, 1986.

35. S. Chakravorty and D. R. F. West, "Intermetallic compound formation in the Ni_3Ta-Ni_3Mo section of the Ni-Ta-Mo system", Journal of Materials Science, vol. 2, 1983, pp.583-586.

36. A. Royer and M. Grantio, "Mecanismes de precipitation et de deformation plastique d'alliages nickel-chrome durcis par precipitation par le niobium et le tantale", Memoires Scientifique Rev. Metallurg., vol. 15, No 1, 1971, pp.1-14.

APPENDIX

(1). Calibration of EDS analysis for the particle $Ni_XTa_YCr_Z$

A 5 cm x 5 cm (estimated from the screen) EDS analysis was done in an un-etched solution treated sample which contained particles and matrix. The counts of Ni, Ta and Cr and the ratios of Ta/Ni, Cr/Ni and Cr/Ta are listed in Table A. The actual chemical composition (see Table A) of this ternary alloy was used to compare with the EDS analysis. Thus, a correction value can be obtained from the relationship between the experimental EDS data and the actual elemental contents and is taken to be

chemical composition ratio / EDS analysis ratio.

The result of EDS analysis for the particles times this correction ratio is the approximate particle ratio. So, the particle ratios of Ta/Ni, Cr/Ni and Cr/Ta after calibration are 0.27, 0.08 and 0.27, respectively (see Table B).

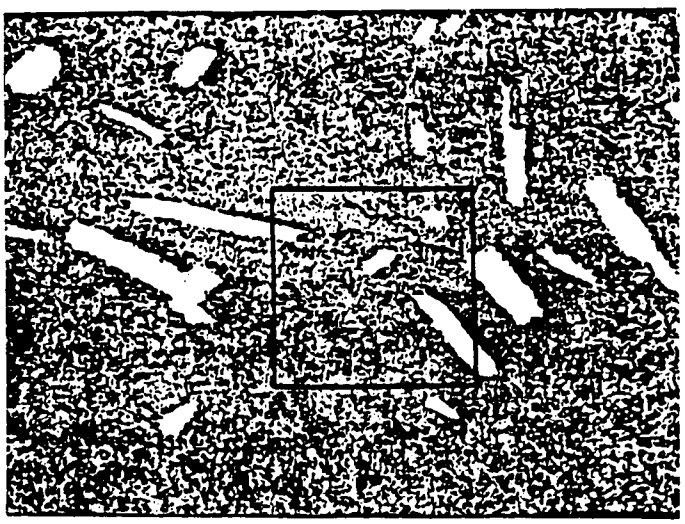

Ni-Ta-Cr alloy, second solution treated at 1280°C for 4 hrs, then water quenched, SEM, 1000 X. The square is 5 cm x 5 cm estimated from the screen.

Table A.

	EDS		chemical composition
	total area	particle	
Ni	8000	8000	73.38 at%
Ta	2616	5333	9.92 at%
Cr	3366	1144	16.70 at%
Ta/Ni	0.327	0.667	0.135
Cr/Ni	0.421	0.143	0.227
Cr/Ta	1.290	0.214	1.680

Table B.

	correction ratio	particle ratio after calibration
Ta/Ni	0.135/0.327 = 0.41	0.667 x 0.41 = 0.27
Cr/Ni	0.227/0.421 = 0.54	0.143 x 0.54 = 0.08
Cr/Ta	1.680/1.290 = 1.30	0.214 x 1.30 = 0.27

(2) The EDS analyses of the un-etched solution treated sample used in calibration in appendix 1.

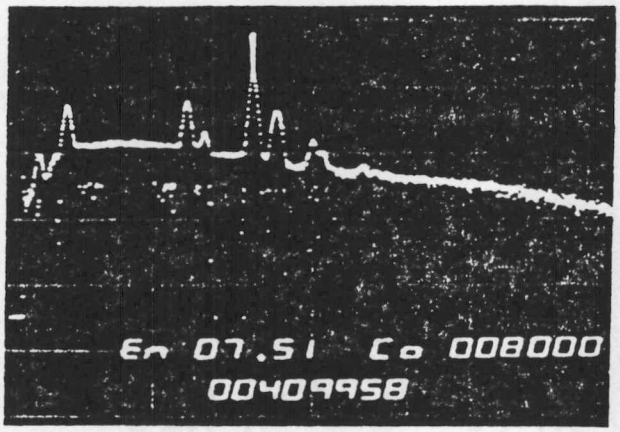

total area
(5cm x 5cm)

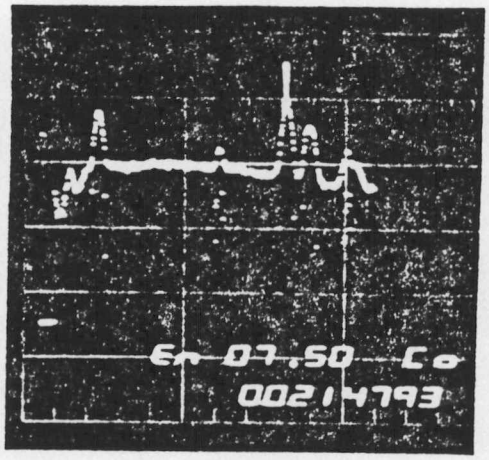

particle
(Ta rich)

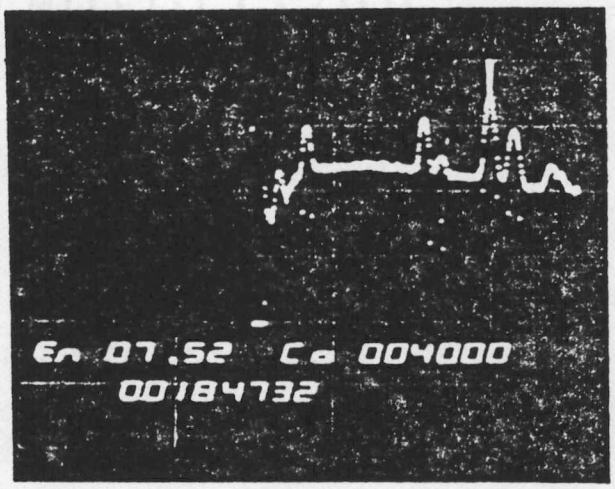

matrix
(Cr rich)

VITA

Yee C. Lin was born in Tainan, Taiwan, R.O.C. on June 15, 1958. He attended high school in Tainan, Taiwan, and graduate from the First Tainan High School in June, 1976.

After attending one year of freshman study in the Chung Yuan University, Chung-Li, Taiwan, he transferred to the National Chung Kung University, Tainan, Taiwan, and received a B.S. degree in the Metallurgical Engineering in June, 1981. He took his military service as an official in the Chinese Air Force from July, 1981 to May, 1983.

In the Fall of 1983, he received the admission from the University of Tennessee, Knoxville and began study toward a Master's degree in Metallurgical Engineering.

He will continue his graduate education toward a Ph.D. at the University of Tennessee, Knoxville.

The author is a student member of the American Society for Metals. His ultimate goal is a career in applied research.